Bar-Ilan University

Effect of Magnetic Zero-Field Lines on the Electric Field in High-Temperature Superconducting Wires and Tapes in the DC and AC Regimes

Offek Marelly

Submitted in partial fulfillment of the requirements for the Master's Degree in the Department of Physics, Bar-Ilan University

Ramat-Gan, Israel 2023

This work was carried out under the supervision of Dr. Shuki Wolfus

Department of Physics, Bar-Ilan University.

Acknowledgements

The work before you would not have come to fruition without the great help and amazing support of countless people. I wish to acknowledge their help and thank all of them here.

First, I would like to thank my advisor, Dr. Shuki Wolfus, from the bottom of my heart. He was always there, ready to answer questions and give advice and counsel. He shared his vast knowledge freely and happily, and was constantly challenging me and helping me push my limits. Through the many difficulties and unexpected twists that arose during this work, he was there to help, teach and encourage, and he always did it with a smile on his face. His patient and dedicated guidance was not just instrumental in the success of this work, it has also had a profound personal effect on me, both as a person and as a researcher. I am better in both respects because of him, and I am forever grateful.

Second, I would like to express my gratitude to Prof. Yosi Yeshurun, the head of the Institute of Superconductivity. His professionalism, boundless knowledge, and emphasis on excellence, combined with his dedication to his group members and peers are truly awe inspiring. Under his leadership, these principles have become an intrinsic part of the lab, making it the perfect environment to start honing my skills and to grow professionally and personally. I cannot think of a better place for me to have started my journey as a Physicist, thank you.

I would also like to thank Dr. Leonid Burlachkov and Nikita Fuzailov. Their help and collaboration were invaluable to the success of this work. Their theoretical analysis of the results as well as the wise and creative ideas they offered over our constant discussions throughout the work were pivotal, and without them this work would have been very different from what it is.

Next, I wish to thank all of my colleagues in the lab. To Dr. Yasha Nikulshin and Eli Perel, for both their indispensable knowledge and advice, as well as for mentoring and patiently helping me in the creation, and constant adjustment and maintenance, of my experimental systems. I would also like to thank Itay Garofy, Ariel Roitman, Jonathan Shvartzberg, Zoharchen Sofer, Michal Wasserman, Omri Tzarfati and Jonathan Smadja. They were always there for helpful discussions and advice, and quick to help me in any way possible. All of them are more than just colleagues, they are also my good friends. This entire experience was made richer because of them. Thank you all.

I also wish to thank the Physics department at Bar-Ilan University. Especially Dr. Yossi Ben-Zion, Rita Dadiomov, and the rest of the amazing administrative staff. Their genuine care for everyone in the department is astounding, no question remained unanswered and no problem unsolved.

And lastly, I wish to thank my family. For their faith in me, which inspired me and has driven me to follow my dreams. And for their unwavering support throughout this journey, which gave me the strength to push forward, no matter the difficulties and challenges. To my parents, for their wise advice and unending assistance. To my mother, who is constantly reminding and inspiring me to push my limits and aim higher and higher, and achieve what at first seemed impossible. And to my sister, who was always there with words of encouragement. There are no words that can describe my gratitude. I especially wish to thank my father, for listening to my ideas for hours on end and giving invaluable input, and for helping me build parts for my experiments – regardless of the time it took and in all manner of hours.

Thank you all.

Contents

Abstract

Recently, a new theoretical model has demonstrated the important contribution magnetic zero-field lines may have to the flux dynamics in superconductors. The local divergence in the current density, where flux vortices of different polarities annihilate each other, redistributes the current density over the superconductor cross-section and leads to a slowdown of the dynamics in the presence of zero-field lines in the sample. In this work, we explore experimentally how the contribution of these zero-field lines affects the induced voltage on High Temperature Superconducting (HTS) tapes. We start in the DC regime, by investigating the current-voltage curves of BSCCO-2223 tapes carrying different DC transport currents and exposed to different external DC magnetic fields. While the transport current naturally creates a zero-field line in the center of the tape, the external field shifts the position of this line and may eliminate the line altogether, depending on the levels of both, current and field. By varying these conditions, we show experimentally that the current-voltage curves change with the crossover from presence to absence of a zero-field line in the sample. We then proceed to investigate the effects of the zero-field line in the AC regime, where two competing regimes of AC magnetic response were previously observed in current carrying HTS tapes. In the usual regime, the voltage induced by flux motion across the tape, is “in-phase" with the external magnetic field. However, as the field frequency grows or transport current decreases, there appears an unexpected, “out-of-phase" peak in the voltage waveform. For different conditions of external magnetic field and transport current, the two regimes coexist. While for some conditions of field and current the out-of-phase peak overwhelms the in-phase one. The aforementioned theoretical model predicts that out-of-phase peak in the voltage waveform is due to the inhibition effect of magnetic zero-field lines on flux motion. A theoretical phase diagram was presented which predicts the conditions of field and current for which each of the peaks in the voltage waveform dominate, and the conditions for which they coexist. By experimentally measuring the voltage waveforms on a BSCCO-2223 tape for varying conditions of transport currents and external magnetic fields we show that the behavior of the waveforms is in qualitative agreement with the theoretical phase diagram. The results in both the DC and AC regimes support the slowdown of flux dynamics in the presence of the magnetic zero-field line. Finally, we discovered an unexpected new phenomenon of asymmetry in the response of the tape which is attributed to the structure of our superconducting tape. This asymmetry drastically effects the voltage waveform in the HTS tape. By adjusting the theoretical model to account for the asymmetric

tape structure, we show that our results are still in qualitative agreement with the phase diagram. We also show that this asymmetry effects primarily the out-of-phase component of the voltage waveform and is more pronounced at higher field frequencies and low transport currents, in agreement with theoretical predictions. With the growing demand for and use of superconducting wires and tapes, these results may play an important role when using these tapes in practical applications. Specifically, the proof we provide for the slowdown of flux motion when annihilation lines are present, strongly recommend to aspire towards allowing operating conditions for HTS tapes that support such lines' presence

1. Introduction

1.1. Goals of this research

The goal of this work is to address experimentally, for the first time, the effect of magnetic zero-field lines, also known as annihilation lines, on the flux dynamics within high temperature superconducting (HTS) wires and tapes and on the voltage induced on them. We experimentally observe how the presence or absence of the zero-field line within the superconductor changes the flux dynamics both in the DC regime and in the AC regime. In doing so, we test the validity of existing theoretical models and predictions regarding the effects of the zero-field lines on the behavior of magnetic flux within the superconductor. We assess how these lines change the induced voltage waveforms within the superconductor and what this means for the practicality and feasibility of HTS wires and tapes in various high-power applications. We determine whether magnetic zero-field lines have a positive or detrimental effect on the performance of HTS in different scenarios and applications and answer the question, should they be utilized or avoided.

1.2. Motivation

Most applications of superconductors today involve low temperature superconductors (LTS). However, due to their low operating temperatures and limited current capacity they are confined to a limited number of applications such as MRI and magnets for accelerators. On the other hand, HTS have much higher current carrying capacity and operating temperatures, as well as the ability to operate in stronger magnetic fields. This makes them much more practical to implement in various applications and they can potentially revolutionize countless industries[1]. A major limiting factor in the adoption of HTS until now was their high cost and low production output. But, recent successful experiments and prototypes of HTS toroidal field coils for tokamak fusion reactors has led to increasing interest and demand for HTS tapes, wires and cables[2]. This has led manufacturers to invest significant resources in expanding and improving their production capabilities. The annual production of HTS wires has greatly increased in the last several years and is expected to continue to drastically increase. Furthermore, the development of more efficient production methods has led to higher quality HTS and prices are expected to decrease. In turn, the growing availability of HTS tapes, wires and cables, and the expected reduction in prices due to the greater and more efficient production have led to interest in using HTS in many more fields and applications.

While the economical and industrial obstacles in the implementation of HTS are beginning to diminish, another major obstacle in the use and implementation of HTS remains. That is the presence of magnetic fields and their detrimental effect on the superconductor's performance. Magnetic flux enters the superconductor in the form of flux quanta, called fluxons, which move within the superconductor due to the Lorentz force and create an electric field and effective resistance. These magnetic fields can either be external to the superconductor or be the self-field of the superconducting wire carrying a current. While the losses generated are small relative to losses in regular conductors, superconductors are highly sensitive to changes in temperature and any rise in temperature due to losses can greatly hinder the efficiency and performance of the superconductor. Furthermore, if dry cryogenic systems (systems that don't rely on cryogenic fluid) are used in the superconducting device, any heat generated will increase the load on the cryogenic system and increase the energy needed to cool the superconductor to its operating temperature. If the device uses cryogenic fluid to maintain operating temperatures, the heat generated by the losses will lead to increased consumption of the fluid. In the worst-case scenario, these losses can lead to thermal runaway in which heat generated by the magnetic field losses decreases the performance of the superconductor, which creates more losses, which lead to more heat etc. until the superconducting phase is ruined, and the superconducting device becomes unusable. It is thus crucial to study and understand losses in superconductors and find ways to mitigate them if we are to create feasible superconducting appliances.

1.3. What are magnetic zero-field lines

Magnetic zero-field lines are places within the superconductor where the magnetic field equals zero ($B = 0$) and is of a different polarity on each side of the point where $B = 0$ (i.e., the magnetic field changes sign). These lines are also called "annihilation lines" because they are the dividing line between magnetic vortices of opposite polarities. The vortices meet at the annihilation line and annihilate each other, hence the name and the zero magnetic field. Due to the inverse relation between the critical current density and magnetic field within the superconductor [3] the current density grows drastically in the presence of the zero-field line. Because the total transport current within the superconductor is constant and determined by the external power supply, this leads to a reduction in current density over the rest of the superconductor's cross section. The current is what drives the vortices within the superconductor and its redistribution has dramatic effects on the flux dynamics within the superconductor, as will be elaborated upon in detail in this work.

1.4. Sources of losses in superconductors

Energy losses in superconductors can arise from the motion of flux quanta – fluxons – within the superconductor due to the Lorentz force. These fluxons are made of a quantized unit of flux in a non-superconducting core which is surrounded by a circular supercurrent which shields the rest of the superconductor from the magnetic flux and allows it to remain superconducting [4]. These circular currents also give fluxons their other name – vortices. Losses due to fluxon motion take several forms including Flux Creep, Flux Flow and, for large enough AC magnetic field amplitudes and a DC transport current, Dynamic Resistance.

In the presence of an external magnetic field, magnetization currents flow in the superconductor to screen out the magnetic field. When fluxons enter the superconductor, the interaction between the fluxon and the screening currents create a Lorentz force, $F = j \times \frac{B}{c}$, which acts on the fluxons in the direction perpendicular to both the screening current and the magnetic field, towards the center of the superconductor. Due to the said Lorentz force, the fluxons should move along the magnetic gradient. As the fluxons move, parts of the superconductor transition from superconducting to normal and vice versa and this will lead to losses in the form of heat. But the fluxons can be trapped by various strains, imperfections and inhomogeneities within the superconductor. These areas, known as "pinning sites", are places within the superconductor where the superconductivity is weakened or nonexistent and thus it is energetically favorable for the fluxons to remain there. Hence the pinning sites act as potential wells for the fluxons. As long as the fluxons remain trapped within the pinning centers, there will be no losses. But, even if the magnetic driving force is weaker than the pinning force, there is still a chance that the fluxon will escape the pinning center due to thermal fluctuations. The fluxon will then move within the superconductor until it reaches another pinning site, generating voltage along the way. This "jumping" of fluxons between pinning sites is called "flux creep"[5]. If the external field and/or the current increase, so too does the Lorentz force (see equation above), this effectively lowers the potential barrier of the pinning sites in the direction of the Lorentz force. Thus, the stronger the external magnetic field or the transport current, the easier it will be for the fluxons to escape via thermal fluctuation (in the direction of the center of the superconductor) – hence the greater the losses from flux creep. Moreover, the higher the temperature, the more thermal fluctuations capable of releasing the fluxon from the pinning site occur, hence higher temperatures facilitate more flux creep. If the magnetic field is large enough so that the Lorentz force is larger than the potential barrier of the pinning sites, or if the current is larger than j_c, the critical current, the

fluxons begin to move within the superconductor in a viscous manner driven by the local field gradient and diffusion mechanisms. This regime of flux dynamics is called “flux flow”[6].

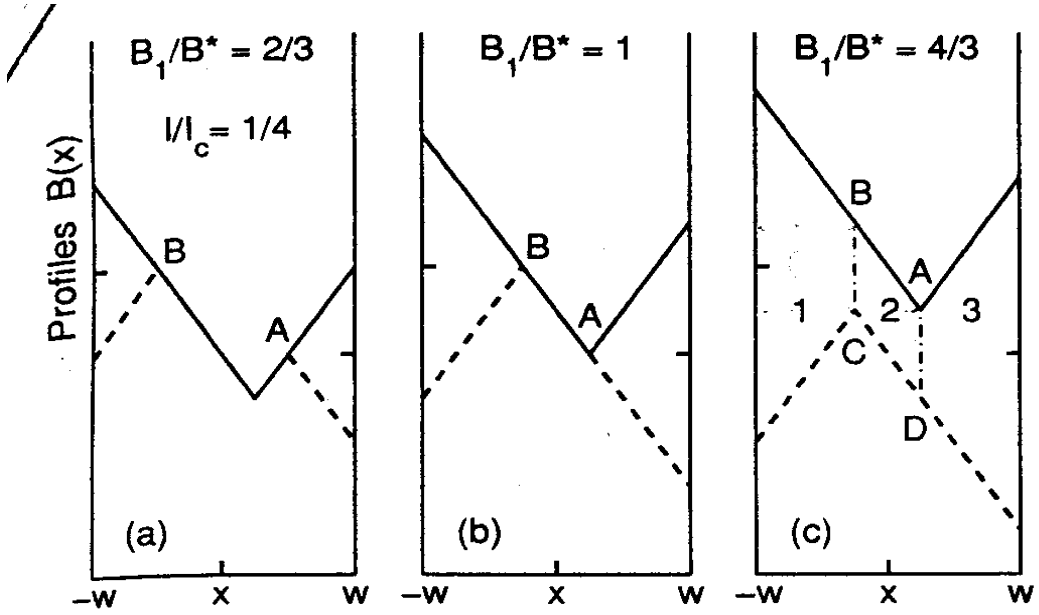

Fig 1. Magnetic field profiles of a superconducting slab carrying a DC transport current and exposed to an AC magnetic field. The asymmetry in the field profiles is due to the DC transport current. The flux enters the slab across the magnetic gradient while the field is positive (solid line) and leaves the slab along the magnetic gradient while the field is negative (dashed line). In (a) and (b), the magnetic field amplitude is $\leq B^*$ so no flux can cross from one side of the superconductor to the other. In (c) $B > B^*$ so all the flux in area 2 crosses the slab.

Another source of losses is due to the entry and exit of fluxons to and from a superconducting wire exposed to AC magnetic field. The situation is described schematically in Fig. 1 which assumes an infinite slab geometry and is based on the Bean critical state model [7], [8]. In this model, the superconductor can carry only a limited, magnetic field independent, current density known as the critical current density (j_c), and any electromotive force the superconductor “feels”, regardless of size, will induce this critical current density to flow where the magnetic field has entered the superconductor. This means that at any given point within the superconductor the current density is either zero, if there was is no magnetic field there, or $\pm j_c$ depending on the magnetic field direction. While the Bean model assumes that the critical current density is independent of the field, its extensions, such as the Kim model [3] [9], have adapted it to account for a field dependent current density. These models imply infinitely fast flux flow when $j > j_c$, and extremely slow flux creep for $j < j_c$. This means

that when j surpasses j_c, the fluxons will quickly flow until they reach a steady state where $j = j_c$, after which they will remain strongly pinned.

The solid lines in the 3 panels of Fig. 1 describe the magnetic field gradient within the superconductor for 3 different external fields: B smaller, equal or larger than the full penetration field (i.e., the field H_p for which the induction B^* reaches the center of the sample), when the AC magnetic field is at its maximum value in the positive direction. The broken lines in the figure describe the magnetic field gradient within the superconductor when the AC magnetic field is at its maximum value in the negative direction. When the superconductor is exposed to an alternating magnetic field, fluxons enter the superconductor from the sides and enter deeper as it increases. When the magnetic field changes direction, the fluxons are forced back out the way they came. The magnetic field at which vortices fully penetrate into the superconductor i.e., it reaches the center, is called the threshold field, or B^*. If there is no transport current within the superconductor, or if there is a current but the AC field is below the threshold, the same number of fluxons that enter from each side also exit from that side. During a full cycle of the AC field, because they follow a closed loop, returning to where they began, the current source does no work and thus does not contribute to the losses. But, if a DC transport current flows through the superconductor, it creates a DC magnetic field that breaks the symmetry between the two sides of the alternating magnetic field. If we have both the transport current and an alternating field larger than the threshold, some of the fluxons that entered from one side will penetrate the superconductor to a point that when the field changes direction, they will be forced out of the side opposite to that from which they came. Now the net flux entering from one side of the superconductor is larger than the flux exiting that side and vice versa for the other side of the superconductor. In transporting flux from side to side the current source does work and thus contributes to the losses. This manifests in the form of voltage on the superconductor, which depends on the amplitude of the magnetic field (determines how many fluxons enter and exit in each cycle), its frequency (number of cycles per second) and the transport current (determines the asymmetry of the magnetic field and thus how many fluxons will reach the point where they will cross the superconductor). This is called “Dynamic resistance”, it was described independently by Adrianov [10], Ogasawara [11]–[13], Brandt-Mikitik [14] and Oomen[15] and experimentally verified by them. It should be noted that because the fluxons are always moving in the direction of the Lorentz force, the voltage generated this way is always positive and has double the frequency of the magnetic field.

In addition to losses related to the motion of fluxons in the superconductor, losses can occur due to other reasons. Many HTS wires and tapes, including BSCCO, are made up of many superconducting filaments within a normal (usually silver) matrix. Induction between these superconducting filaments can lead to losses, known as coupling losses[16], [17]. Superconducting wires and tapes also include several different layers around the superconductor itself, meant to provide protection from oxidation, mechanical strength and thermal capacity. These can be sources for different kinds of losses, such as hysteresis losses in magnetic materials within the wire structure, and losses from eddy currents which flow in the superconductor and also in the non-superconducting layers surrounding it[18]–[20].

In this work we focus on the losses due to the motion of magnetic flux within the superconductor and in particular how magnetic zero-field lines affect them. The reason for this is that losses due to flux motion in the superconductor, particularly for AC fields and currents, are well known to be significant in determining the practicality of superconducting devices and have been studied previously[21][22]. Yet the effect of zero-field lines on the flux behavior and corresponding losses in superconductors is not well studied. As we shall present in this work, the zero-field lines have significant effects on superconducting systems where there exist both a transport current and an external field. The coexistence of transport current and magnetic field is present in the majority of electric and high-power application for which HTS could be implemented. Examples include devices such as Superconducting Magnetic Energy Storage (SMES) systems, where current is put in a closed superconducting coil - thus allowing energy to be stored in the form of a magnetic field without the current decaying due to ohmic resistance[23]. Superconducting Fault Current Limiters (SCFCL) are another example. In SCFCL, a superconducting coil is used to saturate a magnetic core, an AC coil is wound around the magnetic core and is connected in parallel with the electric grid. For normal grid currents the SCFCL is a low impedance component which does not affect the grid. In the case of a fault current, the rise in current through the AC coil creates an AC magnetic field which drives the magnetic core out of saturation, leading to an increase in impedance and limiting the fault current[24], [25]. Both devices usually operate in a mode where DC current flows in a superconducting coil which is exposed to AC field and/or AC current ripple. For instance, in SMES, the magnetic self-field which is how the energy is stored also effects the efficiency of the HTS coil. And while the driven current is DC, the switching required when storing energy in the coil and when releasing it for use creates an AC current which coexists with the DC current component. In such devices, the ability to

predict the level of losses in the coil in a wide range of operating conditions is crucial for the device's design and operation. While contributions of coupling and eddy currents to the losses are generally known and can be calculated for different combinations of currents and fields, this is not the case for the motion of fluxons as they are greatly affected by such conditions and act in novel and difficult to predict ways. As we will describe next, recent theoretical works pointed to the effect of annihilation line on slowing down vortex dynamics in superconductors which operate under conditions discussed here. It is the goal of this research work to study experimentally the dynamics of the flux motion with and without an annihilation line and flux-free zone in the sample, validate the theoretical predictions, evaluate the effect on the induced voltage and contribution to the general AC losses and point to ways for predicting this contribution in high-power applications.

2. Theory

In this section, we will present the theoretical models that have been developed to explain the effect of magnetic zero-field lines on the flux dynamics and losses in HTS. We will divide this section into two parts. First, we will present the model and theoretical predictions for the DC regime – where the external magnetic field is constant. Afterwards, we will expand the model for the case of an AC magnetic field.

2.1. DC regime

As mentioned before, zero-field lines, also called "annihilation lines", are places inside the superconductor where the magnetic field reverses polarity. They divide the fluxons into two different polarities which meet at the zero-field line and annihilate each other. Several studies of the different ways that annihilation lines affect superconductors have been conducted. It was shown by Beasley *et. al.*[26] that when annihilation lines exist within the superconductor, the annihilation of fluxons of opposing polarities leads to instabilities in the form of flux jumps, which manifest as erratic drops in magnetization and voltage pulses on the superconductor. Studies by Kapra *et. al.*[27] and Zadorosny *et. al.*[28] also showed that annihilation of opposing fluxons lead to jumps in the magnetization curve as well as cause an increase of the critical current in the superconductor. It was suggested in these studies that annihilation lines and the interaction between fluxons of different polarities affects flux dynamics and could be used in devices to manipulate flux motion. These studies were conducted in temperatures significantly lower than the critical temperature, currents significantly lower than the critical current, and magnetic fields significantly lower than the upper critical field of the superconductors. In these conditions the flux pinning is very strong and the jumps in the magnetization curve are the result of flux avalanches. These conditions are very different from those in this work. The temperature, current and magnetic field are much closer to their critical values and pinning is very weak. The dominant flux behavior is flux flow and the effects of the zero-field lines will be different.

With regards to the effects of zero-field lines on flux dynamics, it has been recently shown by Burlachkov and Burov[29] that these zero-field lines have a strong retardation effect on flux motion, which manifests in relaxation experiments and magnetization curve measurements when the magnetic field to which the superconductor was exposed is abruptly removed. The model then explained in hindsight studies of magnetic AC response first conducted experimentally by Lukovsky *et. al.*[30]. It was later extended by theoretical studies by

Fuzailov *et. al.*[31]. This is due to the fact that the magnetization current density diverges at the zero-field line (the divergence is cut off by the magnetic penetration depth λ). Since the total current $I = \int j(x)dx$ in the superconductor is finite, so is the total amount of j. The divergence of j at a zero-field line thus "consumes" a lot of j, which leads to the redistribution of the current in the superconductor such that it greatly increases around the zero-field line and decreases everywhere else. Since the local Lorentz force driving the fluxons is proportional to the local current, this leads to a decrease in the driving force. Hence, the zero-field line slows down the fluxon dynamics in the rest of the superconductor and drastically changes the magnetic field profile within it.

A common way to describe fluxon dynamics in a superconductor is the aforementioned Bean critical state model. However, in high temperature superconductors, the energy U_0 of the pinning sites is small due to the short superconducting coherence length (all HTS are type II superconductors) [32]–[34]. Hence, the activation energy required to release fluxons from the pinning sites is small. In addition, HTS have high operating temperatures of around, and even above, liquid nitrogen (77K). The critical current density follows the relation $j_c = j_{c0}\left[1 - \frac{k_B T}{U_0}\right]$ [33]. For low temperatures and strong pinning energies the second term on the right-hand side is small and not significant, but for the high T and small U_0 of HTS the critical current density decreases. This means that for our conditions the flux dynamics are in the flux flow regime and pinning is very weak. In this case, even if the current density is below the critical current, we still have significant ("giant") flux creep [35] and the Bean model and its expansions, which assume extremely slow flux creep for $j < j_c$, do not hold. To properly describe the flux dynamics in high temperature superconductors we must use the flux diffusion equation[34], [36]–[39]. This equation, which is derived from Maxwell's equations and the Lorentz rules for field transformations, treats the fluxons as moving within a viscous medium whose drag coefficient is a property of the superconducting material.

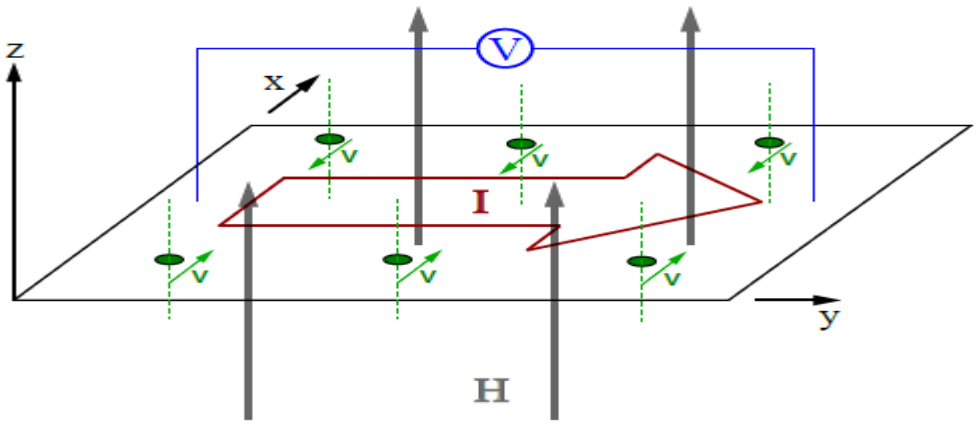

Fig. 2. Transport current I (red arrow) flows in the y direction, and voltage V is measured along the same axis. An external magnetic field H is applied in the z direction. The magnetic vortices of opposite polarities (shown as green dashed lines with circles) enter the sample from both sides, move towards each other along the x axis and annihilate at the $B = 0$ line.

In our experiments, we study the case where the current flows only in the y direction and the magnetic field is applied along the z axis (see Fig. 2). This geometry is that of a tape carrying a transport current and exposed to a magnetic field perpendicular to the flat side of the tape. However, the theory assumes an infinite slab rather than a tape since this allows for analytical solution rather than a cumbersome numerical solution. Despite this assumption, we will show that the experiments on tapes are in qualitative agreement with the theoretical model.

In the slab configuration, the magnetic field B, the electric field E and the current density j are spatially dependent only on x. We can write the flux diffusion equation as:

$$\frac{\partial B}{\partial t} = -c\frac{\partial E}{\partial x} = \frac{\partial}{\partial x}\left[\frac{\phi_0}{4\pi\eta}|B|\frac{\partial B}{\partial x}\exp\left(-\frac{U(j)}{k_B T}\right)\right] \qquad (1)$$

Where $E = \frac{Bv}{c}$ is the induced electric field, v is the fluxon velocity, Φ_0 is the unit flux, η is the Bardeen-Stephen drag coefficient[39], k_B is the Boltzmann constant and c is the speed of light. Now we consider the DC case $\frac{\partial B}{\partial t} = 0$, which reduces the equation to:

$$E = -\frac{\phi_0}{4\pi\eta}|B|\frac{\partial B}{\partial x}\exp\left(-\frac{U(j)}{k_B T}\right) = const \qquad (2)$$

The term $const$ in the equation indicates that the electric field is independent of x. Hence, the voltage measured between to contacts of distance l apart is $V = El$. The boundary conditions of the flux diffusion equation are:

$$B\left(x = \pm\frac{d}{2}\right) = H \mp \beta I \qquad (3)$$

Where the coefficient β can be found using the condition $\beta I = \int_{-\frac{d}{2}}^{\frac{d}{2}} j(x)dx = \frac{2\pi I}{cw}$, which gives us $\beta = \frac{2\pi}{cw}$.

The DC flux diffusion equation was solved with these boundary conditions in the flux flow regime ($U = 0$) and was found to be:

$$E = \begin{cases} \dfrac{\phi_0 IH}{c^2\eta dw}, & H > \beta I \\ \dfrac{\phi_0[H^2 + \left(\frac{4\pi^2}{c^2w^2}\right)I^2]}{4\pi c\eta d}, & H < \beta I \end{cases} \qquad (4)$$

And we can see that for $H = \beta I$ i.e., $B\left(\frac{d}{2}\right) = 0$, which means a zero-field line has just crossed the edge of the superconductor, the two parts of the solution are the same. The solutions clearly show that the $E - I$ curves of the superconductor act very differently depending on whether the zero-field line is present within the sample or not. In the absence of a zero-field line, the voltage increases quadratically to I. Whereas in the presence of a zero-field line the voltage increases linearly with I. While the fluxons are mostly in the flux flow regime, in HTS there still exists some pinning at the inter-grain boundaries. This pinning must be taken into account, so instead of taking $U = 0$ we shall take the well-established dependence of the activation energy U on j: $U(j) = U_0 \ln(\frac{j_c}{j})$. With this dependence, equation takes the form:

$$|E| = s|B|\left|\frac{\partial B}{\partial x}\right|^{u+1} = const \quad (5)$$

Where $u = \frac{U_0}{k_B T}$ and $s = \frac{\phi_0}{4\pi\eta}\left(\frac{c}{4\pi j_c}\right)^u$. The field profiles in the superconductor, and by extension, the solution for equation, are different depending on whether a zero-field line is present or not. In the case where there is no zero-field line, the field profiles that satisfy both equations are:

$$B(x) = (-px + q)^{\frac{u+1}{u+2}} \qquad (6)$$

Where:

$$p = \frac{1}{d}\left[(H + \beta I)^{\frac{u+2}{u+1}} - (H - \beta I)^{\frac{u+2}{u+1}}\right] \qquad (7)$$

$$q = \frac{1}{2}\left[(H + \beta I)^{\frac{u+2}{u+1}} + (H - \beta I)^{\frac{u+2}{u+1}}\right] \qquad (8)$$

At flux flow ($u = 0$), Eq. 6 reproduces the field profiles shown in [31], [40]. The field profiles for different values of u are shown in Fig. 3.

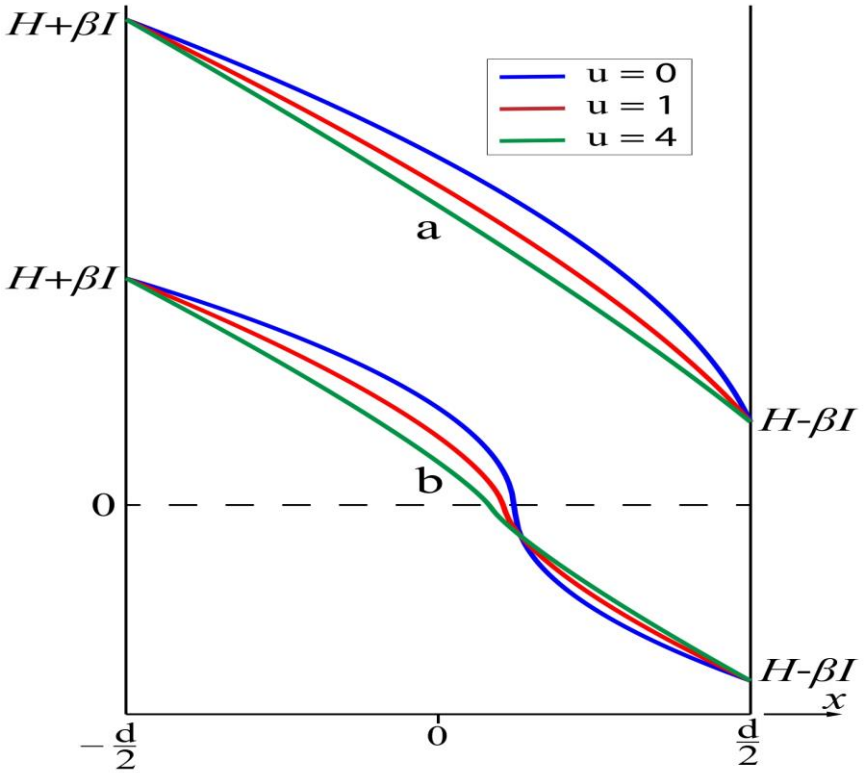

Fig. 3. Profiles of $B(x)$ for (a) $\beta I < H$, no annihilation line; (b) $\beta I > H$, annihilation line $B = 0$ is present. As u grows (pinning increases), the $B(x)$ profiles become straighter.

Fig. 3 visually shows as how the presence of a zero-field line depends both on the external magnetic field and the transport current. The transport current creates a self-field which has opposite signs at the two tape edges ($\mp\beta I$ in Fig. 3). This means that in the absence of an external field the zero-field line exists near the tape's center (Fig. 3 (b)). If an external magnetic field is introduced, it contributes equally to the overall field on both sides of the

tape and in doing so offsets the entire field gradient within the superconductor by H and moves the zero-field line towards one of the tape boundaries. If the external field is greater than the self-field at the tape edge, that is $H > \beta I$, the magnetic field within the tape is finite everywhere and there is no zero-field line inside the tape (Fig. 3 (a)). Otherwise, if $H < \beta I$, then the zero-field line is present within the tape (Fig. 3 (b)).

Substituting Eq. 6 into Eq. 5 gives us the electric field:

$$E = \frac{s}{d^{u+1}}\left(\frac{u+1}{u+2}\right)^{u+1}\left[(H+\beta I)^{\frac{u+2}{u+1}} - (H-\beta I)^{\frac{u+2}{u+1}}\right]^{u+1} \qquad (10)$$

And at $u \gg 1$ Eq. 10 becomes:

$$E = \frac{\phi_0 H I}{c^2 \eta d w}\left(\frac{I}{I_c}\right)^u \frac{1}{e} f\left(\frac{\beta I}{H}\right), \qquad H > \beta I \qquad (11)$$

Where I_c is the critical current, e is the Euler number and $f(a) = (1-a)^{\frac{(a-1)}{2a}}(1+a)^{\frac{(a+1)}{2a}}$.

In the case where a zero-field line is present, the magnetic field profiles are:

$$B(x) = -sign(x - x_0)m|x - x_0|^{\frac{u+1}{u+2}} \qquad (12)$$

Where $m^{u+2} = \frac{1}{d^{u+1}}\left[(H+\beta I)^{\frac{u+2}{u+1}} - (H-\beta I)^{\frac{u+2}{u+1}}\right]^{u+1}$ and x_0 is determined by the condition $m\left(x_0 + \frac{d}{2}\right) = (\beta I + H)^{\frac{u+2}{u+1}}$.

Substituting Eq. 12 into Eq. 5 we find that:

$$E = \frac{s}{d^{u+1}}\left(\frac{u+1}{u+2}\right)^{u+1}\left[(H+\beta I)^{\frac{u+2}{u+1}} + (H-\beta I)^{\frac{u+2}{u+1}}\right]^{u+1} \qquad (13)$$

And for $u \gg 1$, the electric field becomes:

$$E = \frac{2\pi\phi_0 I^2}{c^3 \eta d w^2}\left(\frac{I}{I_c}\right)^u \frac{1}{e} g\left(\frac{H}{\beta I}\right), \qquad H < \beta I \qquad (14)$$

Where $g(a) = (1-a)^{\frac{(1-a)}{2}}(1+a)^{\frac{(1+a)}{2}}$, functions $f(a)$ and $g(a)$ are presented in Fig. 4. Both equations and provide good approximations for $E(I)$ at $u > 4$.

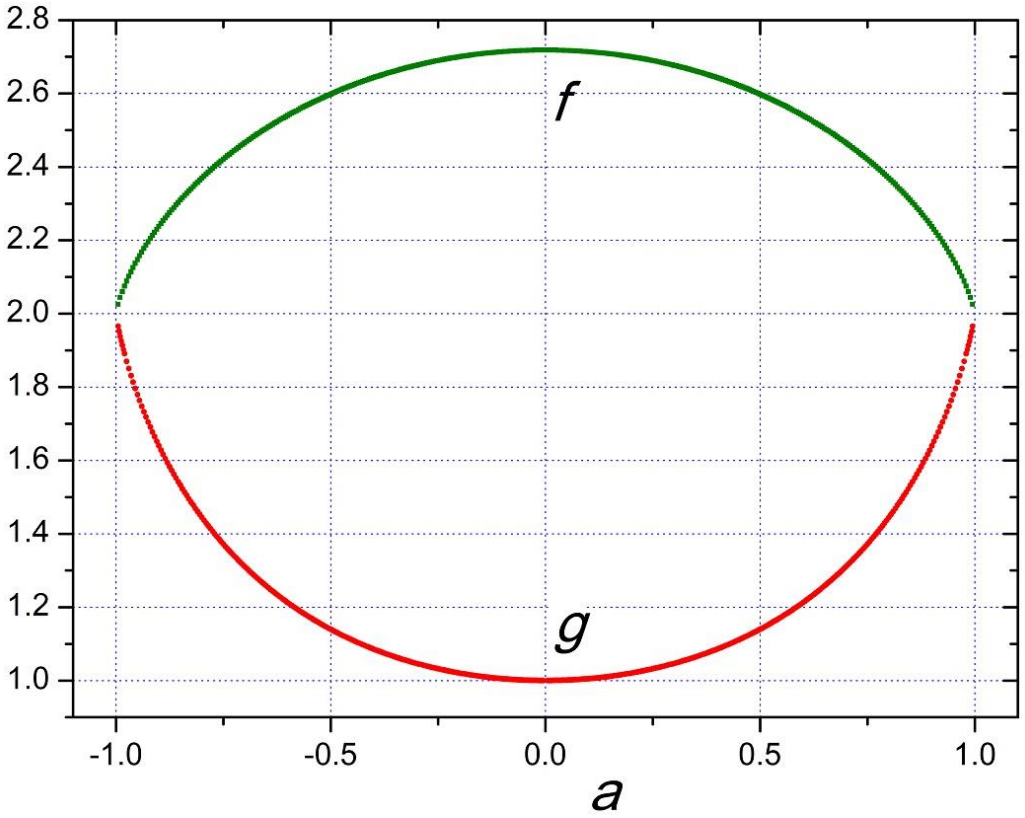

Fig. 4. Functions $f(a)$ and $g(a)$

The main prediction of this theoretical model is the change in the dependence of the electric field on the current in the presence an annihilation line. If such a line is absent then $E \sim I^{u+1}$, whereas if it exists within the superconductor, we obtain $E \sim I^{u+2}$. The experimental examination of this prediction, its results and analysis and discussion of the results will be done in the following sections.

2.2. AC regime

In this section we will address the effects of zero-field lines on the flux dynamics in the case of an alternating external magnetic field, which were theoretically modeled in [29], [31], [40], [41]. We shall show how the zero-field lines greatly influence the magnetic field profiles, especially with growing magnetic field frequency. This will be followed by how the change in the magnetic field profiles gives rise to highly unusual voltage waveforms. We will use the same infinite slab geometry as in the previous section.

While both the phenomena described in the previous section about the DC regime and those that will be described below about the AC regime are as a result of magnetic zero-field lines and their effect on the flux dynamics in the superconductor, there is a difference between the

regimes that leads to different physical phenomena. Unlike the DC regime, for AC external fields the experimental time window is frequency dependent. Due to the fact that the flux dynamics are in the flux flow regime and the fluxons are moving as if in a viscous medium, they lag behind the external field, and the greater the frequency, the greater the viscous drag and by extension the delay. This delay means that the experimental time windows observed in the AC regime are further back in time in comparison to those observed in the DC regime. Also, the fact that the external field is always changing and the internal field is constantly trying to follow it, while lagging behind due to the viscous drag, leads to non-linear and time varying field profiles within the superconductor. This, by extension, leads to non-linear and time varying current distribution. In this section we shall show how this non-linearity changes and magnifies the way zero-field lines affect the flux dynamics.

Moreover, in the AC regime the pinning energies holding the fluxons in place are much weaker – which leads to more substantial flux creep and the transition to flux flow occur for lower temperatures, transport currents and magnetic fields. This is because alternating magnetic fields induce shielding currents within the superconductor and the greater the external magnetic field frequency, the greater the currents. These currents contribute to the Lorentz force driving the fluxons and effectively weakens the pinning energy.

In terms of the magnetic field profiles in the superconductor, we shall again start with the flux diffusion equation seen previously in Eq. 1:

$$\frac{\partial B}{\partial t} = -c\frac{\partial E}{\partial x} = \frac{\partial}{\partial x}\left[\frac{\phi_0}{4\pi\eta}|B|\frac{\partial B}{\partial x}\exp\left(-\frac{U(j)}{k_B T}\right)\right]$$

And again, we shall start with the flux flow regime $U = 0$ and the same boundary conditions in Eq. 3:

$$B\left(x = \pm\frac{d}{2}\right) = H \mp \beta I$$

To reduce the number of variables, the problem was converted to dimensionless variables. Starting with dimensionless length: $\xi = \frac{x}{d}$, where d is the width of the wire, along which the fluxons are moving. In or geometry $-\frac{d}{2} < x < \frac{d}{2}$, which in turn means $-\frac{1}{2} < \xi < \frac{1}{2}$ the dimensionless magnetic field inside the superconductor is $b = \frac{B}{H_{max}}$ and $h = \frac{H}{H_{max}}$ outside it, where H_{max} is the amplitude of the external magnetic field. We define $\tilde{t} = \frac{t}{\tau}$ and $\tilde{\omega} = \omega\tau$,

where $\tau = \frac{\pi\eta d}{2\phi_0 H_{max}}$ is the characteristic time of the relaxation of the magnetization currents in the superconductor as shown in [36]. And lastly, we define the dimensionless current $\tilde{I} = \frac{4\pi I}{H_{max} c}$. These dimensionless variables, combined with the flux flow regime $U = 0$, reduce the flux diffusion equation to:

$$\frac{\partial b}{\partial \tilde{t}} = \frac{1}{8}\frac{\partial}{\partial \xi}\left(|b|\frac{\partial b}{\partial \xi}\right) \qquad (15)$$

And the boundary conditions are:

$$b\left(\xi = \pm\frac{1}{2}, \tilde{t}\right) = h(\tilde{t}) \mp \beta\tilde{I} \qquad (16)$$

In the context of zero-field lines, the boundary conditions imply two different regimes, one in which the fields at the superconductor's boundaries are always of opposite sign i.e., there is a zero-field line within the superconductor the entirety of the external field cycle – this can be seen for example in Fig. 6, $\tilde{\omega} = 0.25$, where the field at the edges are of opposite signs throughout the external field cycle and the magnetic field profile always changes sign inside the superconductor. And a second regime in which the fields at the edges change sign throughout the external field cycle i.e., zero-field lines enter and exit the superconductor – this can be seen for example in Fig. 5, $\tilde{\omega} = 0.25$, where at the beginning of the field cycle (blue and orange curves) the external field is small and the profile changes sign inside the superconductor. As the external field reaches its peak value (green and purple curves), the entire field profile is positive and the zero-field line is absent. Looking at the boundary conditions in Eq. 16, it is clear that for a given field the regime is determined by $\beta\tilde{I}$. For a sinusoidal magnetic field $H(t) = H_{max} sin(\omega t) \Rightarrow h(\tilde{t}) = sin(\tilde{\omega}\tilde{t})$, the first regime exists for $\beta\tilde{I} > 1$ and the second regime exists for $\beta\tilde{I} < 1$. Hence, the physical meaning of $\tilde{I}$, beyond reduction of variables, is to demarcate between the two regimes. $\tilde{I} = \frac{1}{\beta}$ is the boundary between "low currents" i.e., zero-field lines enter and exit the superconductor, and "high currents" where the zero-field line is always in the sample. In addition, the physical meaning of $\tilde{\omega}$ is to demarcate between what can be called the "quasistatic limit" $\tilde{\omega} \ll 1$, where $\frac{\partial B}{\partial t} \ll 1$ and the magnetic field profiles are mostly straight and the affect of the zero-field line is small. Conversely at $\tilde{\omega} \simeq 1$ the magnetic field profiles are not linear and the effect of the zero-field line is much more substantial. It is important to note that from the definitions of the dimensionless variables $\tilde{I}$ and $\tilde{\omega}$ that they are dependent not only on the

respective current I and frequency ω, but also on the external magnetic field amplitude H_{max}, the tape geometry (tape width d) and the material properties of the superconductor (η is the Bardeen-Stephen drag coefficient which is material dependent[39]). Hence, the values of variables $\tilde{I}$ and $\tilde{\omega}$ for different I and ω will be different for different types of superconductors, different types of tape geometries and even for different field amplitudes.

The behavior of the flux dynamics in the different regimes as well as how and why they affect the voltage waveform and losses in the superconductor will be explained below.

For low frequencies, in the limit $\frac{\partial B}{\partial t} \ll 1$ and $\tilde{\omega} \ll 1$, which we called the quasistatic regime, Eq. 15 with the boundary conditions of Eq. 16 can be solved analytically. This was solved by Fuzailov and Burlachkov [31] with the solution being:

$$b(\xi) = \sqrt{h^2 - 2\tilde{I}h\xi + \frac{\tilde{I}^2}{4}} \qquad (17)$$

If $b = 0$ i.e., there is no zero-field line in the superconductor, this condition only exists if $\beta\tilde{I} < |h(\tilde{t})|$. Otherwise, when a zero-field line exists within the sample and its location is denoted as ξ_0, the solution is:

$$b(\xi) = \sqrt{\left(2h^2 + \frac{\tilde{I}^2}{2}\right) \cdot |\xi - \xi_0|} \quad (18)$$

Unlike the DC regime in the previous section or the quasistatic regime above, for moderate and high frequencies where $\frac{\partial B}{\partial t} \simeq 1$ there is no analytical solution for the flux diffusion equation. Instead, a numerical solution was calculated by Fuzailov[41]. The calculated magnetic field profiles in the superconducting slab for different values of $\tilde{\omega}$ are presented in Fig. 5 and Fig. 6.

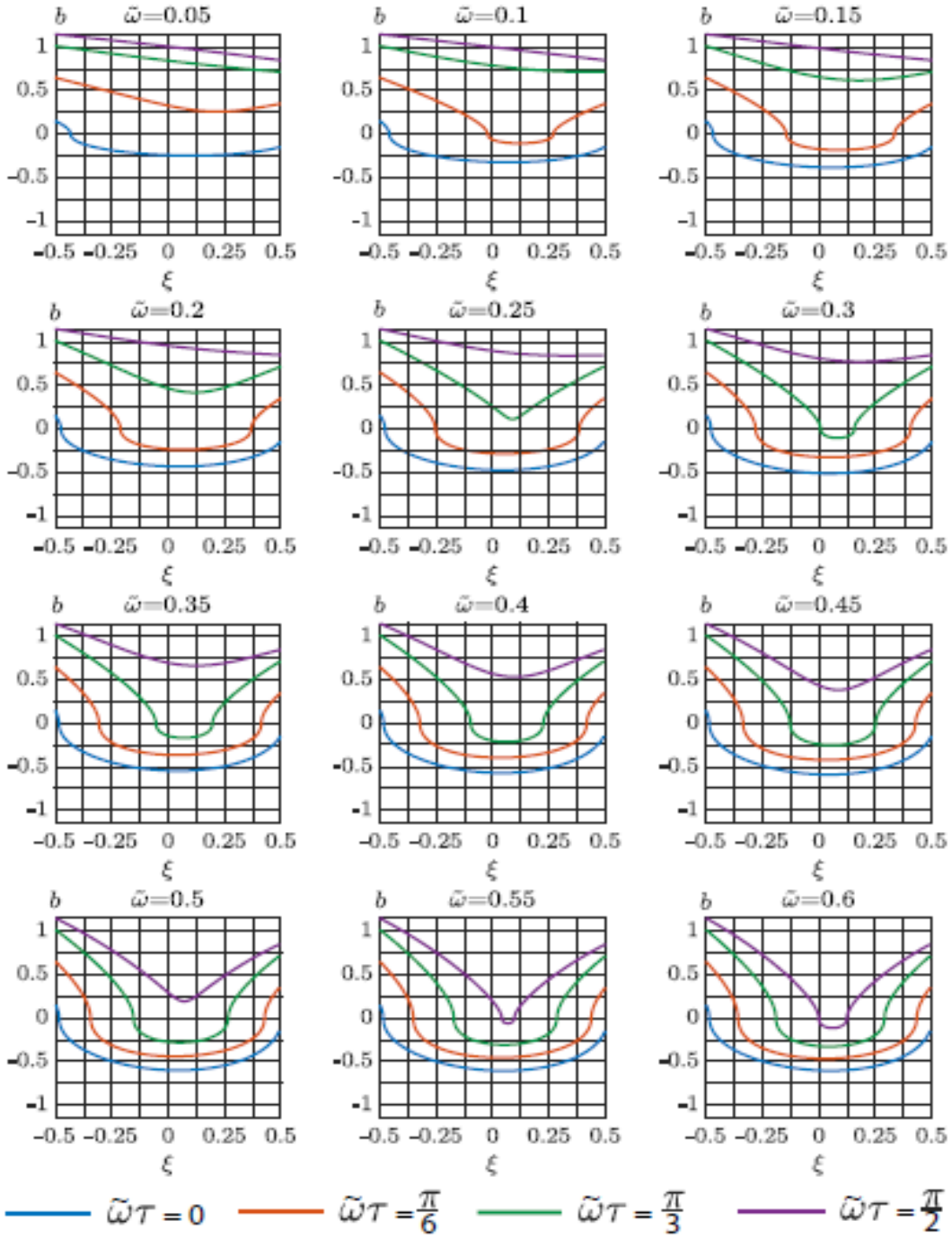

Fig. 5. The magnetic field profiles inside the superconducting slab for different values of $\tilde{\omega}$ for $\beta\tilde{I} < 1$. Each colored line represents the magnetic field profile for a different phase of the external magnetic field, starting from $h = 0$ (external field equals zero) to $h = 1$ (external field at maximum).

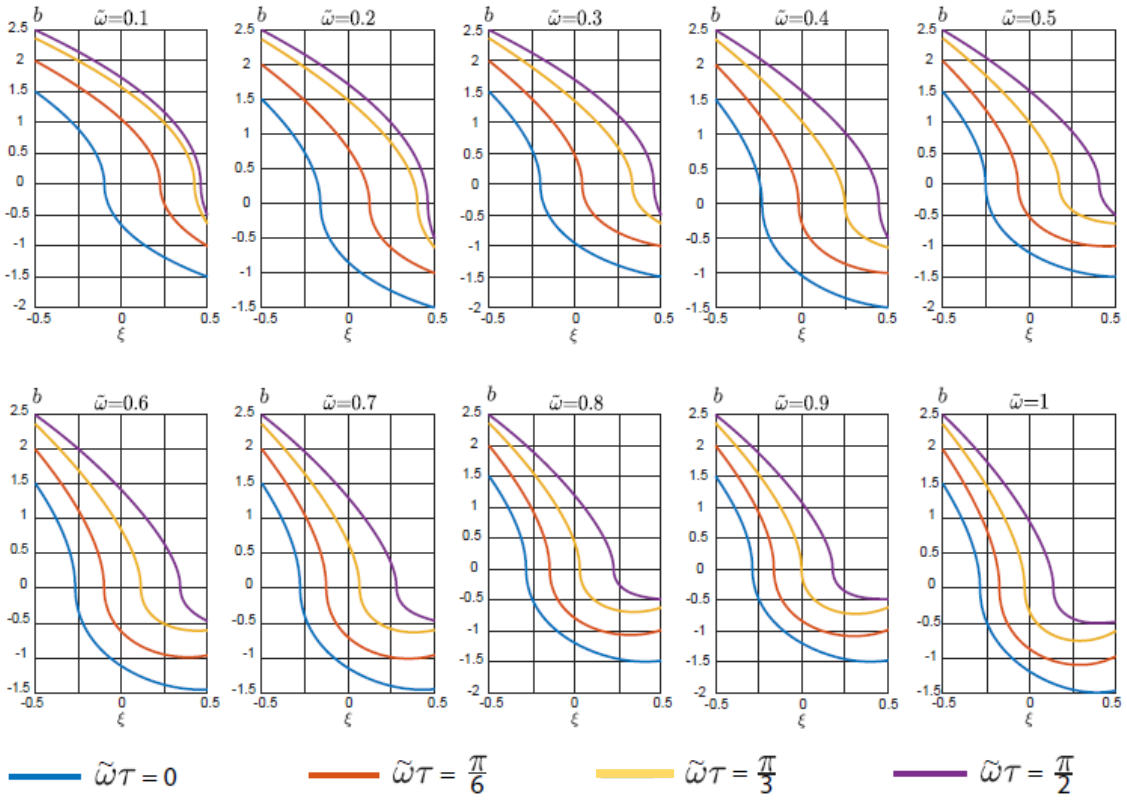

Fig. 6. The magnetic field profiles inside the superconducting slab for different values of $\tilde{\omega}$ for $\beta\tilde{I} > 1$. Each colored line represents the magnetic field profile for a different phase of the external magnetic field, starting from $h = 0$ (external field equals zero) to $h = 1$ (external field at maximum).

Fig. 5 shows the magnetic field profiles for different $\tilde{\omega}$ for $\beta\tilde{I} < 1$, whereas Fig. 6 shows the profiles for $\beta\tilde{I} > 1$. The different colored lines represent different stages of the external field as it rises from zero to its maximum value. It is immediately clear that the greater the frequency, the greater the effect of the zero-field lines on the flux dynamics and the less linear the profiles become. In Fig. 5 we can see that at low frequencies, let's take for example, $\tilde{\omega} = 0.05$, the magnetic field profiles are mostly straight. Only at $\tilde{\omega}\tau = 0$ (blue curve), as a zero-field line enters the superconductor, the profile becomes slightly curved – particularly near the left boundary of the superconductor where the zero-field line is located. At the location of the zero-field line we see a square root behavior $b(\xi) \propto \sqrt{|\xi - \xi_0|}$ as calculated by Fuzailov[41] and shown above. As the external field grows, the zero-field line leaves the superconductor and the profiles straighten out.

As the frequency grows, the profiles become less and less linear. Let's take, for example, $\tilde{\omega} = 0.6$ in Fig. 5. At the location of the zero-field lines, the slope of the magnetic field, which is

also the current, diverges, $j(\xi) = \frac{\partial b}{\partial \xi} \propto \frac{1}{\sqrt{|\xi - \xi_0|}}$. As discussed before, this leads to a decrease of the current throughout the rest of the superconductor. This in turn leads to a slowdown in the magnetic relaxation processes throughout the superconductor, as shown in [29]. This can be seen in Fig. 5, $\widetilde{\omega} = 0.6$, purple curve, as a steep slope in the magnetic field profiles at the zero-field lines in the center of the superconductor which becomes shallower as we move towards the edges – away from the zero-field lines.

In Fig. 6 we can see that for low frequencies the field profiles coincide with Eq. 18. In this quasistatic regime, as the external field rises, the zero-field line approaches the boundary where the field is decreasing by absolute value. Looking at Fig. 6 $\widetilde{\omega} = 0.1$, for $\widetilde{\omega}\tau = 0$ (blue curve) the field at the right boundary is far from zero and the zero-field line is closer to the left boundary. As the external field rises, the field at the right boundary approaches zero and the zero-field line moves towards the right. When the external field reaches its maximum ($\widetilde{\omega}\tau = \frac{\pi}{2}$, purple curve) the zero-field line is almost at the right boundary.

As the frequency grows, the internal magnetic field profile, and by extension the zero-field line, can no longer keep up with the changing external field and when the external field is at its maximum ($\widetilde{\omega}\tau = \frac{\pi}{2}$) the zero-field line is located close to the center of the superconductor This can be seen, for example, in Fig. 6, $\widetilde{\omega} = 1$, for $\widetilde{\omega}\tau = 0$ (blue curve) the zero-field line is further to the left in comparison to the case of $\widetilde{\omega} = 0.1$ and for $\widetilde{\omega}\tau = \frac{\pi}{2}$ (purple curve), the zero-field line is near the center of the superconductor.

To understand how the aforementioned behavior of the flux dynamics affects the losses, we must observe what it does to the voltage across the superconductor. The voltage is measured along the direction of the transport current flow and its equation is derived from Kirchoff's law, the voltage per unit length is:

$$V(x) = \varepsilon(x) - j(x) \cdot \rho(x) \quad (19)$$

Where $\varepsilon(x)$ is the induced electric field, $j(x)$ is the current density and $\rho(x)$ is the effective resistivity. Using Maxwell's equations, integration, and the boundary conditions as done in [31] and [41], we get the following equation for the voltage at the superconductor boundary, but since the voltage is constant across the superconductor width[40], this is the voltage over a given length of the superconductor:

$$V = \frac{\Phi_0}{8\pi c\eta}\left(|B|\frac{\partial B}{\partial x}\right)_{\frac{d}{2}} + \left(|B|\frac{\partial B}{\partial x}\right)_{-\frac{d}{2}} \quad (20)$$

The dimensionless voltage is [31], [40], [41]:

$$\tilde{V} = \frac{8ct_0}{H_{max}d}V = \left(|b|\frac{\partial b}{\partial \xi}\right)_{\frac{1}{2}} + \left(|b|\frac{\partial b}{\partial \xi}\right)_{-\frac{1}{2}} \quad (21)$$

Using the numerically calculated magnetic fields shown above, the dimensionless voltage waveform can be plotted for different frequencies. This is shown in Fig. 7.

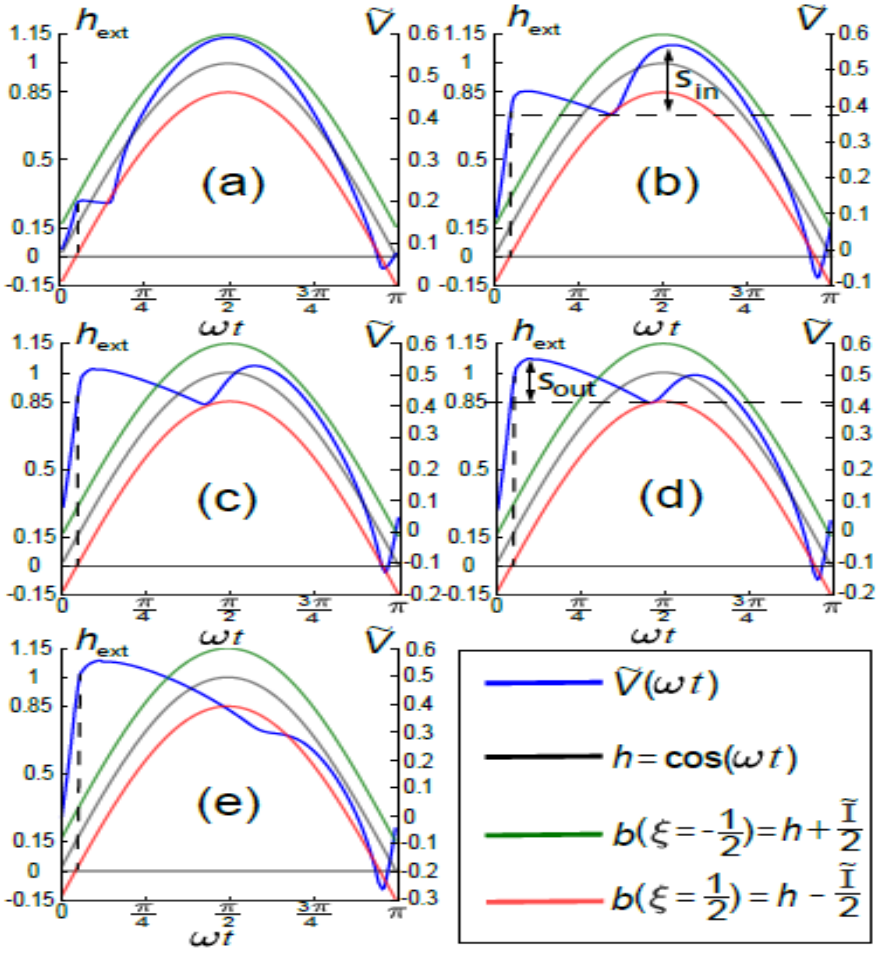

Fig. 7. Dimensionless voltage $\tilde{V}$, along with the external magnetic field h and the magnetic field b at the superconducting slab edges. For $\beta\tilde{I} < 1$ and different values of $\tilde{\omega}$. (a) $\tilde{\omega} = 0.05$ (b) $\tilde{\omega} = 0.25$ (c) $\tilde{\omega} = 0.35$ (d) $\tilde{\omega} = 0.4$ (e) $\tilde{\omega} = 0.6$.

For low frequencies, like in Fig. 7 (a), the voltage waveform (blue) mostly mirrors the external magnetic field (gray). This is to be expected because for low frequencies the

magnetic field profiles are almost straight (see Fig. 5, $\widetilde{\omega} = 0.1$) i.e., $\frac{\partial b}{\partial \xi} \approx const$. This means the voltage behaves like $|b|$. Despite this, we can already see a small "kink" in the voltage waveform due to the non-linearity of the magnetic field profile when the zero-field line enters the superconductor. As the frequency grows, the magnetic field profile becomes highly non-linear (see, for example, Fig. 5, $\widetilde{\omega} = 1$). Now $\frac{\partial b}{\partial \xi} \neq const$ and the kink in the voltage waveform becomes a peak that is out-of-phase with the external magnetic field, now there are two peaks in the voltage waveform, one in-phase with the external magnetic field and one out-of-phase with it (see Fig. 7 (b) (c) and (d)). Henceforth we shall refer to them as the "in-phase-peak" and the "out-of-phase-peak", respectively. And as the magnetic field inside the superconductor moves further out of phase with the external magnetic field, the out-of-phase peak in the voltage waveform grows and eventually overwhelms the original "in-phase peak" (see Fig. 7 (e)). To further understand the appearance of the out-of-phase peak and its location we must observe that, as can be seen in Eq. 21 and in [14], the voltage depends on the amount of fluxons that enter and exit through the superconductor's boundaries at $\xi = \pm\frac{1}{2}$. As a zero-field line enters the superconductor and is located at one of its boundaries, it greatly slows down the flux dynamics and effectively blocks the entry of fluxons from that boundary[29], [31]. This means that as the zero-field line enters from one of the boundaries, we get either $b_{\xi=\frac{1}{2}} = 0$ or $b_{\xi=-\frac{1}{2}} = 0$. This means one of the terms on the right side of equation 21 is suppressed. It is important to note that while the magnetic field is zero, the magnetic field gradient diverges at the zero-field line so that the term does not get canceled out entirely, only greatly suppressed. In the quasistatic regime, where, as we mentioned before, the magnetic field profile is linear and both terms in the voltage follow the external field, the suppression of one of the terms in Eq. 21 has little effect on the shape of the voltage waveform (see Fig. 7 (a)). But for higher frequencies, where the flux dynamics are non-linear and the two terms not only don't follow the external field but can have different signs such that both terms are large by absolute value but their opposite signs limit the size of the overall voltage. In such cases suppression of one of the terms leads to a sharp increase in voltage and the appearance of the out-of-phase peak (see Fig. 7 (b) (c) and (d)). Furthermore, as the frequency grows, the field within the superconductor becomes more and more desynchronized from the external field, to a point where while the external field reaches its maximal value, the internal field is still negative (see Fig. 5, $\widetilde{\omega} = 1$, purple line). Thus, the in-phase voltage peak diminishes and eventually disappears (see Fig. 7 (e)).

As was shown in Fig. 6, for $\beta\tilde{I} > 1$ the zero-field line is always inside the superconductor and never reaches its boundaries. This means that the zero-field line never completely suppresses the fluxon motion at any of the boundaries. The closer it gets to any of the boundaries, the greater the suppression which will give rise to an out-of-phase peak. Because of the less pronounced suppression of the fluxons at the boundaries for high currents ($\beta\tilde{I} > 1$), the out-of-phase peak is expected to appear at higher frequencies compared to lower currents $\beta\tilde{I} < 1$.

We define the heights of the in-phase and out-of-phase peaks to be S_{in} and S_{out}, respectively, as can be seen in Fig. 7. Fig. 8 shows a phase diagram of $\tilde{\omega}$ and $\tilde{I}$, where any combination of $\tilde{\omega}$ and $\tilde{I}$ below the red line will result in an in-phase peak only, any combination of $\tilde{\omega}$ and $\tilde{I}$ above the blue line will result in an out-of-phase peak only, and any combination of $\tilde{\omega}$ and $\tilde{I}$ confined between the red and blue lines will result in a double peak. The distance from the blue and red lines indicates which peak is more dominant, with the black line representing where $S_{in} = S_{out}$.

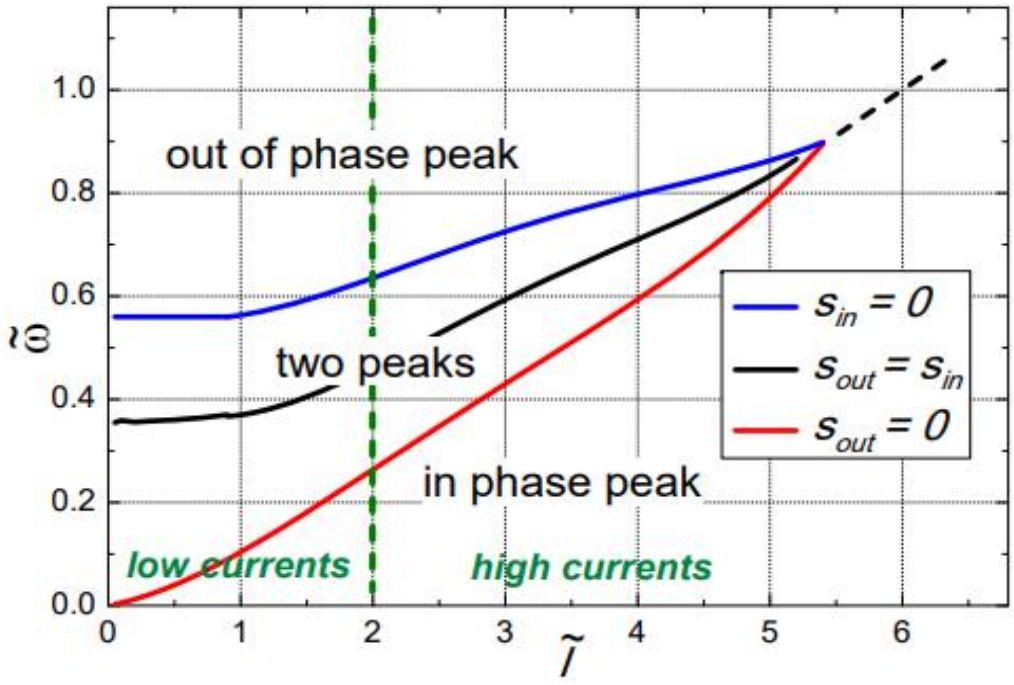

Fig. 8. Phase diagram of the appearance of in-phase and out-of-phase peaks for different values of $\tilde{\omega}$ and $\tilde{I}$. The diagram consists of three phases: only in-phase peak (below the red line), only out-of-phase peak (above the blue line) and double peak (between the red and blue lines).

3. Experiment

3.1. Experimental setup

In this work, we are focusing on the induced voltage in type II superconductors exposed to either constant or alternating magnetic fields while carrying a DC transport current. We are using commercial tapes of Bi-Sr-Ca-Cu-O (BSCCO 2223) superconductors manufactured by American Superconductors. BSCCO is a type-II high temperature superconductor which is made up of many superconducting filaments within a silver matrix. As illustrated in Fig. 9, The tapes are placed between two racetrack coils through which flows either a DC or AC current, thus creating a DC or AC magnetic field, respectively. The tapes are soldered at the edges to two large cables which are connected to a DC current source. The voltage on the tape is measured through two voltage taps on the tape, which are spaced 2 cm apart. The whole setup is submerged in liquid nitrogen to keep it at 77K, below the critical temperature.

The DC transport current was driven by an Agilent 6681, 8V, 580A power supply. For DC field measurements the field was generated by driving a DC current through the coils using a Lipman 30V, 12A power supply, and the voltage across the taps was measured using a Keithley 182 sensitive voltmeter. For AC field measurements, the field was generated by driving an AC current using a HP 8904A waveform synthesizer which feeds a Berlinger audio amplifier. The voltage waveform induced on the superconducting tapes was measured using a Picoscope oscilloscope.

Due to the presence of an AC magnetic field all wires in the vicinity of the system, namely the voltage taps, will have voltage induced on them. If left untreated, this induced voltage can obscure the voltage on the superconductor. To minimize said pickup and allow for good observation and study of the voltage and losses in the superconductor itself, proper orientation of the voltage taps is required. The most obvious solution is to arrange the taps parallel to the field, so as to prevent the existence of a current loop, and have the two taps be a twisted pair for as much of their length as possible, so as to prevent the existence of a pickup loop. While this is good in theory, in practice it was difficult to execute. At some point the taps must diverge from the twisted pair to connect to the superconducting tape with some distance between the taps. At this point, the voltage taps must be arranged so that they run perfectly straight along the tape center until they meet into a twisted pair. Any deviation from the straight line, whether during the manufacturing process or while submerged in the

nitrogen, would create a loop which would induce voltage on the taps. Due to the very small margin of error, this technique proved unfeasible. We used a different technique, first introduced by Rabbers *et. al.*[42]. After the voltage taps diverge, instead of keeping them straight we arranged them in a figure eight formation. In this setup, we intentionally create two loops in our voltage taps where each loop has an opposite induced voltage on it. Now, by making both loops identical in size, the induced voltages cancel each other out and we are left only with the voltage on the superconductor. To ensure the loops are identical in size we manufactured a plate with channels that hold the voltage taps in the right formation from the point where they are welded until the point they converge. This method has proven to be far easier to implement and more robust when submerged in nitrogen and has allowed has to almost completely remove the induced pickup voltage. A schematic drawing of the figure eight setup is presented in Fig. 10. To further reduce the pickup, we used a coaxial shielded twisted pair rather than just a twisted pair.

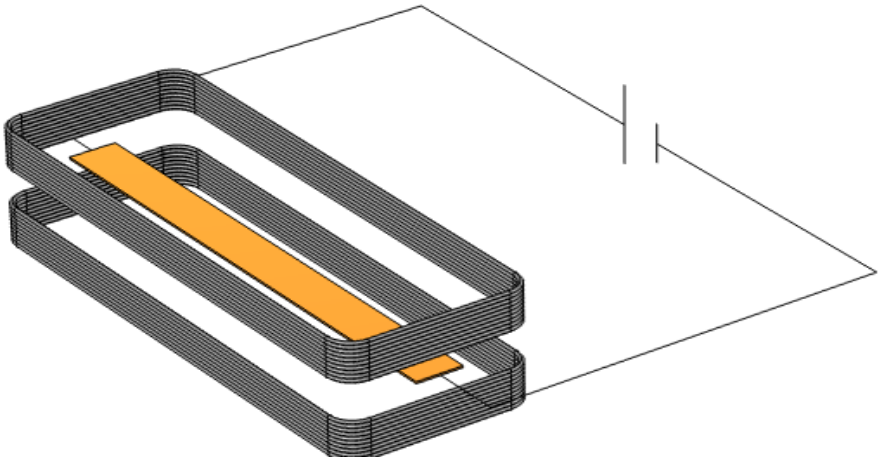

Fig 9. Experimental system setup.

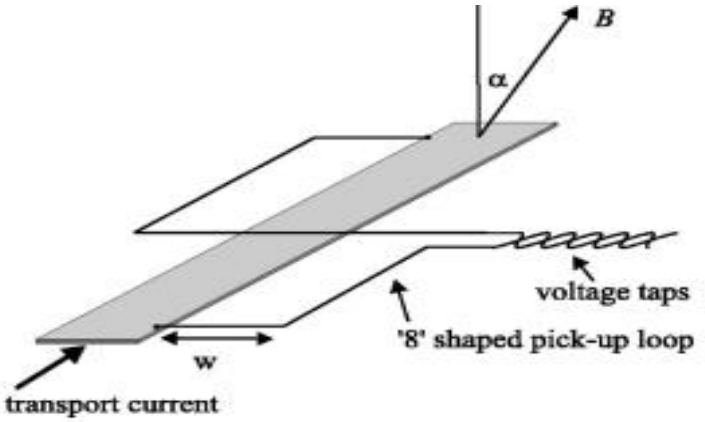

Fig. 10. Schematic drawing of the figure eight setup used in our experiment (from Rabbers *et. al.*[42]*)*.

4. Results

4.1. E-I curves in the DC regime

We conducted volt-ampere measurements of the BSCCO tape in the presence of different external DC magnetic fields and obtained E-I curves for the tape (V is converted to E via the relation $V = El$, where l is the distance between the voltage taps). As we approach the critical current I_c, the field begins to grow and assumes the power law forms shown in Eq. 11 and 14. To better observe the exponent in the $E(I)$ power law relation, and to more easily compare between the exponents of different curves, the curves are drawn in a log-log scale. Thus, we get a linear dependence between the field E and the current I, where the gradient of the linear curve of the log-log plot is equivalent to the exponent in the regular $E(I)$ power law relation. Our equations for the $E(I)$ relation turn from the power law form:

$$E(I) \sim I^{u+1}, \qquad H > \beta I \qquad (22)$$

$$E(I) \sim I^{u+2}, \qquad H < \beta I \qquad (23)$$

To the linear form:

$$\log(E(I)) \sim (u+1)\log(I), \qquad H > \beta I \qquad (24)$$

$$\log(E(I)) \sim (u+2)\log(I), \qquad H < \beta I \qquad (25)$$

In this form, it is much simpler to see the different gradients of the different curves, and these different gradients clearly correspond to the different exponents in the $E(I)$ power law relation.

Our model predicts that the presence of a zero-field line will change the exponent in the $E(I)$ relation. We expect the gradients of the curves in the log-log plot to be greater when a zero-field line is present in the superconductor, as opposed to when it is absent. The measured $E(I)$ curves in the log-log scale are shown in Fig. 11:

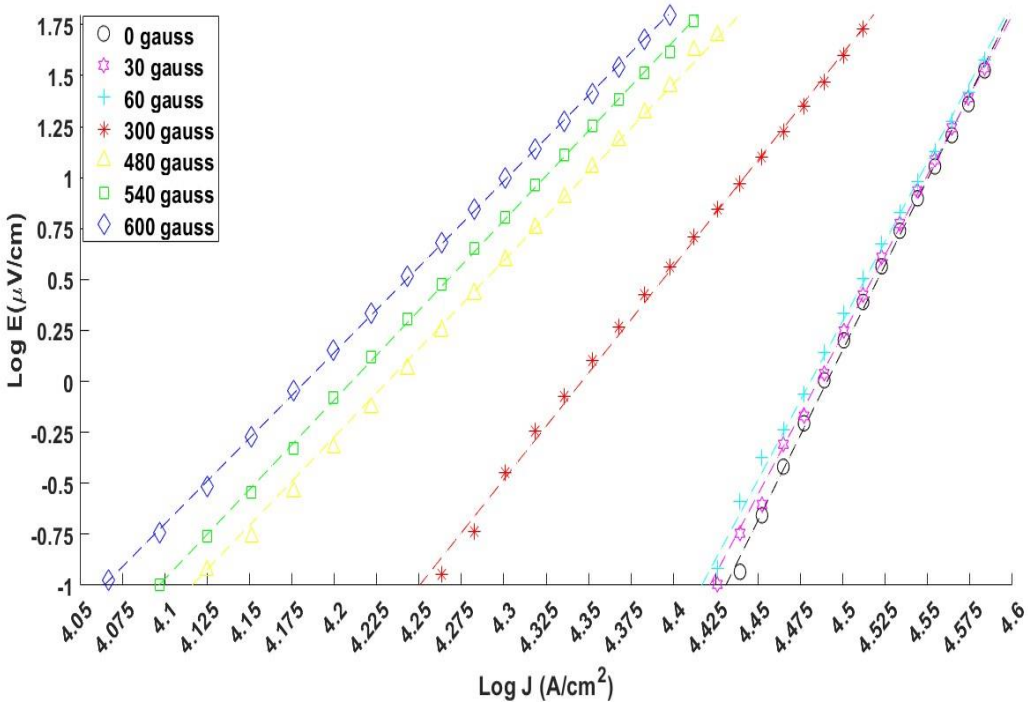

Fig. 11. $E(I)$ curves of BSCCO HTS tape in the log-log scale for various external DC magnetic fields. Dashed lines are linear fits in the log-log scale

As shown in the theory chapter, the presence of the zero-field line within the superconductor is determined by both the self-field βI and the external field H. As we measure the $E - I$ relation, the external magnetic field H remains constant. On the other hand, the transport current I, and by extension the self-field, is gradually increased. Thus, there are multiple different behaviors of the logarithmic E-I curves. For no external field, or if the magnetic fields are smaller than the self-field ($H < \beta I$) throughout the entire $E - I$ measurement, the zero-field line is always present and the gradient is steep, this behavior can be seen in the three rightmost curves in Fig. 11, where the exponent's value is approximately 16. If the magnetic fields are higher than the self-field ($H > \beta I$) throughout the entire $E - I$ measurement, the zero-field line is always absent. Thus, we expect to see a smaller exponent. This behavior can be seen in the three leftmost curves in Fig. 11, where the gradient is approximately 8. These measurements qualitatively agree with the theory which suggests that the presence of a zero-field line changes the $E(I)$ relation within the superconducting tape. As was mentioned before, for the infinite slab geometry $\beta = \frac{2\pi}{cw}$. For a slab width $w = 0.4cm$ this gives us $\beta \approx 20 \frac{Gauss}{ampere}$. However, taking into account that the actual tape is flat

with a thickness to width ratio of $\frac{h}{w} \approx 13$, the prediction for β should be smaller. The value of β for the finite tape geometry was found by Zeldov *et. al.*[43] to be $\beta = \frac{2 \cdot \sqrt{2}}{c \cdot \sqrt{h \cdot w}}$ and for our tape's dimensions this gives $\beta = 2.58\ Gauss$.

The results are in qualitative agreement with the theory, in that the slopes of the E-I curves in the log-log plot are greater in the presence of a zero-field line within the tape. However, quantitively, the theory and experiment are somewhat apart. The slopes of the curves where the zero-field line is present are approximately 8 whereas for the curves where the zero-field line is absent the slope is approximately 16. The zero-field line changes the slopes by approximately 8. This is significantly greater than the theoretical prediction, which expects a difference of 1 between the slopes. There are several possible factors that may contribute to this discrepancy. Firstly, the theoretical model considers an infinite slab geometry, while in reality the geometry is that of a finite tape. Secondly, the theoretical assumption of $u \gg 1$, which the theoretical model assumed in order to obtain Eq. 11 and 14 may be exaggerated. The theory observes that Eq. 11 and 14 give good approximations of $E(I)$ for values as low as $u > 4$. But for the experimental conditions, with operating temperatures of 77K and currents that approach and even exceed I_c, the measured BSCCO HTS tape may be deep in the flux flow regime and therefore it could very well be that that $u < 4$ in the experiment. The model will need to be refined and adjusted to account for the much smaller pinning energies.

Both of these factors affect the value of β. While we have already adjusted the predicted value of β to account for the tape geometry and decreased it by roughly an order of magnitude from ~20 to ~2.5, this adjustment may still be insufficient. This is due to the fact that we did not take into account how the geometry affects the homogeneity and direction of the magnetic self-field at the edge of the superconductor. The infinite slab geometry assumed by the theory dictates that the self-field created by the transport current at the slab edges is constant throughout, as well as always being parallel to the slab. For a finite tape geometry, the self-field will eventually curve around the ends of the tape. This means that the self-field at the edge of the tape is not uniform. It is also not parallel to the edge of the tape for the entirety of the tape height. For a tape as thin as ours, it might not even be parallel to the tape edge at the half height of the tape. Considering the differences between the theoretical assumptions and the experimental conditions, and to determine how much these affect the value of β, we conducted numerical simulations of the magnetic self-field around a finite,

current carrying, superconducting tape with the dimensions of the experimental tape using COMSOL Multiphysics. The results are presented in Fig. 12:

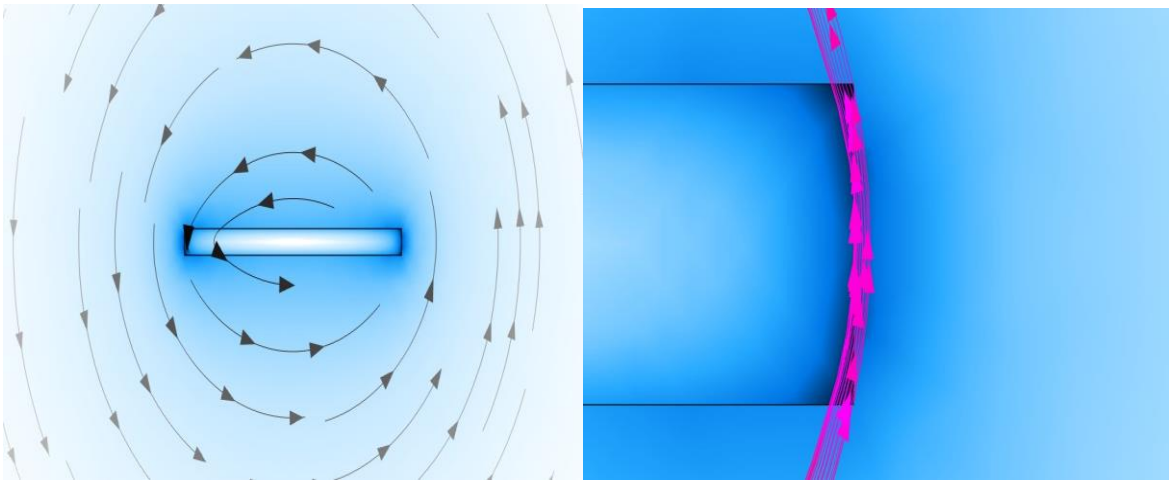

Fig. 12. Numerical simulation of the magnetic self-field of a current carrying, finite HTS tape. Left: Around the entire tape cross section. Right: Along the edge of the tape.

The numerical simulations in Fig. 12 clearly show that for a finite tape geometry the magnetic self-field at the tape edge is not uniform and this will clearly affect the predicted value of β. The field lines cut through the edge of the tape such that even at half of the tape height they are slightly curved. By taking the calculated magnetic field near the tape edge at half the tape height and dividing by the transport current, we get $\beta \approx 1.6$. This is smaller than the theoretical prediction by almost 1. Considering that β is found both in the magnetic field profile equations (Eq. 6 and 12) and by extension in the electric field equations (Eq. 10 and 13), the smaller value of β will affect the exponent in the $E(I)$ power law relation. For β of around 2, we expect that for transport currents of around 150A we will see the zero-field line enter the tape for an external magnetic field of approximately 300 Gauss (the zero-field line enters the tape when $H = \beta I$). Looking again at Fig. 11, we can see that for an external field of 300 Gauss (red center curve in Fig. 11), we get a curve with an intermediate exponent of ~10. This is the transition point between the high exponents due to the presence of the zero-field line and the low exponents where there is no zero-field line. The external field for this field transitional line is in agreement with the value of β which was calculated in the numerical simulations.

The dependence of the exponent n on various factors has been studied in the past. It has been shown that n is affected by various factors such as the temperature of the superconductor, its homogeneity and its structure, in particular the filament diameter in multifilamentary superconductors, the presence of impurities and even the method of manufacture of the superconductor[44]. Studies have also shown that for larger external magnetic field amplitudes the exponent n grows smaller. The explanation given for the decrease of n with the growing magnetic field is that n is dependent on the critical current j_c, which itself decreases as the external field grows[45], [46]. In these experiments, the value on n was measured in the same way as was done in this work - by measuring the $E-J$ curves of the superconductor under different external fields, moving to the log-log scale, and comparing the slopes of the curves. We present here a new interpretation for the change of n due to the change in the external field, where the entry of a zero-field line and the subsequent change in flux dynamics lead to a change in n. It is important to emphasize that to observe the effects of the zero-field line one needs to be able to compare between $E-J$ curves where zero-field lines are always present and ones where they are always absent. This means choosing magnetic field amplitudes and driving transport currents which ensure cases where $H > \beta I$ or $H < \beta I$ inside the superconductor all the time. Previous studies on changing n were done in higher fields (several Teslas as opposed to several hundred Gauss in this work [45], [46]) and lower temperatures (4.2K-30K as opposed to 77K in this work [45], [46]), it is possible that in these conditions the interplay between the external field and the self-field are such that the zero-field line was either present or absent in all the measurements and throughout the entirety of the measurements. In such cases, the changes in values of n would not be due to the zero-field lines and since the zero-field line either never enters or never leaves the superconductor, the value of n cannot be associated to its affect. Moreover, for the lower temperatures measured in previous works, the pinning would be very strong and the flux dynamics are in the flux creep and not the flux flow regime. The flux diffusion equation no longer describes the flux dynamics and the effect of zero-field lines would not conform to the theory. The zero-field line is probably just one factor that affects the value of n, along with those mentioned above.

To summarize this chapter, in the DC regime, the zero-field changes the flux dynamics. This results in a change in the exponent of the $E(I)$ relation of the superconductor. It is thus important to consider whether a zero-field line is present inside a superconductor when designing superconducting applications.

4.2. Voltage waveform measurements in the AC regime

4.2.1. Broken symmetry

We begin this chapter, which describes the results for the AC regime, with unexpected and surprising results. As was mentioned in the introduction (see Fig. 1 and its corresponding text), that for a combination of an external AC magnetic field and DC transport current, one normally expects to see a double frequency, symmetric response in the AC voltage signal. That is, we expect two peaks in the voltage for each cycle of the external magnetic field, and both peaks should be of equal height. The reason that the frequency of the voltage is double that of the magnetic field has to do with the dependence of the electric field (and by extension, the voltage) on both the direction of the magnetic field and the direction of the motion of the fluxons. We know that $\vec{E} = \vec{B} \times \vec{v}$, where for the case of a magnetic field perpendicular to the tape and flux motion only along the width of the tape this can be simplified to $E = B \cdot v$. Hence, the voltage induced in the superconductor depends on the net motion of fluxons from one side of the superconductor to the other (fluxons which enter and leave from the same side of the superconductor do not contribute to the field, the voltage they contribute going in is canceled by the opposite voltage they contribute going out). If we take, for example, a sinusoidal external magnetic field, during the positive half of the field cycle fluxons of positive polarity (positive B) move across the superconductor in one direction (we shall choose this direction to be the positive direction – hence positive v). For the negative part of the field cycle, fluxons of negative polarity (negative B) move across the superconductor in the opposite direction (negative v). For both parts of the field cycle B and v have the same sign, thus the induced voltage throughout the entire field cycle is always positive and we shall observe two voltage peaks per field cycle. Both voltage peaks in the field cycle are symmetrical and of identical height and shape. This is because the positive and negative parts of the external field are symmetrical, hence the number and velocity of fluxons of positive polarity is identical to the number and velocity of fluxons of negative polarity. The only difference is the direction of motion which ensures the voltage is always the same sign.

This double frequency of the induced voltage was observed and explained by Adrianov[10], Ogasawara[11]–[13], Brandt and Mikitik[14], and Oomen[15]. The models presented in these works assumes strong pinning of the vortices. In such scenario, the gradient $\frac{\partial B}{\partial x}$ within the sample is quite constant hence E reaches its maximum value when B is maximal hence, the peaks in the waveforms of E are in-phase with the magnetic field. This was also observed

experimentally by Lukovsky[30], whose voltage waveform measurement is presented in Fig. 13 below. The figure clearly demonstrates the double frequency effect. For each frequency of the applied field presented in the figure, we see peak marked as “in-phase peak” which appears twice during a field cycle. However, Lukovsky has demonstrated a second peak (per half-cycle) which emerges as a small bump in the major peak and increases with increasing frequency to become dominant. This peak was named “out-of-phase peak” in these experiments and it was suggested there, without theoretical support, that the annihilation of vortices and anti-vortices may play a role here.

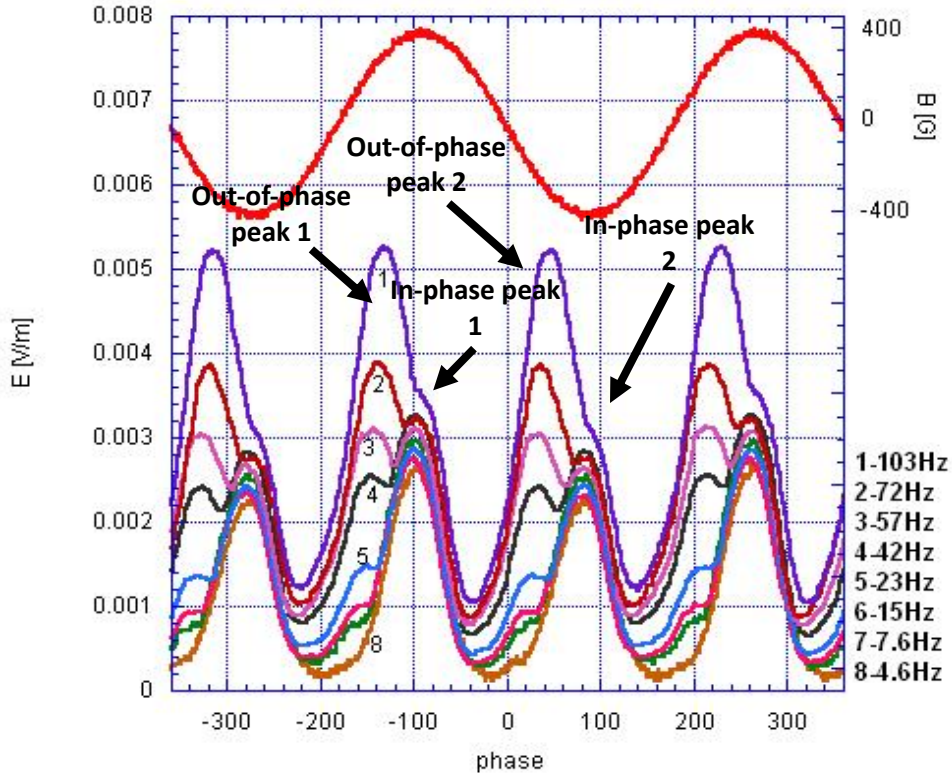

Fig. 13. Voltage waveforms on a HTS tape carrying a DC transport current and exposed to an external AC field (from Lukovsky *et. al.*[30]). The double frequency of the voltage relative to the field is clearly visible.

Notice that in Lukovsky’s measurements we can see the coexistence of the out-of-phase and the in-phase peaks in each half cycle of the field (black arrows in Fig. 13). It is important to emphasize that the double peak which results from the zero-field line is not the double frequency of the voltage waveform in comparison to the field. The transition between in-

phase and out-of-phase peaks happens for every half cycle such that when the two peaks coexist, we see four peaks per external field cycle.

Surprisingly, when we measured the AC voltage waveforms, the picture was very different. The voltage peaks where asymmetrical, having different heights and different shapes. In some cases, the voltage waveform had the same frequency as the external magnetic field. One of these waveforms we measured, where both peaks are out of phase with the external field and asymmetrical to one another is presented below in Fig. 14:

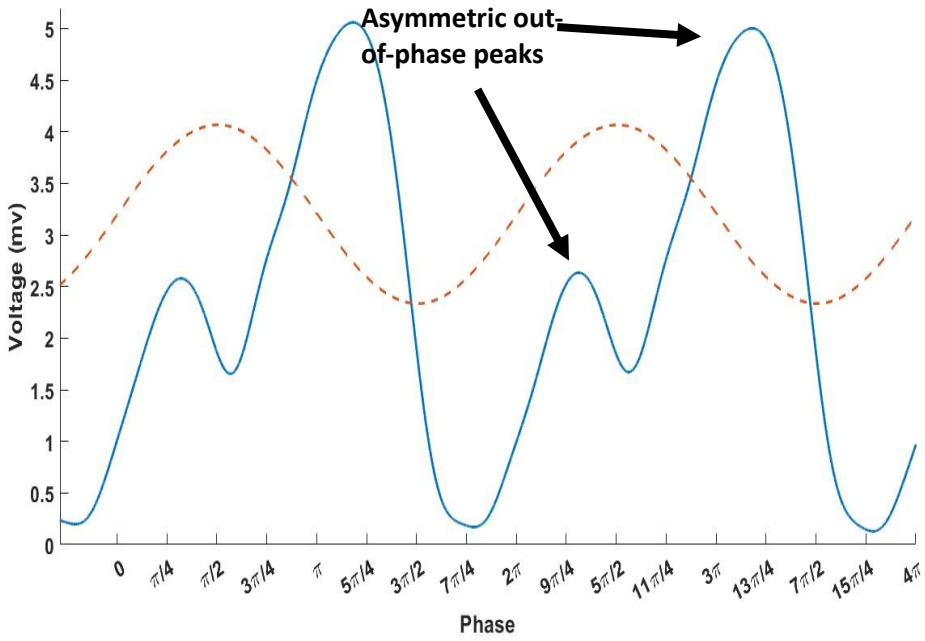

Fig. 14. Voltage waveform on a HTS tape carrying a DC transport current and exposed to an external AC field. The asymmetry between the peaks in every half cycle is clearly visible.

The asymmetry in Fig. 14 is quite evident, for each cycle of the external magnetic field (dashed line in Fig. 14) we have two peaks which are out-of-phase with the field. The right peak in each field cycle is considerably larger than the left peak – about twice as large.

This asymmetry remained after ensuring that no experimental factors, such as voltage pickup in the measurement setup or DC components in the external magnetic field, where at play. Initially, this behavior does not make sense as it implies that the tape behaves differently for the case where the perpendicular magnetic field is pointing up and for the case where it is pointing down. The only possible explanation is that the tape itself is asymmetrical, and that the motion of fluxons in one direction is different than the motion of fluxons in the opposite direction despite identical external factors. Such an asymmetry can be due to uneven

distribution of the superconducting filaments in the BSCCO tape – which could be the result of improper manufacture of the tape or degradation of some of the superconducting filaments over time. Or, it can be the result of different surface barriers on each side of the tape. Interestingly, asymmetry in the behavior of BSCCO tapes has been observed in the past by Chesneau *et. al.*[47]. They measured the magnetic field profiles within BSCCO tapes carrying different transport currents and exposed to an external magnetic field. In their results they found that the field profiles measured for the same current but in different directions was asymmetrical (Fig. 15). This is also unexpected, just as the behavior of the superconducting tape should not change just because the external magnetic field is in the opposite direction, neither should it behave differently because the current is reversed. Chesneau *et. al.* attributed this asymmetry to relaxation effects, namely different times between the application of the current and the measurement of the field. Because the current in one direction was applied longer than the current in the opposite direction, this means that the flux that penetrated the tape when the current was in the positive direction did not have enough time to fully exit when the current was reversed. While this might be the reason for the asymmetry they observed, asymmetry of the tape itself could also cause this behavior. In any case, uneven application times of the current or field in one direction cannot explain the asymmetry we observe. The applied external field is sinusoidal and completely symmetric in terms of time.

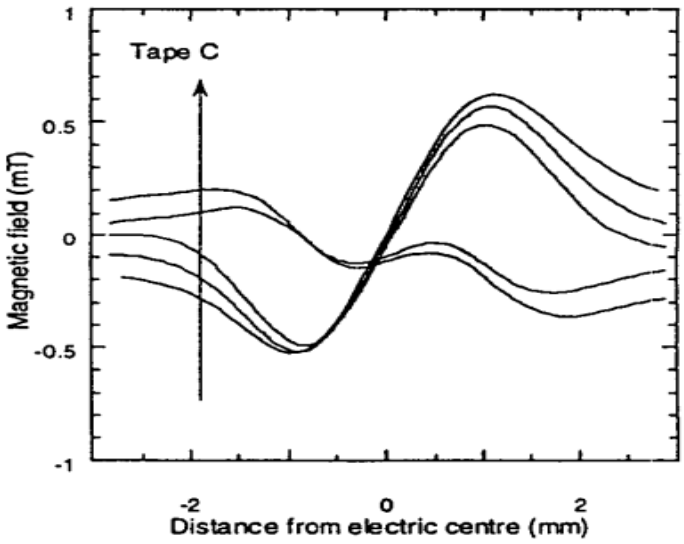

Fig. 15. Magnetic field profiles inside a BSCCO tape for different current directions, the profiles are different for the same current in opposite directions (from Chesneau *et. al.*[47]).

To verify whether the tape is indeed asymmetric, we measured the I-V curve of the tape under different external DC magnetic fields perpendicular to the flat side of the tape. For each

magnetic field we measured the I-V curve twice, once for the field pointed up, and once for the field pointed down. If the superconductor is symmetric, the curves for each magnetic field amplitude should overlap. The results are presented in Fig. 16 below:

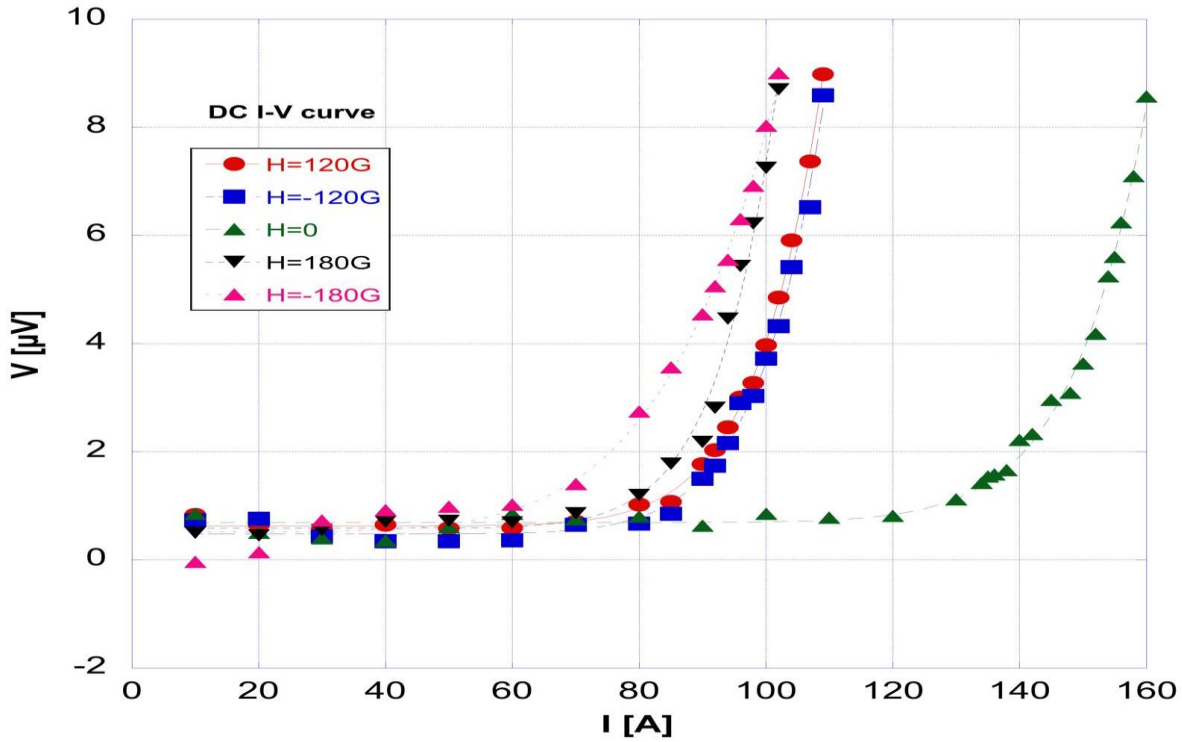

Fig. 16. I-V curves of the HTS tape exposed to DC magnetic fields of different amplitudes and directions.

In Fig. 16, it is clearly visible that the tape is asymmetric. The curves for magnetic fields of identical magnitudes but different polarities are offset from each other, with one curve rising in voltage earlier than the other. This disparity between curves was observed in multiple I-V measurements conducted for each field. It is also interesting to notice that for greater magnetic field amplitudes the difference between the curves of different field directions is greater (compare curves of 180 Gauss to curves of 120 Gauss).

To better understand how this asymmetry should affect the voltage waveform results, we worked in collaboration with Nikita Fuzailov and Leonid Burlachkov from the Physics department at Bar Ilan University. They have adjusted the theoretical model to account for an asymmetrical superconductor. They did this by artificially applying different barriers on each of the tape boundaries and defined an adjustable variable that determines what is the height of the barrier on the left boundary as a fraction of the barrier on the right boundary. Based on this adjusted model, they run numerical simulations of the magnetic field profiles and voltage waveforms expected for different dimensionless currents and frequencies and for different

asymmetries. The numerical simulations, along with experimental waveforms, are presented below:

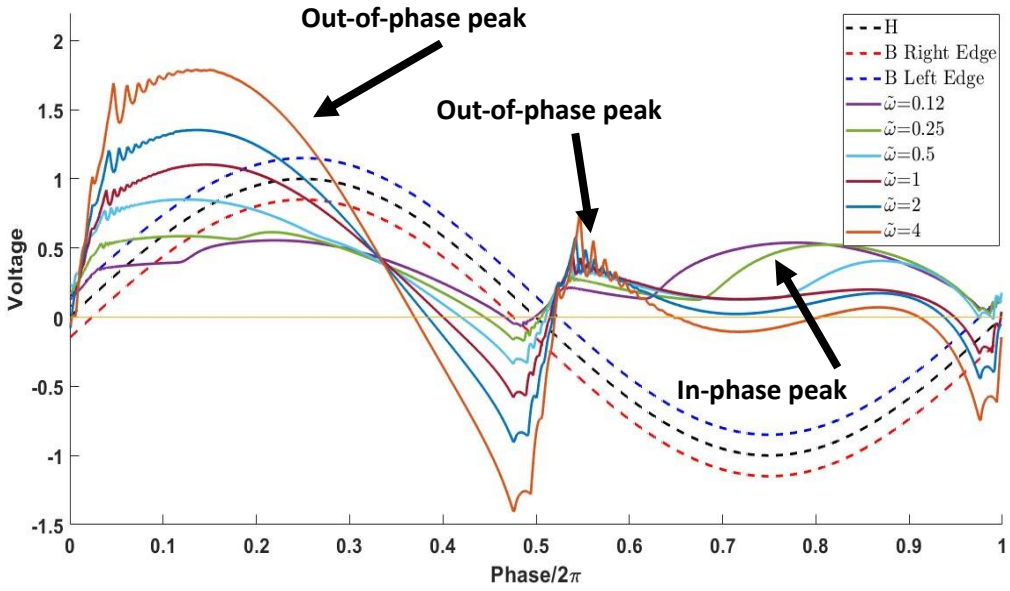

Fig. 17. Numerical simulation of voltage waveforms on a current carrying HTS tape exposed to external fields of different frequencies. The surface barrier on the right boundary is 80% of the height of the surface barrier on the left boundary.

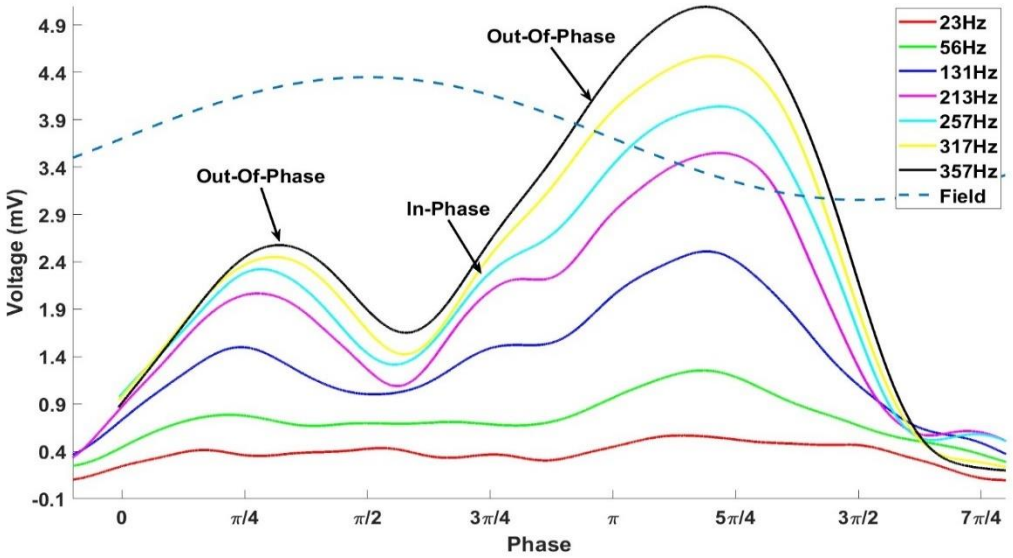

Fig. 18. Experimental voltage waveforms on a current carrying HTS tape exposed to external fields of different frequencies.

Before describing the predictions and results for asymmetric tapes, let us start with a description of what would be seen for a symmetric tape. Looking again at Lukovsky's results

in Fig. 13, we can see that at low frequencies the voltage starts with two peaks percycle (Fig. 13, bottom curve), both peaks are in-phase with the magnetic field – hence we start in the in-phase regime. We can see that the two peaks in each external field cycle are of identical height and shape, as is expected for a symmetric tape. As the frequency grows, the double peak regime is reached and an out-of-phase peak grows in every half cycle of the field. We now have four peaks per half cycle of the external field – two in-phase ones and two out-of-phase ones. The out-of-phase peaks which grow with the frequency are identical to each other in shape and height, thus symmetry of the waveform always remains. For high enough frequencies, the out-of-phase peaks become dominant (Fig. 13, upper curves), and eventually the in-phase peaks will disappear. The out-of-phase regime will be reached and again we will have two peaks per external field cycle.

Now, we can describe how the asymmetry changes the voltage waveform in the tape. In their modified model, Fuzailov and Burlachkov assumed that the source of the asymmetry was unequal barriers on the tape boundaries. Let us recall that the voltage on the tape is created by the net crossing of fluxons across the tape boundaries. The voltage is thus dictated by the magnetic field and its gradient at the tape boundaries (see Eq. 20). For low frequencies, where the magnetic field profiles are close to linear, the contribution of each boundary to the voltage is the same whether the magnetic field is positive or negative. If the surface barriers on the tape are unequal, then this will change the voltage contribution of each boundary somewhat, but because the contribution is the same regardless of the field's sign, it will be the same change in both halves of the magnetic field cycle. Hence, the effects of the asymmetry on the voltage waveform at low frequencies, and in particular on the in-phase peak which is a product of the linear field profiles, are predicted to be small. On the other hand, as the frequency grows, the magnetic field profiles become very non-linear. Not only does each boundary contribute differently to the voltage, the contributions can be of opposite signs. And so, when one boundary contributes positively and the other negatively, they balance each other out. That is until a zero-field line enters the tape through one of the boundaries. We have shown that when this happens, the zero-field greatly inhibits the flux motion at the boundary and suppresses its contribution to the voltage. If the zero-field line enters through the boundary that contributes negatively to the voltage, it suppresses it – leaving the positive unchecked and creating the out-of-phase peak. When the external magnetic field changes sign every half field cycle, the voltage contributions of the boundaries also change sign. If one boundary contributes positively when the external field is positive, it will contribute

negatively when it is negative and vice versa for the other boundary. If the tape is symmetric, for one half cycle a zero-field line will enter from the left boundary, suppressing that boundary, leaving the only the positive contribution of the right boundary and creating the out-of-phase peak. The shape of the field profile when the zero-field line enters from the left is presented below:

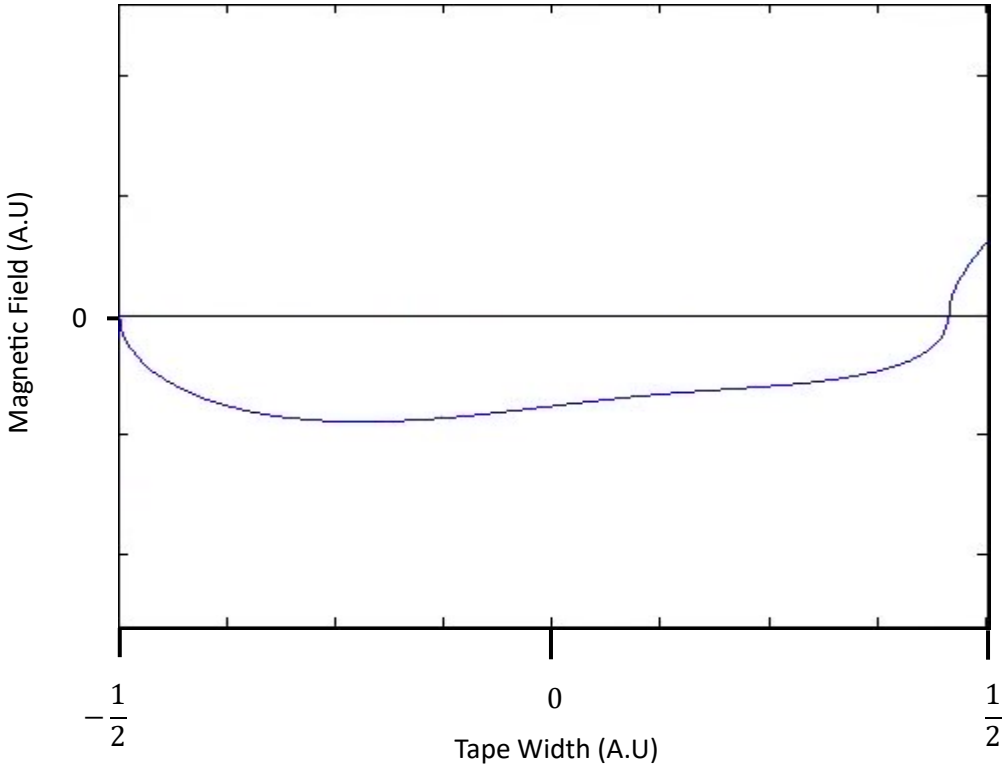

Fig. 19. Magnetic field profile inside the tape when the zero-field line is at the left boundary of the tape.

On the other half of the field cycle a zero-field line will enter from the right boundary and suppress it. But, because the gradients of the magnetic field profile at the boundaries changed signs, the signs of the voltage contributions also flip. This will again leave only the positive voltage contribution and lead to the creation of the out-of-phase peak. The shape of the field profile when the zero-field line enters from the right is presented below:

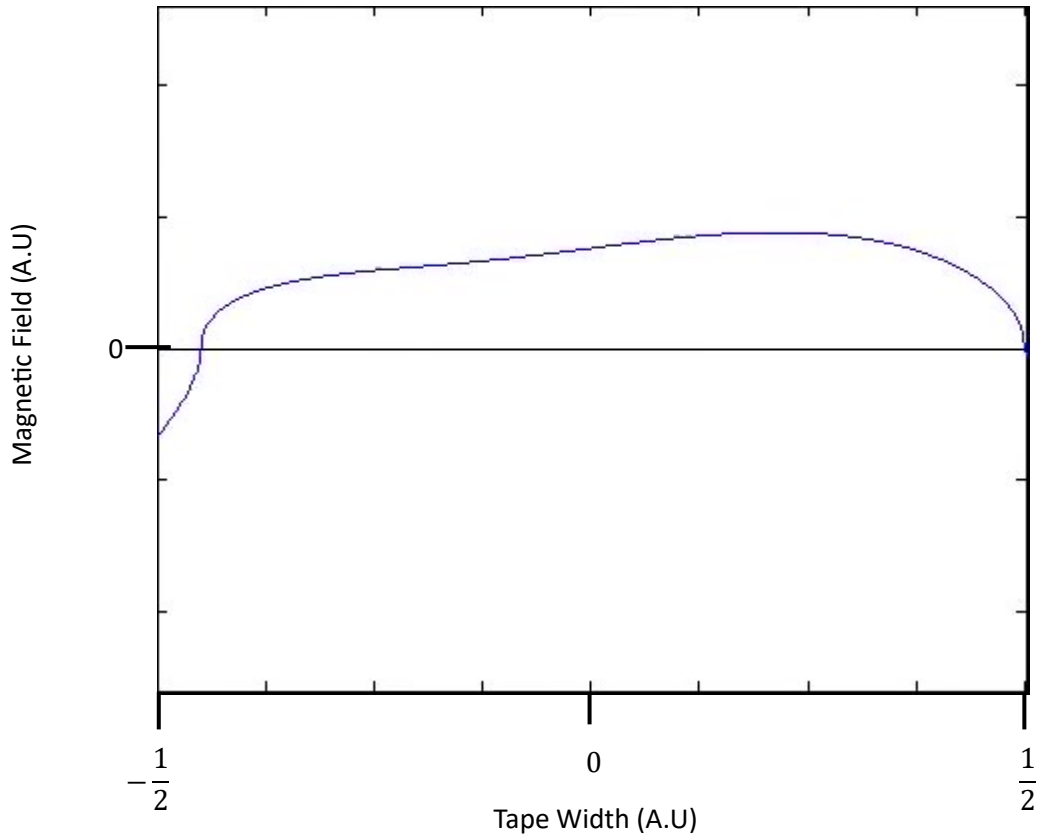

Fig. 20. Magnetic field profile inside the tape when the zero-field line is at the right boundary of the tape.

Thus, the voltage waveform of each half cycle will be identical to the other. If the tape is asymmetric, the picture changes. Now, each boundary contributes differently, the one with the larger surface barrier has less flux crossing it in comparison to the other. This means that on the field half cycle where the boundary with the weaker barrier contributes positively, its contribution is larger and thus when the zero-field line enters, we will get a large peak. On the next field half cycle, the boundary with the stronger barrier contributes positively, now when the zero-field line enters from the other side, the resulting out-of-phase peak will be smaller than the previous one. Hence, for higher frequencies, we expect that the asymmetry of the tape will strongly affect the voltage waveform. It will cause the out-of-phase peak in one half cycle of the field to be larger than that in the other. The higher the frequency, the less linear the field profiles, and the greater the difference between the out-of-phase peaks is expected to be. With these predictions in hand, we can now look at the results and see if they agree with our theory.

In Fig. 17 above, we presented a simulation of an asymmetric tape carrying a constant current and exposed to different field frequencies. Before addressing the voltage waveforms, we shall look at the waveforms of the external magnetic field. In Fig. 17 there are three dashed lines, they are all identical waveforms, but are offset from one another in the y axis by some constant. The middle of the three (black dashed line) is the external field to which the tape is exposed. The blue and red dashed lines are the magnetic fields at the left and right tape edges, respectively. The reason for the offset at the tape edges is the self-field created by the transport current in the tape. The self-field will contribute a constant and positive magnetic field at one edge of the tape and an identical but negative magnetic field at the other edge. Because of this, the fields at the tape edges are offset from the applied field, the size of the offset depends on the transport current in the tape. It is important then to note that the zero-field line does not enter the tape when the black dashed line is zero, but rather when the blue or red dashed lines are zero. Moving to the voltage waveforms, for low frequencies, the voltage waveform is almost completely symmetrical, with one peak only slightly higher than the other. Fig. 17, starts in the double peak regime and so we initially see four peaks per cycle. As the frequency grows, one of the out-of-phase peaks is suppressed, and grows less than the other out-of-phase peak, creating a height disparity between the two (compare the height difference between the out-of-phase peaks at $\widetilde{\omega} = 0.12$ with the height difference at $\widetilde{\omega} = 4$). We can see that the higher the frequency, the greater the height disparity that is expected between the peaks i.e., the stronger the suppression. Moreover, looking at the in-phase peaks, we can see that they shrink with rising frequency, as expected. But they remain almost identical in height throughout. This implies that the suppression of the out-of-phase peak is more powerful than that of the corresponding in-phase peak. We can see that at a certain frequency, the larger of the two out-of-phase peaks is large enough as to completely overwhelm it corresponding in-phase peak. But at the same time, the other out-of-phase peak is so suppressed that its in-phase peak is still visible. Thus, for certain conditions of current and field, it is predicted that one of the in-phase peaks will be gone and the other will still be visible such that there are three peaks per field cycle. Fig. 18 presents an example from our experimental series of measurements, where the current is constant and the frequency is increased. The disparity between the two out-of-phase peaks is clear, and so is the existence of three peaks per field cycle predicted by the simulation (see Fig. 18, three arrows). To test if the suppression of the out-of-phase peak increases with the field frequency, we analyzed the voltage waveforms measured for identical transport currents and field amplitudes, but

different frequencies. We measured the height of the two peaks in the same external field cycle and plotted the height of the peaks as a function of the frequency. We also calculated the ratios between the small and large peaks in the voltage waveform and plotted the ratios as a function of the frequency. The resulting graphs are presented below:

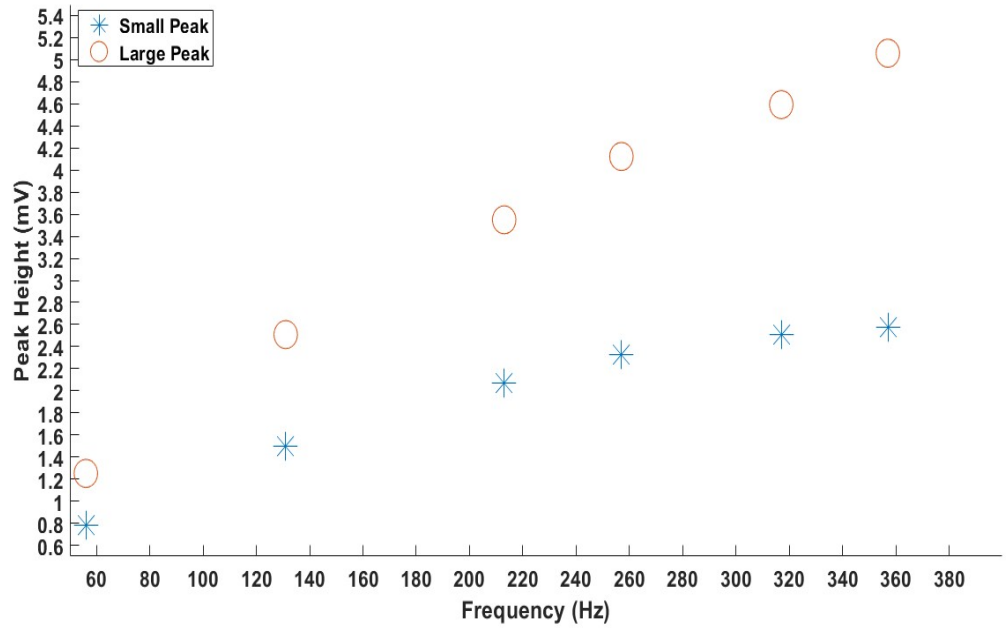

Fig. 21. Height of the two voltage peaks in Fig. 18 in one field cycle for different frequencies.

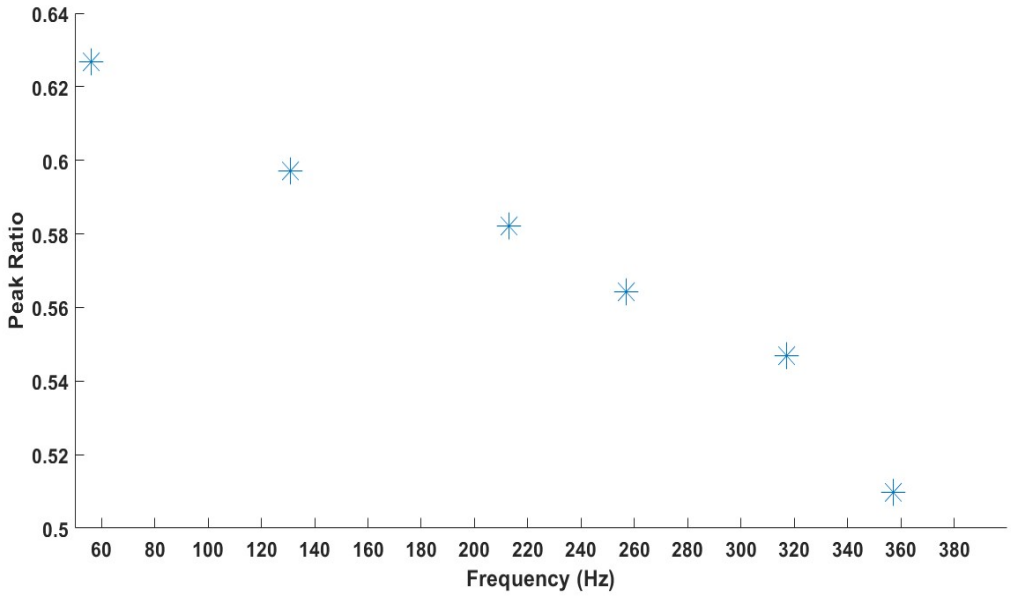

Fig. 22. Ratio between the height of the small and large peaks presented in fig. 18 for different frequencies.

In Fig. 21 we can see the height of each of the voltage peak for different frequencies. Initially, at low frequencies, both peaks grow in size. Looking at Fig 22, where the ratio between the heights is presented as a function of the frequency, the ratio between the peaks decreases, meaning that the larger of the two peaks grows faster than its smaller counterpart. At a frequency of about 213Hz, the growth of the smaller peak stalls and by 257Hz it virtually stops, the larger peak continues to grow at an unchanged rate. This is exemplified when looking again at Fig. 22, at around 257Hz the ratio between the peaks drops faster than it did for the lower frequencies. This is as predicted by the numerical simulations.

In Figs. 17-22, we studied the effect of frequency on the asymmetry. But the origin of the voltage is the combination of both the external field and the transport current and its shape is determined by both the frequency of the field and the magnitude of the current. As such, it is pertinent to study how the current effects the asymmetry of the waveform. To do this, we measured the voltage waveform for a constant external magnetic field and changing currents. The experimental waveforms are presented below:

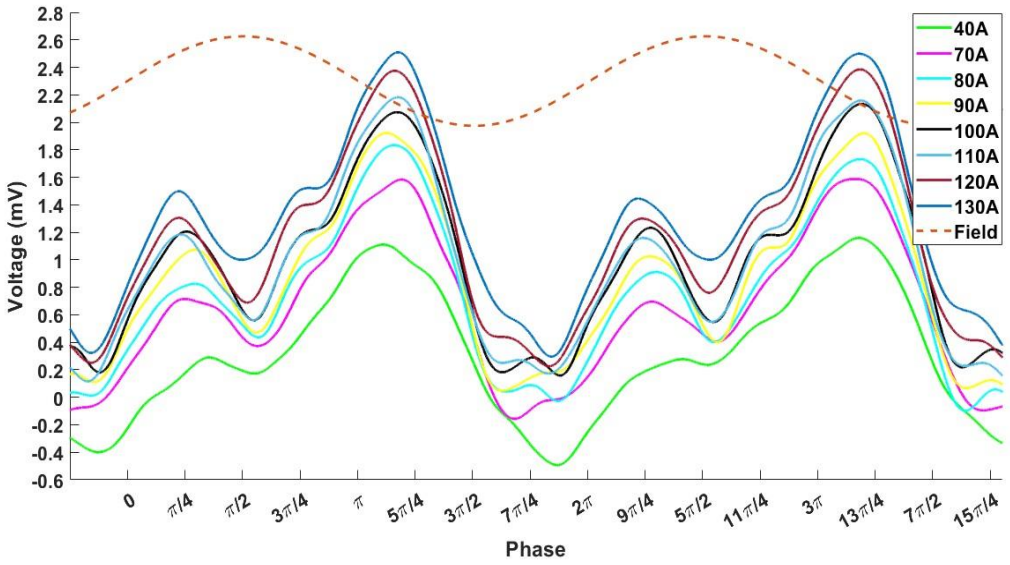

Fig. 23. Experimental voltage waveforms on an HTS tape exposed to an external magnetic field with an amplitude of 764 Gauss and frequency 131Hz and carrying different transport currents.

Like the analysis for changing frequencies, we measured the height of two out-of-phase peaks in the same external field cycle in Fig. 23 and plotted the height of the peaks as a function of the current. We also calculated the ratios between the small and large out-of-phase peaks in the voltage waveform and plotted the ratios as a function of the frequency. At present, we are working on numerical simulations to compare with these results. But we can already study

the experimental results with the theory itself to see if they are in agreement. The results are presented below:

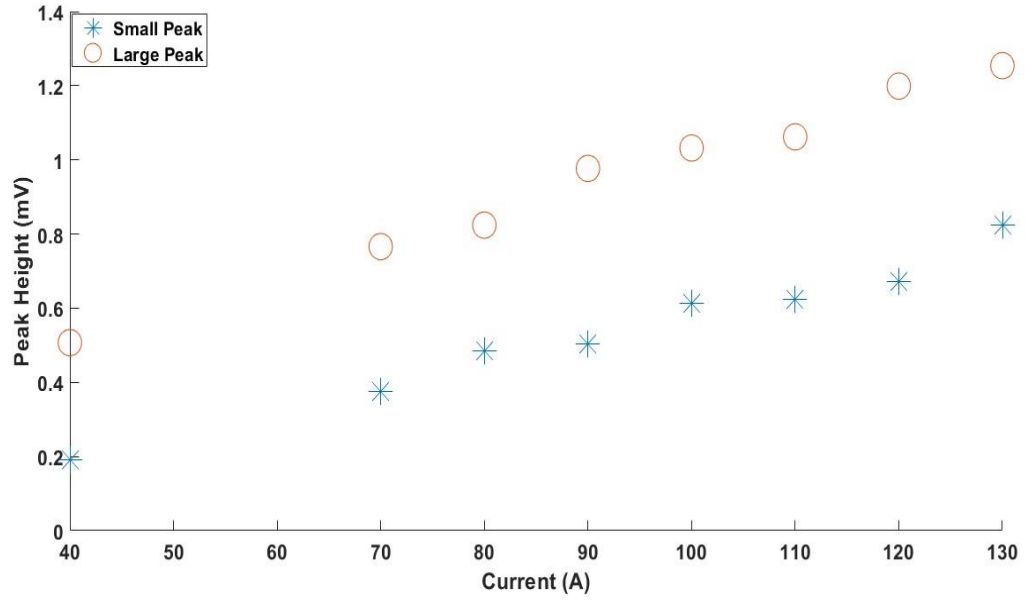

Fig. 24. Height of the two voltage peaks in Fig. 23 in one field cycle for different transport currents.

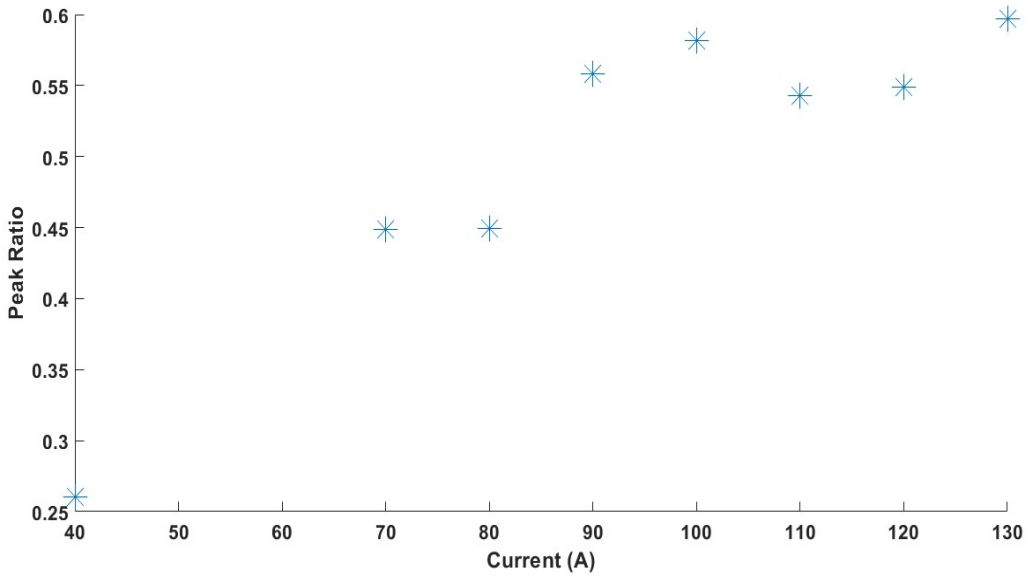

Fig. 25. Ratio between the height of the small and large peaks presented in Fig. 23 for different currents.

Figs. 24 and 25 clearly show that the height difference between the two out-of-phase peaks, and thus the asymmetry of the voltage, shrinks with growing transport current. In Fig. 24 we see that both peaks grow with the current, but the initially smaller peak grows faster. The difference between them shrinks. This can be seen even better in Fig. 25, the ratio between

the small peak and the large peak grows with the current. Interestingly, the asymmetry does not shrink at a constant rate. At first it shrinks rapidly, with the ratio growing quickly, but at about 90A the growth of the ratio slows down quite drastically. These results are in agreement with the theory. This is due to the fact that the suppression depends on the non-linearity of the magnetic field profiles and the corresponding out-of-phase regime. For higher currents, the out-of-phase regime is less dominant and appears at higher frequencies. The magnetic field profiles are linear at higher frequencies and for very large currents the zero-field line is trapped in the center of the tape (see Fig. 6). When this happens, they cannot effectively stop the motion of flux on the tape boundaries and we should not see any asymmetry.

To summarize, we have shown that the measured HTS tape has an asymmetric structure. This asymmetry drastically changes the voltage waveform, suppressing one peak of the voltage waveform in every half cycle of the external field. The theoretical model was adjusted to account for the asymmetry of the tape. Comparing the predicted waveforms obtained by numerical simulations to our experimental waveforms, there is good qualitative agreement between the two. Further analysis of our results shows that the asymmetry of the tape primarily affects the out-of-phase peak in the voltage waveform and has very little effect on the in-phase peak. Also, we showed that the suppression effect of the asymmetry is stronger for higher field frequencies and lower transport currents. These results are in agreement with the theoretical predictions.

4.2.2. Traveling in the predicted phase diagram

As mentioned in the theory section, we expect the presence of magnetic zero-field lines and their entry and exit from the superconductor to drastically affect the voltage waveform induced in the superconductor. Specifically, we expect that for different values of DC transport current, AC magnetic field amplitude and AC magnetic field frequency, the wave form will exhibit either an in-phase peak, an out-of-phase peak, or both peaks simultaneously. The conditions for which each one of these regimes will exist has been predicted in [31] in the form of a phase diagram which has been presented in Fig. 8 above. While the appearance of an out-of-phase peak and its coexistence and replacement of the in-phase peak has been experimentally observed by Lukovsky *et. al.* [30], [48], the validity of the theoretical predictions and the conditions for which each peak dominates have yet to be experimentally verified. In this work we measured the voltage waveform on BSCCO tapes under different DC transport currents and AC external field amplitudes and frequencies so as to validate the theoretical model. For the readers convenience, we display Fig. 8 again.

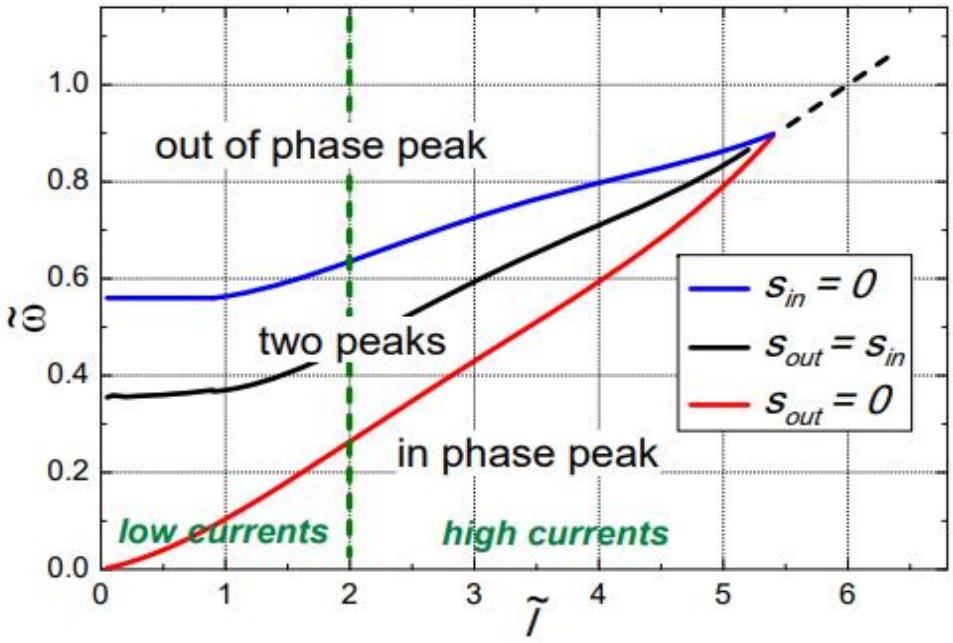

Fig. 8. Phase diagram of the appearance of in-phase and out-of-phase peaks for different values of $\tilde{\omega}$ and $\tilde{I}$. The diagram consists of three phases: only in-phase peak (below the red line), only out-of-phase peak (above the blue line) and double peak (between the red and blue lines).

Following the theoretical phase diagram suggested in Fig. 8, we started with two types of measurements. First, we kept the DC transport current constant and gradually increased the external AC magnetic field's frequency while keeping a constant field amplitude. Looking at the phase diagram in Fig. 8, this means starting at some value $\tilde{I}$ and increasing $\tilde{\omega}$ so that we move "up" the phase diagram from the region of only the in-phase peak to the region of the double peak and finally to the region of only the out-of-phase peak. Second, we kept the external magnetic field constant and gradually increased the DC transport current. Looking again at Fig. 8, this means starting at a constant value of $\tilde{\omega}$ and increasing $\tilde{I}$ so as to move from "left" to "right" across the phase diagram. Starting either from the region of the double peak and moving into the region of the in-phase peak alone, for the smaller values of $\tilde{\omega} \lesssim 0.6$. Or starting from the region of the out-of-phase peak alone, moving to the region of the double peak and ending in the region of the in-phase peak alone, for the larger values of $\tilde{\omega} \gtrsim 0.6$. Both types of measurements (constant $\tilde{I}$ and constant $\tilde{\omega}$) have been conducted for different fixed values of current and frequency so as to observe the transitions in different parts of the phase diagram. The goal of these measurements was to observe the transition

between the different regimes and compare these results to the phase diagram and confirm its predictions.

Before presenting our results, we should revisit the relations between I and ω and their dimensionless counterparts $\tilde{I}$ and $\tilde{\omega}$. We have already shown the relations, but these relations must be adjusted to account for the differences between the theory and the experiment. The theory considers an infinite slab, while the experiment is conducted on a finite tape. The necessary correction to the relation was done by Fuzailov[41]. Where it is shown that $\tilde{I}$ can be written as:

$$\tilde{I} = 2 \cdot \frac{B_{edge}}{H_{max}} \cdot \frac{h}{w} \qquad (26)$$

Where B_{edge} is the magnetic self-field at the edge of an infinite wire with a rectangular cross section (a finite tape). Fuzailov derived the relation between B_{edge} and I and found it to be:

$$B_{edge} = \left(h \cdot \ln\left(1 + 4 \cdot \left(\frac{w}{h}\right)^2\right) + 4 \cdot w \cdot tan^{-1}\left(\frac{h}{2 \cdot w}\right)\right) \cdot \frac{j}{c}$$
$$= \left(h \cdot \ln\left(1 + 4 \cdot \left(\frac{w}{h}\right)^2\right) + 4 \cdot w \cdot tan^{-1}\left(\frac{h}{2 \cdot w}\right)\right) \cdot \frac{I}{c \cdot w \cdot h} \qquad (27)$$

Where w is the tape width and h is the tape height, while j is the current density.

For our measured tape $w = 0.4cm$ and $h = 0.03cm$. Substituting these into Eq. 27, and then substituting Eq. 27 into Eq. 26 gives us:

$$\tilde{I} \approx \frac{3.213}{H_{max}} \cdot I \qquad (28)$$

In the theory section we presented the relation between ω and $\tilde{\omega}$:

$$\tilde{\omega} = \frac{\pi}{2} \cdot \frac{\eta d^2}{\Phi_0 H_{max}} \cdot \omega \qquad (29)$$

Where $\eta \approx 5 \cdot 10^{-7} \frac{g}{cm \cdot sec}$ is the Bardeen-Stephen drag coefficient, $\Phi_0 = 2.07 \cdot 10^{-7} Gauss \cdot cm^2$ is the unit flux, and $d = 0.4cm$ is the tape width. Substituting these variables into Eq. 30 gives us:

$$\tilde{\omega} \approx \frac{0.61}{H_{max}} \cdot \omega \qquad (30)$$

With the relations in Eq. 29 and 31 in hand, we have three variables to control, I, ω, and H_{max}. By choosing a constant value for the external field amplitude H_{max}, we can then measure the transition between the different regimes of the phase diagram in Fig. 8. The results are presented below, starting with the transition from the left to the right of the phase diagram (along the $\tilde{I}$ axis), the external magnetic field amplitude is set at 764 Gauss. In each of the following figures, we display such scans of current (left to right on the phase diagram) for a different value of $\tilde{\omega}$.

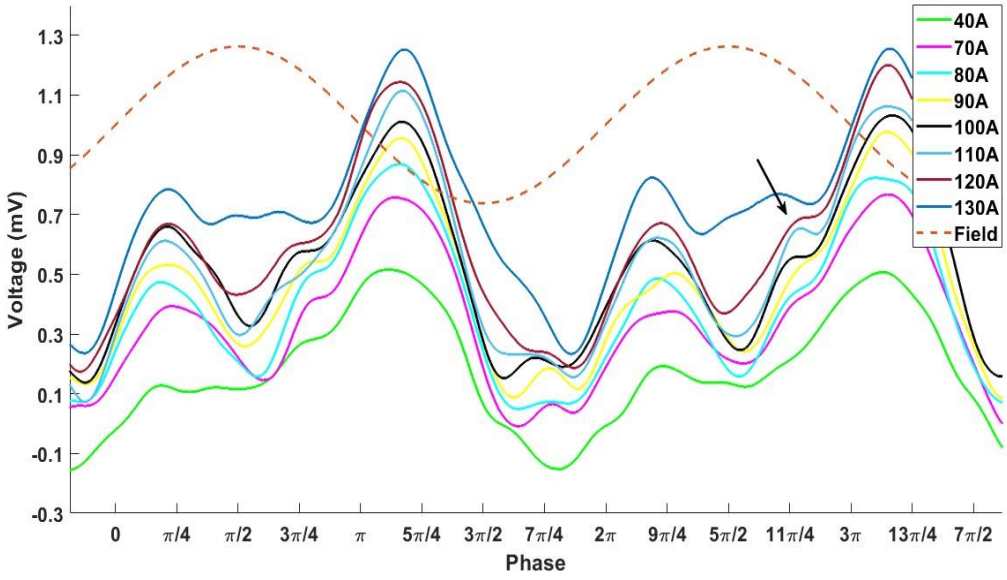

Fig. 26. Voltage waveforms for an external AC magnetic field with a frequency of 56Hz and an external field amplitude of 764 Gauss, carrying different transport currents. The dashed line is the normalized magnetic field waveform and it is for comparison of the phase. The arrow denotes the shoulder caused by the in-phase peak.

We start with a frequency of 56Hz. At low transport currents, such as the lower green curve of 40A, we can see that the voltage peaks are out-of-phase with the external field. We are clearly in the out-of-phase regime, above the blue line in Fig. 8. We can see that as we increase the transport current, the larger out-of-phase peaks develop a shoulder (denoted by the black arrow in Fig. 26), it can already be seen for transport currents of 70A (purple curve). This shoulder becomes more and more pronounced as the transport current grows and at the highest measured current of 130A (upper blue curve), it is already an independent peak. As it grows, we can see that this peak moves in-phase with the external field. We identify this "semi-hidden" peak as the in-phase peak. As can be seen in Fig. 26 and in the figures that

follow, this in-phase peak is not actually in phase with the external field. Looking at the numerical simulations of Fuzailov and Burlachkov, we can see that there is a phase shift of the in-phase peak (see Fig. 17). This shift is dependent on the transport current, external magnetic field, and tape asymmetry. The theory predicts that for higher frequencies the phase shift will be greater due to the greater viscous drag on the fluxons. While for higher currents the phase shift will be smaller due to the linearity of the field profiles. The in-phase peak in our measurements qualitatively agrees with the theory, moving towards the peak of the external field with growing current and away from it with growing frequency. But, without a quantitative characterization of the asymmetry of the tape so as to factor its effect on the phase shift, we cannot make quantitative conclusions about the phase shift of the in-phase peak.

Recalling our findings regarding the asymmetry and its effects on the voltage waveform, this in-phase peak corresponds to the smaller of the out-of-phase peaks. We can see that it is of comparable height to the suppressed out-of-phase peak for all the currents in which it appears, but we must remember that the asymmetry suppresses the out-of-phase peak more than it does the in-phase one, and that the suppression is lesser with growing current. It thus follows that for the lower currents, if the tape was symmetric, the out-of-phase peak would be taller than the in-phase one. As the current grows, we expect the in-phase peak to grow while the out-of-phase peak is less suppressed. Thus, for the higher currents, if the tape was symmetric, the difference between the peaks would shrink. Hence, what we see is the in-phase peak growing with the rising current and approaching the out-of-phase peak. Now, repeating the transition for a higher frequency of 131Hz we get:

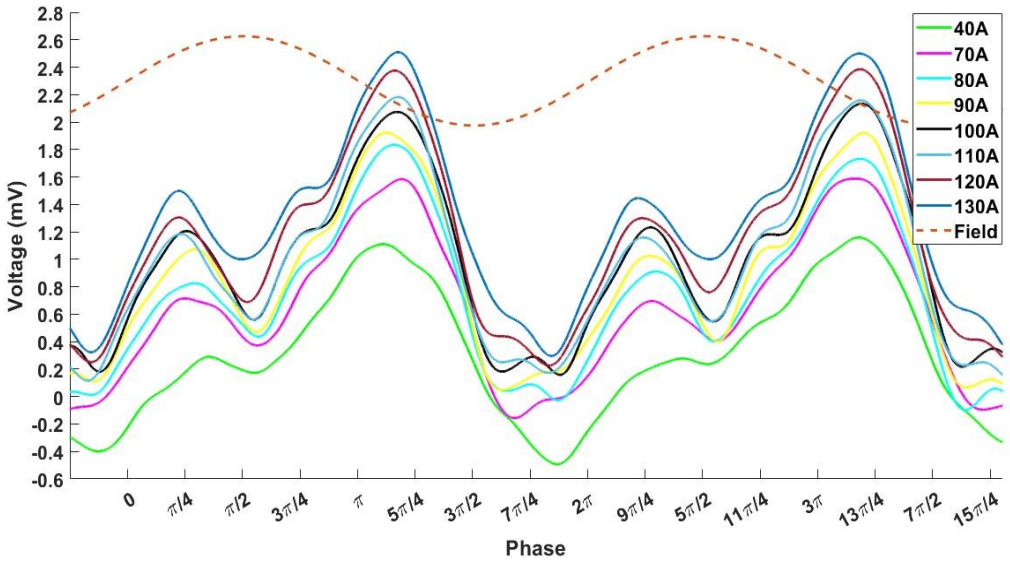

Fig. 27. Voltage waveforms for an external AC magnetic field with a frequency of 131Hz and an external field amplitude of 764 Gauss, carrying different transport currents.

Like in Fig. 26, at low currents we start in the out-of-phase regime. However, as the transport current is increased, the in-phase peaks in Fig. 27 appear later when compared to Fig. 26 (at 80A, light blue curve). Like in Fig. 26, the in-phase peak and its corresponding out-of-phase are almost equal in height for all the currents, for the lower currents the in-phase peak is even slightly higher. But if we again consider the asymmetry, the higher frequency means greater suppression, especially of the out-of-phase peak. This means that for the symmetric case the out-of-phase peak would be higher and the difference between it and the in-phase peak would be greater in Fig. 27 than for the lower frequencies seen in Fig. 26. Further increasing the frequency gives us:

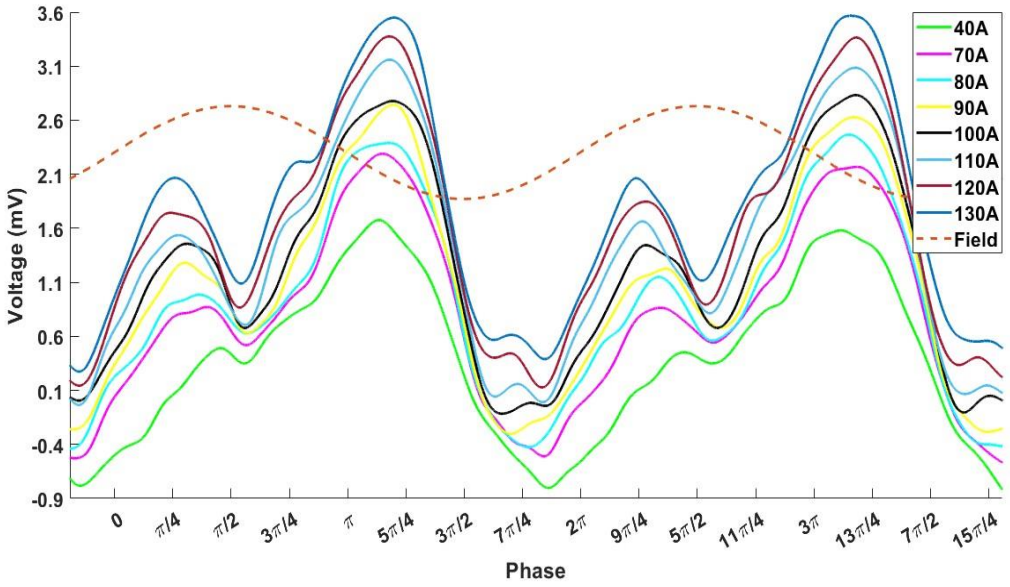

Fig. 28. Voltage waveforms for an external AC magnetic field with a frequency of 213Hz and an external field amplitude of 764 Gauss, carrying different transport currents.

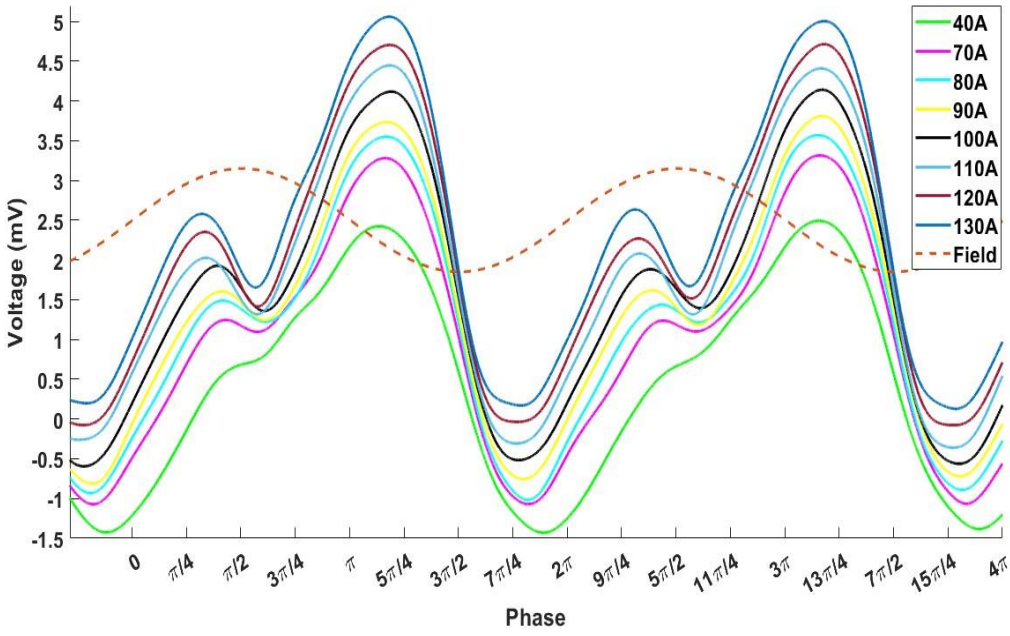

Fig. 29. Voltage waveforms for an external AC magnetic field with a frequency of 357Hz and an external field amplitude of 764 Gauss, carrying different transport currents.

As can be seen in Figs. 28 and 29, as we increase the frequency, the in-phase peak begins to appear at higher currents. For 213Hz a shoulder appears only at around 110A, and at 357Hz it doesn't appear at all. The heights of the in-phase and out-of-phase peaks in Fig. 28 are of similar height, like in Figs. 26 and 27. But recalling that the suppression of the peaks due to asymmetry is greater for greater frequencies, this actually corresponds to a greater height

disparity between the in and out-of-phase peaks in the case of symmetry when compared to Figs. 26 and 27.

In practice, we were unable to complete the entire transition between the three different regimes of the phase diagram. This is due to the frequency limits of our experimental setup. We intend to extend the capabilities of the setup and add measurements at the very low frequency range, even lower than 1 Hz. Despite this, the transition between the out-of-phase and double peak regimes was observed. Thus, we can investigate this transition qualitatively, and indeed, we see that Figs. 26-29 are in agreement with the phase diagram. We always start in the out-of-phase regime i.e., above the blue line in Fig. 8. Looking at Fig. 8, we can see that the blue curve separating between the out-of-phase and double peak regimes starts with a low slope for $\tilde{I} < 1$ and above that begins to curve upwards with $\tilde{I}$. As the transport current is increased, we move right along the $\tilde{I}$ axis in Fig. 8 and eventually we shall cross the blue line. At that point, we have entered the double peak regime, and the in-phase peak begins to appear and grows as we move further into the double peak regime with increasing current. This is what we see in the experiments. We start with only out-of-phase peaks at lower currents and at higher currents we cross into the double peak regime and an in-phase peak begins to appear. Moreover, as we saw, the higher the frequency, the higher the currents at which the in-phase peak begins to appear. This is also in agreement with the phase diagram. As the blue line in Fig. 8 curves upward it also curves further to the right. This means that the higher up we are in the phase diagram i.e., the higher the frequency, the further we need to move to the right to cross into the double peak regime. Hence the in-phase peak will appear at higher currents, as observed. The fact that we observed the transition from the out-of-phase to the double peak regime indicates that the transport currents driven in the tape are in the region where the transition line rises with I, meaning they should correspond with values of $\tilde{I} > 1$. Calculating $\tilde{I}$ based on Eq. 28 for an external field amplitude of 764 Gauss, the dimensionless current for the highest driven current (130A) is $\tilde{I} \approx 0.55$, which is lower than expected. This quantitative discrepancy will be addressed later in this work.

Next, we shall follow experimentally the transition from the bottom to the top of the phase diagram (along the $\tilde{\omega}$ axis) for different values of $\tilde{I}$, the results are presented below:

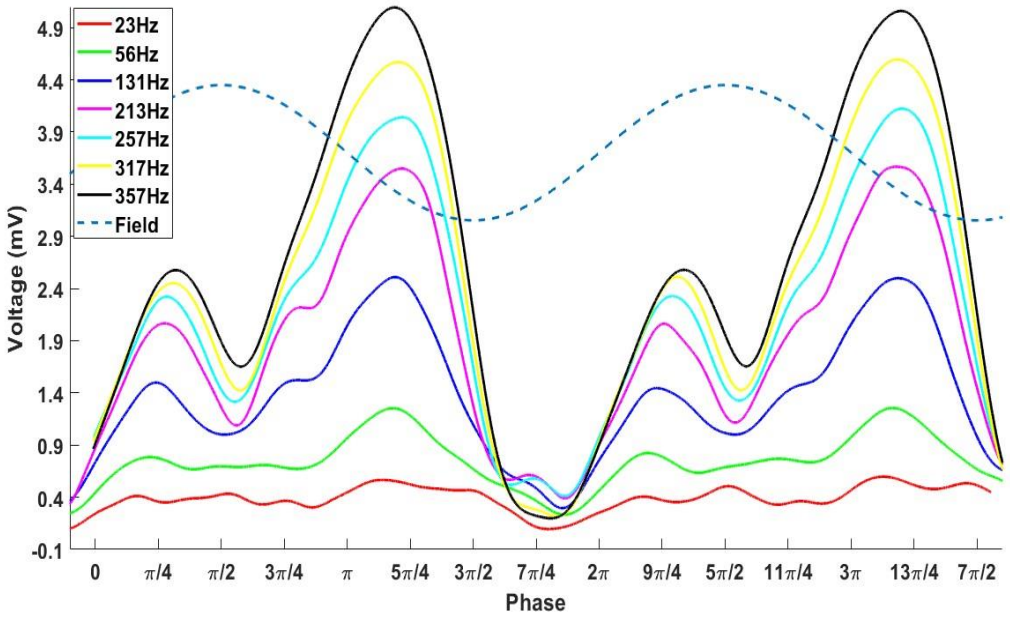

Fig. 30. Voltage waveforms for 130A transport current and external field amplitude of 764 Gauss and different frequencies.

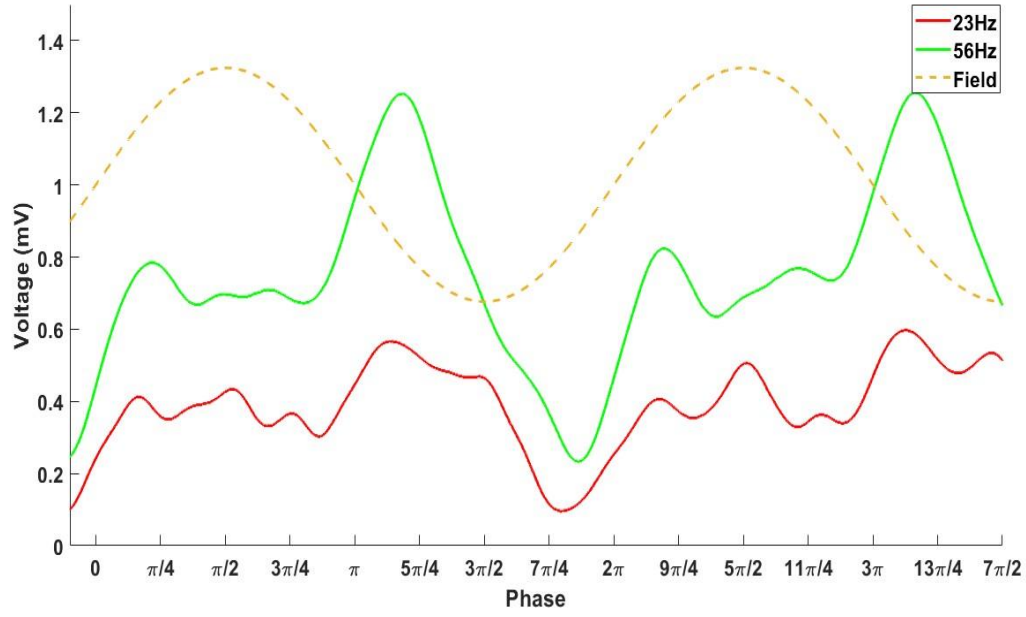

Fig. 31. Lower two waveforms in Fig. 30. I = 130A, H_{max} = 764 Gauss.

Let us recall that due to the asymmetry of the BSCCO tape, there will be an asymmetry between the peaks in the voltage waveform in every cycle of the external field. Starting with the highest measured transport current, 130A. We can see in Fig. 30 that for lower frequencies there are three peaks in every cycle of the external field, where the two lower

peaks being the suppressed out-of-phase and corresponding in-phase peak while the larger peak is the non-suppressed out-of-phase peak, which has already suppressed its in-phase peak (red and green lower curves in Fig. 30 and the same curves closer up in Fig. 31). Hence, we begin in the double peak regime. At the lowest frequency of 23 Hz, the in-phase peak is most pronounced and higher than the out-of-phase one (bottom red curve in Figs. 30 and 31). As the frequency increases, it first shrinks to become equal in size to the out-of-phase peak (green curve in Figs. 30 and 31), and then appears as though it remains the same in height compared to its out-of-phase peak. Again, we must take into account that the suppression of the out-of-phase peak grows with growing frequency, so for the case of symmetry the in-phase peak would actually be shrinking compared to the out-of-phase peak. The in-phase peak diminishes and becomes a shoulder in the enlarged out-of-phase peak (see Fig. 30, 131Hz-257Hz) and at the highest frequencies (see Fig. 30, 317Hz and 357Hz) it disappears altogether. Repeating the transition for a lower transport current of 120A, we get:

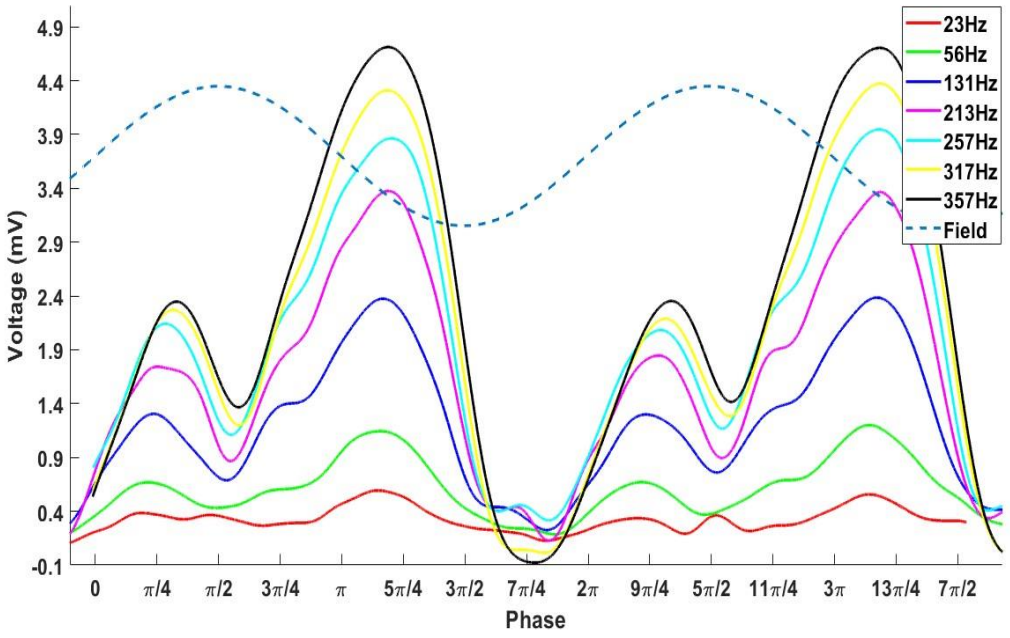

Fig. 32. Voltage waveforms for 120A transport current and external field amplitude of 764 Gauss and different frequencies.

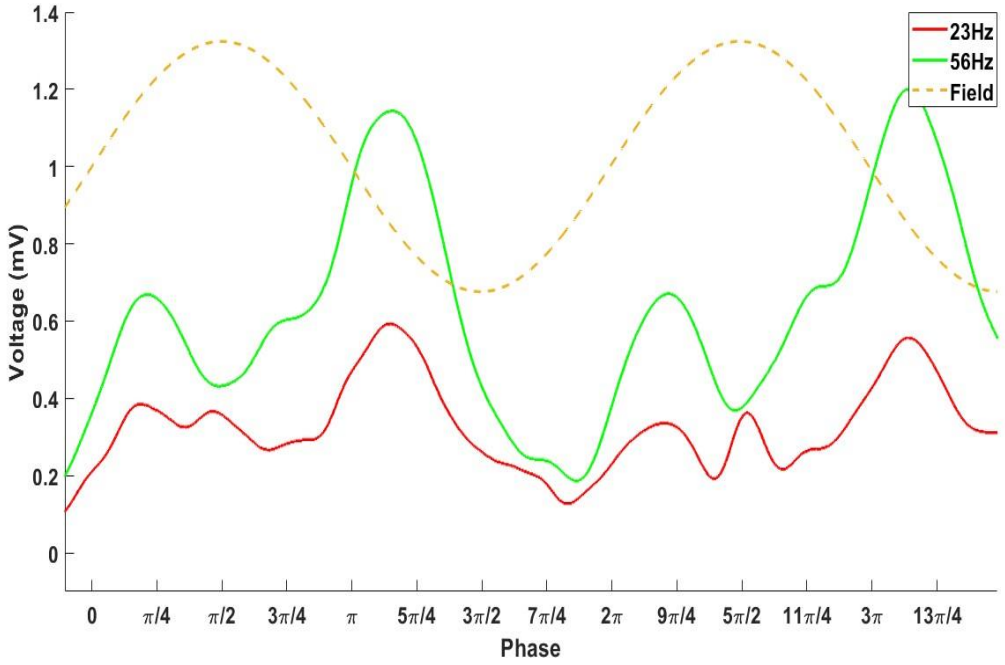

Fig. 33. Lower two waveforms in Fig. 32. I = 120A, H_{max} = 764 Gauss.

Similarly to the previous transition, at low frequencies we start with three peaks. A suppressed out-of-phase peak, its corresponding in-phase peak, and a non-suppressed out-of-phase peak which has overwhelmed its in-phase peak. At the lowest frequency of 23Hz (bottom red curve in Figs. 32 and 33) the in-phase peak is most pronounced and slightly higher than the out-of-phase peak. As the frequency increases it shrinks and becomes equal to the out-of-phase peak and eventually disappears. As we explained before, the reason that it remains of comparable height to the out-of-phase peak is the asymmetry. The asymmetry suppresses the out-of-phase peak more than it does the in-phase one, thus for the symmetric case the in-phase peak would be shrinking in relation to the out-of-phase peak. At first glance, the results in Figs. 32 and 33 are very similar to those in Figs. 30 and 31, and it would be tempting to say that the decrease in transport current did not affect the results. But, the suppression of the out-of-phase peak due to asymmetry is predicted to be more powerful at lower currents. So, for the case of symmetry, we would actually see the out-of-phase peak overtake the in-phase one at a lower frequency compared to the case of 130A transport current. This is a predicted by the theory.

Further lowering the transport current to 85A gives us the following results:

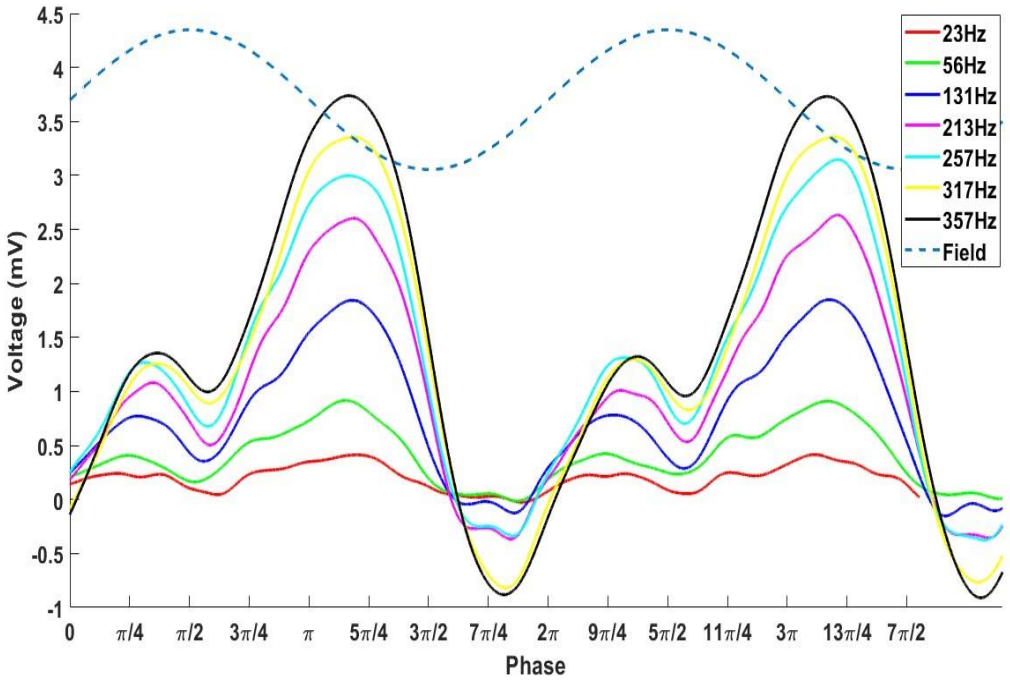

Fig. 34. Voltage waveforms for 85A transport current and external field amplitude of 764 Gauss and different frequencies.

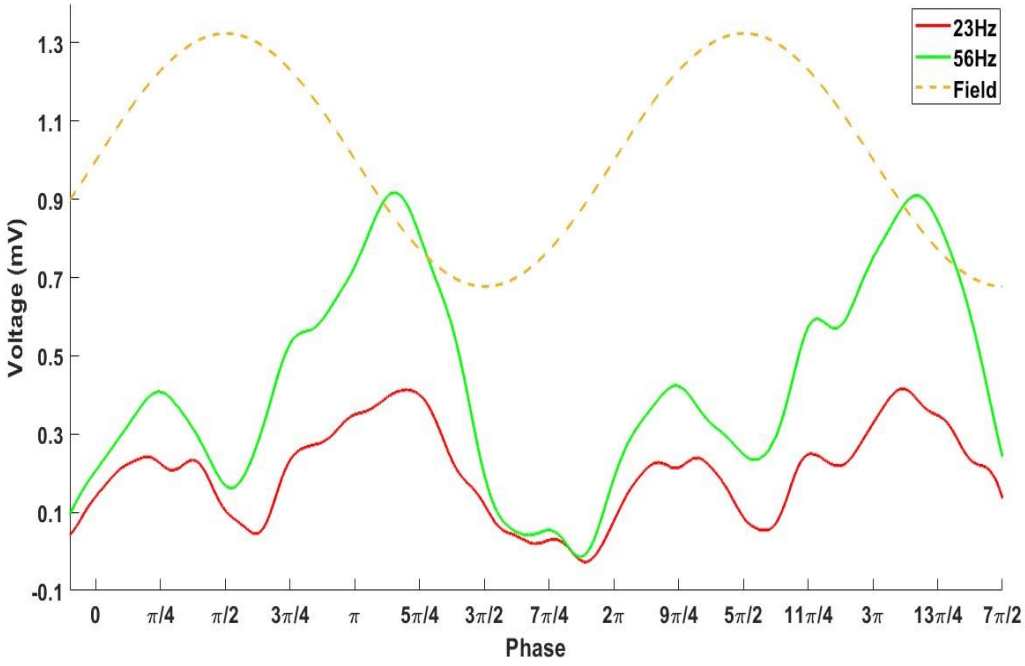

Fig. 35. Lower two waveforms in Fig. 34. I = 85A, H_{max} = 764 Gauss.

Figs. 34 and 35 give us a seemingly contradictory image. On one hand, the in-phase peak disappears at a lower frequency compared to measurements in higher currents (at 213 Hz in

Fig. 34 as opposed to 317 Hz in Figs. 30 and 32). This is very much in agreement with the theory, which predicts that at lower currents the transition to the out-of-phase regime will happen at lower frequencies. On the other hand, while the in-phase and out-of-phase peaks start at the same height at 23 Hz (red curve, Figs. 34 and 35), the in-phase peak actually grows taller than the out-of-phase one for higher frequencies, and remains so until it disappears. This supposed contradiction to the theory can be explained by the asymmetry of the tape. For the lower current, the suppression of the out-of-phase peak becomes stronger. It is possible that at this transport current the suppression of the out-of-phase peak is stronger relative to the weakening of the in-phase peak to the extent that the out-of-phase peak actually becomes smaller than the out-of-phase one. If this is the case, for the symmetric case we would expect the out-of-phase peak to dominate.

As for the transitions at constant frequencies and changing transport currents, we were unable to transition between all three regimes in the theoretical phase diagram in Fig. 8. We did again succeed in transitioning between the out-of-phase regime and the double peak regime, and we can investigate this transition to see if it supports the theoretical phase diagram. For this experiment the transition is from the double peak to the out-of-phase regime, the opposite of what happened when the frequency was constant and the current was changed. This is expected from the phase diagram, for a given transport current, as we increase the frequency we move "up" the phase diagram along the $\widetilde{\omega}$ axis. This means we should start in the in-phase regime, move to the double peak regime and from their continue to the out-of-phase regime. For the lower accessible frequencies in our experimental setup, we evidently start our measurement in the double peak regime. After accounting for the effects of the asymmetry, the size of the in-phase peak indicates that we start at the top half of the double peak regime, above the black line where the peaks are of equal height and close to the blue line that demarcates between the double peak and the out-of-phase regime (see Fig. 8). And so, we expect that as we increase the frequency, we move closer to the blue line which leads to the shrinking of the in-phase peak until finally, we cross into the out-of-phase regime and the in-phase peak disappears altogether. This is exactly what happens in our measurements. Moreover, we have observed that as the transport current is decreased i.e., we move to the left of the phase diagram, the transition from the double peak regime to the out-of-phase regime – signified by the disappearance of the in-phase peak – happens at lower frequencies. Looking at the theoretical phase diagram, we can see that for lower values of $\tilde{I}$, the transition line is near horizontal (see blue line in Fig. 8, $\tilde{I} < 1$). This means that the point of transition should

exhibit low or no dependence on the transport current. But at high values of $\tilde{I}$ ($\tilde{I} > 1$), the transition line curves up and begins to grow with $\tilde{I}$. Our experiments clearly show that the point of transition from the double peak regime to the out-of-phase regime is proportional to the transport current. This means that the transport currents used in this experiment should correspond to values of $\tilde{I} > 1$, exactly the conclusion we reached previously when measuring the voltage for changing currents.

In addition to the transport current I and the external field frequency ω, the dimensionless variables both depend on the external magnetic field amplitude H_{max}. By comparing the voltage waveforms for fixed values of $\tilde{I}$ and $\tilde{\omega}$ and different values of H_{max}, we can study the effects of the external field amplitude on the voltage waveforms in the superconductor and compare them to the theoretical predictions. The results are presented below. The previous measurements indicated that for our measurements the transition between the out-of-phase and double peak regime happens at our lowest measured frequencies and our highest measured currents, we shall thus begin our analysis of the effect of H_{max} at low frequencies and high currents:

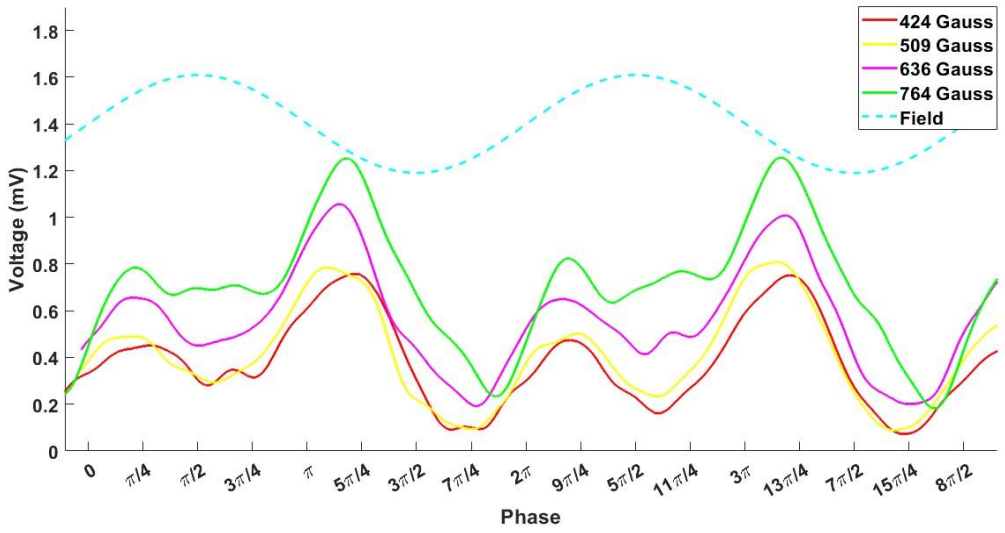

Fig. 36. Voltage waveforms for 130A transport current an external field frequency of 56Hz and different amplitudes.

Starting with Fig. 36, where the transport current was fixed at 130A and the external field frequency was 56Hz, we can see how the voltage waveform changes with rising field amplitude. For the lowest applied amplitude of 424 Gauss (bottom red curve), the voltage waveform is in the out-of-phase peak regime, with two asymmetric out-of-phase peaks for

every external field cycle. Increasing the field amplitude to 509 Gauss (yellow curve) leads to an increase of the voltage, but the waveform is still clearly out-of-phase with the external field. Only at 636 Gauss do we see the appearance of an additional peak in the voltage waveform for every half cycle of the external field. These peaks trend toward being in-phase with the external field and signify that we have just entered the double peak regime. Further increase in the external field to 764 gauss leads to an increase in this in-phase peak, such that it is comparable in size to the out-of-phase peak. Remembering that low frequencies and high currents are predicted to result in weak suppression from asymmetry, the closeness in height between the peaks indicates that we are close to the black line in Fig. 8. Looking at Eq. 29 and 31, we can see that both $\tilde{I}$ and $\tilde{\omega}$ are inversely proportional to H_{max}. This means that, for fixed value of transport current and frequency, both $\tilde{I}$ and $\tilde{\omega}$ should decrease for increasing field amplitudes. While a decrease in $\tilde{\omega}$ should facilitate the appearance of the in-phase peak, a decrease in $\tilde{I}$ should do the opposite, push us further into the out-of-phase regime. Thus, it is expected that increasing the external field amplitude should both push us towards the appearance of the in-phase peak and at the same time push us deeper into the out-of-phase regime. Moreover, as increasing the external field amplitude decreases the dimensionless frequency, it should weaken the asymmetry. Yet, at the same time it decreases the dimensionless current, thus strengthening the asymmetry. We should thus expect that changing the external field amplitude should not strongly affect the asymmetry of the voltage waveform. But as we have observed that the in-phase peak appears with growing field amplitude, it appears that the inverse relation between $\tilde{\omega}$ and H_{max} is stronger than the one between $\tilde{I}$ and H_{max}. Hence, we should also expect that the asymmetry will decrease with the growing field amplitude. The stronger relation between $\tilde{\omega}$ and H_{max} could indicate that the drag coefficient η in Eq. 30 is positively dependent on external field amplitude, an assumption that needs to be further investigated in future experiments.

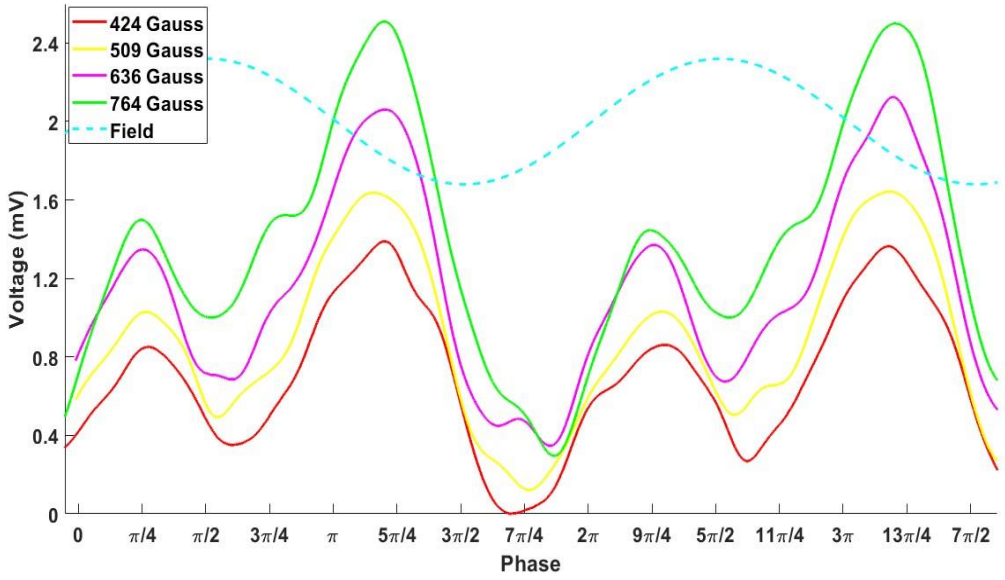

Fig. 37. Voltage waveforms for 130A transport current an external field frequency of 131Hz and different amplitudes.

In Fig. 37 we have increased the frequency from 56Hz to 131Hz and maintained a transport current of 130A. In terms of our location on the phase diagram, each voltage waveform remains at the same point along the $\tilde{I}$, axis in relation to the voltage waveform of the same amplitude in Fig. 36, but is higher up on the $\tilde{\omega}$ axis. As in Fig. 36, for the lowest field amplitude we start in the out-of-phase regime (Fig. 37, 424 Gauss, bottom red curve), and as the amplitude is increased, we move toward the double peak regime, as can be seen by the appearance of a small peak in the voltage waveform for 509 Gauss (Fig. 37, yellow curve) which continues to grow with increasing field amplitude. At higher frequencies we expect to start deeper within the out-of-phase regime, meaning that the appearance of the in-phase peak will happen at higher field amplitudes and the peak will be less prominent than that in Fig. 37 for the same field amplitude. We can see that for the higher fields in Fig. 37 (purple and green curves), the in-phase peak is about the same height as its out-of-phase counterpart whereas in Fig. 36 it is slightly smaller than out-of-phase peak. Again, we must take into account that when comparing between individual curves of the same field amplitude in Figs. 36 and 37, the difference in frequency means that the out-of-phase peaks in Fig. 36 are less suppressed than those in Fig. 37. So that for a symmetric tape the out-of-phase peak in Fig. 37 would be more dominant in the waveform as compared to the out-of-phase peak in Fig. 36.

Continuing to increase the frequency, we obtain the following results:

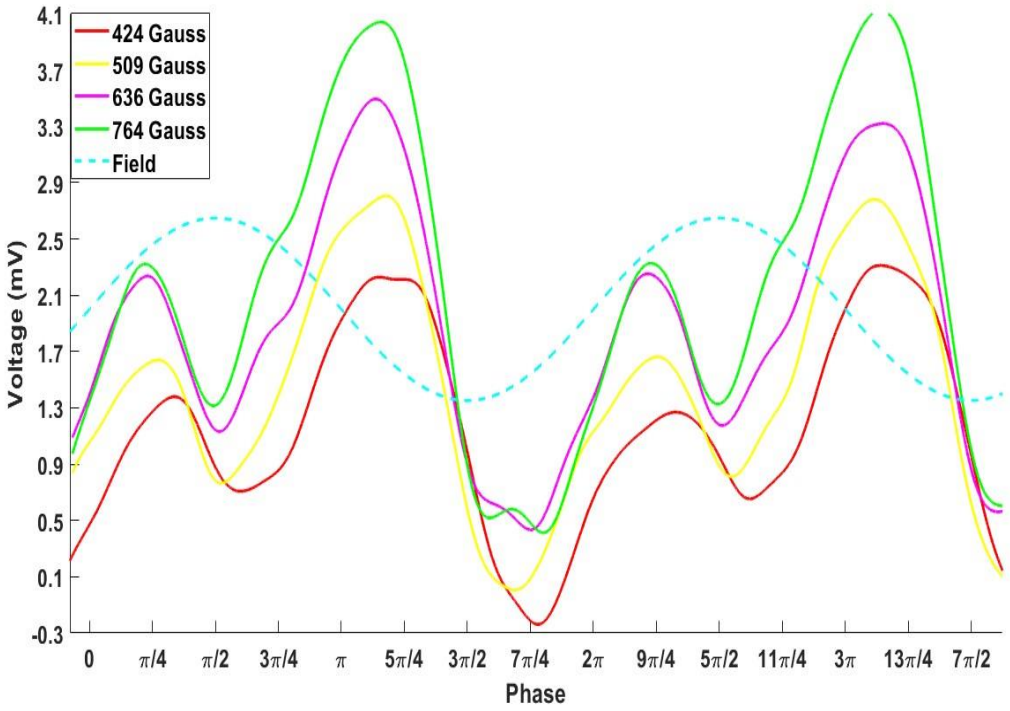

Fig. 38. Voltage waveforms for 130A transport current and an external field frequency of 257Hz and different amplitudes.

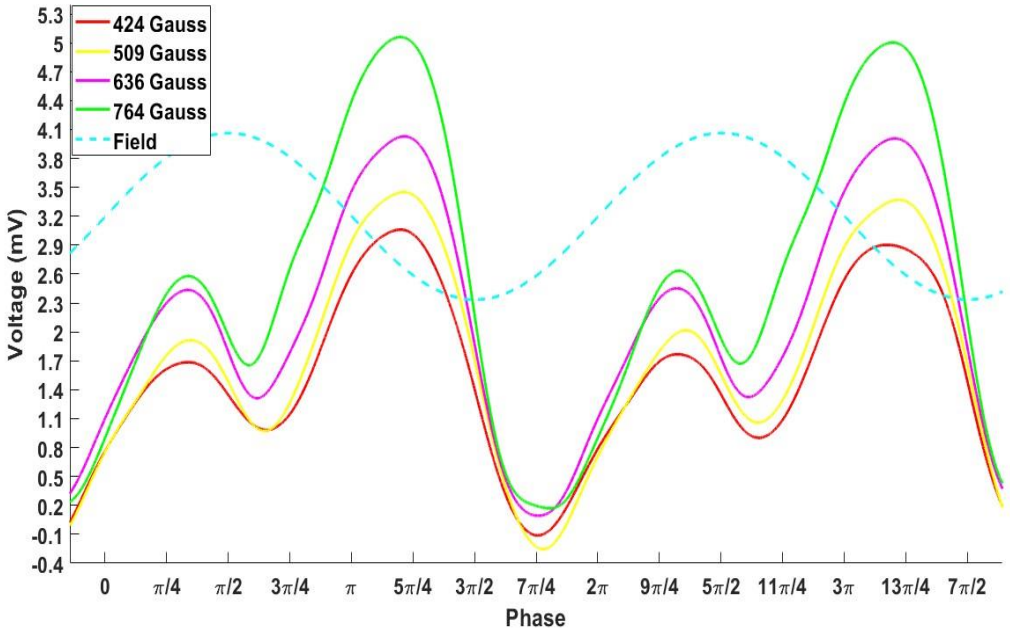

Fig. 39. Voltage waveforms for 130A transport current and an external field frequency of 357Hz and different amplitudes.

Figs. 38 and 39 show the voltage waveforms on the superconductor carrying a transport current of 130A and exposed to external fields of varying amplitudes and frequencies of 257Hz and 357Hz, respectively. We can compare Fig. 38 to Fig. 36 and 37 and notice that the in-phase peak is nonexistent for the smaller amplitudes of 424 and 509 Gauss (two bottom curves in Fig. 38), and only appears for high field amplitudes (two upper curves in Fig. 38). And while its height in relation to its out-of-phase peak is comparable to those of the corresponding in-phase peaks for lower frequencies, the increased suppression of the out-of-phase due to the higher frequency means that it would in fact be smaller than its out-of-phase peak, more so than in Figs. 36 and 37. This is in agreement with the theoretical prediction as mentioned above, the higher the frequency the deeper into the out-of-phase regime we begin. This is further exemplified by the results of Fig. 39, for a field frequency of 357Hz the in-phase peak is absent for all measured field amplitudes. We start so far in the out-of-phase regime that the decrease in $\tilde{\omega}$ brought by the increase in H_{max} is not enough to cross the blue line in the phase diagram and reach the double peak regime.

To further verify our conclusions on the effect of the external field amplitude on the voltage waveforms, we have also checked what happens to the waveforms when instead of changing the frequency, we change the currents. To be able to see as many transitions as possible, we shall return to the lower frequency 56Hz, and start with a lower current of 100A, working our way back up 130A. Looking at the theoretical phase diagram in Fig. 8, we predict that for the lower currents we will begin deeper in the out-of-phase regime and the in-phase peak will be absent in the lower field amplitudes and only begin to manifest for the high field amplitudes. The reason we expect the appearance of an in-phase peak at all, despite the fact that the growing field amplitude decreases $\tilde{I}$, is that as observed above in experiments of changing field amplitude, the inverse relation between $\tilde{\omega}$ and H_{max} appears stronger than the one between $\tilde{I}$ and H_{max}. This means that it should be possible for $\tilde{\omega}$ to decrease enough to move the waveform into the double peak regime despite the decreasing $\tilde{I}$. As the transport current increases, we expect that we shall begin closer to the transition between the regimes and that we shall observe the beginning of the in-phase peak for lower field amplitudes and that it will be more prominent.

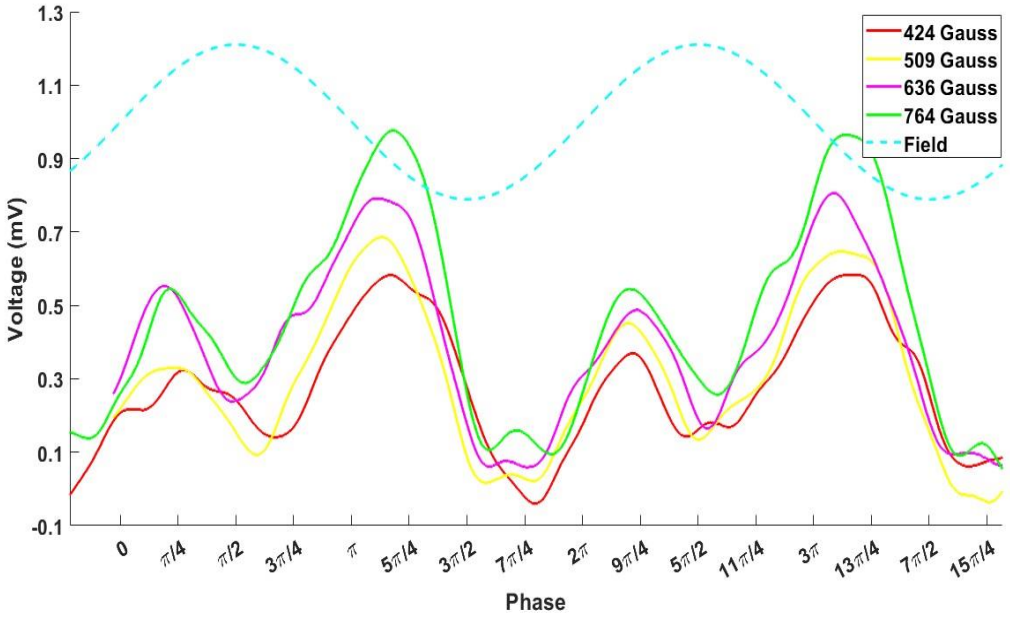

Fig. 40. Voltage waveforms for 100A transport current and an external field frequency of 56Hz and different amplitudes.

Having returned to lower frequencies (56Hz) we can see that for the lower field amplitudes of 424 and 509 Gauss – the two lower curves in Fig. 40 – we are in the out-of-phase regime with only the out-of-phase peaks present. For the higher field amplitudes of 636 and 764 Gauss – the two upper curves in Fig. 40 – we can see the beginning of the double peak regime with the appearance of a new peak. This agrees with our prediction and previous observations that the relation between $\tilde{\omega}$ and H_{max} is stronger than the relation between $\tilde{I}$ and H_{max}. At the same time, comparing the results in Fig. 40 to those of Fig. 36 – which is also exposed to fields of 56Hz but while carrying a higher transport current of 130A. We can see that for the two upper curves representing field amplitudes of 636 and 764 Gauss, the in-phase component for the lower current (Fig. 40) starts smaller than the out-of-phase peak for 636 Gauss (Fig. 40, purple curve) and then overtakes it at 764 Gauss (Fig. 40, green curve). For the higher current (Fig. 36), the in-phase peak starts smaller than the out-of-phase peak and then closes the gap but is still just slightly smaller (Fig. 36, purple and green curves). But taking into account that the suppression due to asymmetry grows with decreasing field, in a symmetric tape the out-of-phase peak in Fig. 40 would be much larger in comparison to the in-phase one. Thus, we are again in agreement with our theoretical expectations.

To summarize this chapter, we have experimentally investigated how three different variables, the DC transport current, the external AC magnetic field amplitude, and the

external AC field frequency, affect the induced voltage waveform on a BSCCO-2223 HTS tape. We studied how changing each of these variables contributed or hindered the appearance of an in-phase peak in the voltage waveform. We did this by fixing two of the three variables and changing the third. We thus obtained a series of voltage waveforms that differed only in one variable, allowing us to see how the waveform evolved for every variable. Each of these series represents motion along the theoretical phase diagram in a specific direction. Changing the frequency represents vertical motion along the $\tilde{\omega}$ axis of the phase diagram, changing current represents horizontal motion along the $\tilde{I}$ axis of the phase diagram, and changing the magnetic field amplitude represents diagonal-like motion along the phase diagram. We repeated each type of measurement, changing frequency, changing current, and changing amplitude, for different fixed values. This means we repeated the same motion along the different axes of the phase diagram with different starting points. Within the limits of the experimental setup, we were successfully able to observe the beginning of the transition between two different regimes in the phase diagram – the out-of-phase and the double peak regimes. As we have shown, the change in the voltage waveform due to the changing of the different external variables is in qualitative agreement with the theoretically predicted phase diagram.

5. Discussion and Summary

5.1. Effect of zero-field lines on the $E(I)$ relation in HTS for the DC regime

For HTS at high operating temperatures (~70K), fluxon motion involves the non-activated, flux flow regime. Therefore, a description of flux dynamics in HTS has to include an analysis of the flux diffusion equation (Eq. 1). By taking the well-established dependence of the activation energy U on j - $U(j) = U_0 \ln(\frac{j_c}{j})$, and the boundary conditions of a current carrying HTS slab (Eq. 3), the $E(I)$ relation for the current carrying slab exposed to an external field were derived. The $E(I)$ relation obtained for the case where the zero-field line is absent in the HTS is different than the one for the case where the zero-field line is present (Eq. 11 and 14). This indicates that the presence of a zero-field line changes the flux dynamics in the superconductor, and by extension its $E-I$ characteristics. For both instances the $E(I)$ relation is a power-law one, but the presence of the zero-field line is predicted to increase the exponent in the relation by one.

To verify this prediction, we measured the $E-I$ curves of a BSCCO-2223 HTS tape exposed to different external DC magnetic fields. The fields were chosen so as to allow for cases where the zero-field line is present in the tape, and for cases where it is absent. We then compared the exponents of the different curves to see if there was a change between them, and if so – is it by one as predicted by the theory.

Our results showed that the exponents do increase in the presence of a zero-field line, in qualitative agreement with the theory. However, quantitatively the results and the theory diverge. Where the theory predicts that the exponent will increase by one, the results show a larger increase of about 8. We have shown that this discrepancy is a result of both the assumption of stronger pinning energies than those that probably occur in the tape as well as the difference between the infinite slab geometry of the theory and the finite tape geometry of the experiment. The theory needs to be refined to account for these differences so as to give a correct prediction of the change to the exponent. Also, we must rule out the possibility that the asymmetry described in the previous chapters does not play a role in the DC regime and affects the E-I curves. We will therefore extend our measurements to other BSCCO and YBCO tapes and wires. Despite the quantitative differences, we have shown that the presence of a zero-field line inside a superconductor does change the exponent of its $E(I)$ relation.

5.2. Effect of zero-field lines on the voltage waveforms in the AC regime

For the AC regime, our main goal was to measure the voltage waveform of a superconducting tape in which a zero-field line is present and observe how it affects the induced voltage on the tape. For a superconductor carrying a DC transport current and exposed to an external AC magnetic field, the voltage depends on the motion of fluxons entering and leaving the superconductor. Magnetic zero-field lines have a drastic effect on the flux dynamics inside the superconductor. The motion of flux in the superconductor is drastically slowed down in their presence. If a zero-field line is on or near one of the boundaries of the superconductor, it strongly suppresses entry and exit of fluxons on that boundary. Whether a zero-field line can approach and cross the boundary to suppress flux motion there, and how much the suppression of flux motion at the boundary affects the voltage waveform depends on the combination of three variables: the frequency of the external magnetic field, the amplitude of the external magnetic field, and the DC transport current. Fuzailov *et. al.*[31], [41] simplified the problem from three variables into two normalized variables $\tilde{I}$ and $\tilde{\omega}$ and created a phase diagram which predicts for which values of $\tilde{I}$ and $\tilde{\omega}$ the voltage will be in-phase, out-of-phase or have two peaks. And if it has two peaks, which one will be more dominant.

In this work we measured the voltage waveforms on a BSCCO-2223 HTS tape carrying different DC transport currents and exposed to different AC magnetic fields. By controlling the three variables, transport current, frequency, and field amplitude, we experimentally investigated the effects of the zero-field line within the superconductor on the induced voltage and tested the validity of the theoretical model presented by Fuzailov *et. al*. From our results we have learned several things:

First, we learned that the tape has an asymmetric structure. It behaves differently if the direction of the perpendicular external field is flipped, or conversely if the direction of the transport current is reversed. In collaboration with Fuzailov and Burlachkov, the theoretical model was adjusted to account for this asymmetry and new predicted voltage waveforms were made accordingly. Comparison of the numerical voltage waveforms with the experimental results confirmed major predictions of the theory. We showed that the asymmetry greatly effects the out-of-phase peaks in the voltage waveform, but has almost no effect on the in-phase peaks. We showed that this is very much in line with the fact when the voltage is in the in-phase regime, the magnetic field profile is close to linear. Hence, it is not greatly affected by changes to the amount of flux crossing the boundaries. On the other hand, in the out-of-phase regime, where the field profile is very non-linear, changes to the amount

of flux at the boundaries have a big impact on the voltage. We showed that the asymmetry suppresses one voltage peak in each cycle of the external field, and that the suppression is stronger for higher frequencies, leading to reduced peak growth with frequency and eventually stopping peak growth altogether. Conversely, the suppression effect caused by the asymmetry is weaker for higher currents, the greater the current, the more similar the voltage peaks. This again is in line with the theory, because the out-of-phase regime dominates at higher frequencies and lower currents while the in-phase one dominates at higher currents and lower frequencies. This asymmetry greatly affects the shape of the voltage waveforms induced on the tape and can have many implications for the feasibility and practicality of HTS tapes in different applications, which require further investigation.

Second, we were able to qualitatively confirm the existence of the theoretical phase diagram predicted by Fuzailov and Burlachkov. Our experiments were able to show that the voltage waveform on the HTS tape reacts to changes in the transport current, external field frequency and external field amplitude in the manner predicted. By fixing two of the aforementioned variables and changing the third, we moved along the phase diagram in different directions looking for the transition between the regimes. In our experiments, we successfully observed the beginning of the transition between the out-of-phase and double peak regimes and vice versa. We saw that for fixed frequencies and amplitudes the in-phase peak appears as the current increases whereas for fixed currents and amplitudes the in-phase peak disappears as the frequency increases. For higher fixed frequencies the applied transport current needed for the in-phase peak to appear was greater. Conversely, for higher fixed currents, the in-phase peak persisted at higher frequencies. Both these observations agree with the phase diagram. When changing only the current I or the frequency ω, we change only one of the dimensionless variables in the phase diagram, $\tilde{I}$ and $\tilde{\omega}$ respectively. When changing the magnetic field amplitude H_{max}, both $\tilde{I}$ and $\tilde{\omega}$ are changed. In our experiments, higher field amplitudes led to entry into the double peak regime and the appearance of the in-phase peak. Seeing as both $\tilde{I}$ and $\tilde{\omega}$ should decrease with growing H_{max}, this implies that $\tilde{\omega}$ is more strongly dependent on H_{max} than $\tilde{I}$. A possible reason for this is that H_{max} also affects the Bardeen-Stephen drag coefficient η, which also affects $\tilde{\omega}$. This will be investigated in future experiments.

This qualitative agreement with the theory, despite the asymmetry of the measured tape and the fact that the measured tape is multi-filamentary in structure whereas the theory assumes a homogenous structure, indicates that the zero-field line does affect the flux dynamics inside

the superconductor. Hence the zero-field line needs to be taken into account when evaluating the potential losses in superconductors and their viability in various applications.

However, quantitatively the theoretical values of the dimensionless variables that correspond to the experimental currents and fields applied are not in agreement with the experimental results. Our measurements indicate that we are on the border between the out-of-phase and double peak regimes in an area of the phase diagram which corresponds to moderate dimensionless frequency values of $\tilde{\omega} \gtrsim 0.6$ and dimensionless current values of $\tilde{I} > 1$. But plugging the values of I, ω and H_{max} into Eq. 28 and 30 gives much lower values of $\tilde{\omega}$ and $\tilde{I}$, we get $\tilde{\omega} < 0.3$ and $\tilde{I} < 0.6$ for all combinations of variables. This suggests that we should have observed mostly the double peak behavior with the in-phase peak being the dominant of the two peaks, and for the lower frequencies and higher currents we could even expect to enter the in-phase regime. This is very different from the experimental results. There are several factors that could contribute to the fact that while the experiment agrees qualitatively with the behavior of the phase diagram and the changes in the waveforms agree with the theoretical predictions, the theoretical values of $\tilde{\omega}$ and $\tilde{I}$ are quantitively far from those indicated by the experiment. First, the theory assumes an infinite slab geometry when in reality the superconductor has a finite tape geometry. Second, the theory assumes that the superconductor is homogenous and superconducting throughout, but BSCCO is made of many superconducting filaments embedded in a non-superconducting silver matrix. This raises several questions, for instance, how does the moving of the current between filaments through the matrix affect the model? Third, the theory assumes that the superconductor is symmetric, where our superconductor is clearly asymmetric. Considering the fact that many HTS are have a filamentary structure and that there is a possibility that many commercial superconducting tapes could be asymmetric, either due to manufacturing issues or decay of some of the filaments over time, it is of great interest to adjust the theory to account for these factors.

In light of the quantitative discrepancy and the fact that the properties of HTS tapes can differ greatly from those assumed in the theory, there are many more experiments that can be done to shed more light on how zero-field lines affect the voltage waveforms and the losses in HTS and refine the theory. We plan on repeating the above measurements for more HTS tapes, both filamentary ones like BSCCO and homogenous ones like YBCO, and improving our experimental setup to allow for greater ranges of magnetic field frequency and field amplitude. Comparing between HTS tapes with different internal structures will provide

insight as to what part the internal structure plays in losses in HTS tapes exposed to AC current and field combinations in general and when zero-field lines exist in the tape in particular. We also plan on investigating the different tapes symmetry, through volt ampere and magneto-optic measurements, and compare the voltage waveforms and losses of symmetrical tapes to those of asymmetrical ones and see how this affects the losses. If there is a possibility of superconductors decaying and losing symmetry over time, shedding light on the effects of asymmetry in HTS tapes could be crucial in determining their feasibility and effective lifetime. In addition, we also plan on repeating these measurements at different temperatures. Seeing as temperature affects the appearance of flux flow inside the superconductor and changes the viscous drag coefficient η, changing the temperature should increase or decrease the effects of the zero-field line. Hence investigation of different temperatures will contribute greatly to determining ideal operating temperatures of HTS in different applications. Finally, we plan to conduct magneto-optic measurements not only to determine the internal structure and symmetry of the tape, but also to observe the zero-field line inside the HTS tapes and directly observe how they change the flux dynamics in the tape.

6. References

[1] A. Godeke, “High temperature superconductors for commercial magnets,” *Supercond Sci Technol*, 2023, doi: 10.1088/1361-6668/acf901.

[2] A. Molodyk and D. C. Larbalestier, “The prospects of high-temperature superconductors,” *Science (1979)*, vol. 380, no. 6651, 2023, doi: 10.1126/science.abq4137.

[3] Y. B. Kim, C. F. Hempsteadp, and A. R. Strnad, “Magnetization and Critical Supercurrents,” *Physical Review*, vol. 129, pp. 528–536, 1963.

[4] A. A. Abrikosov, “On the Magnetic Properties of Superconductors of the Second Group,” *SOVIET PHYSICS JETP*, vol. 5, no. 6, 1957.

[5] Anderson P.W., “Theory of Flux Creep in Hard Superconductors,” *Phys Rev Lett*, vol. 9, no. 7, pp. 309–311, 1962.

[6] Y. B. Kim, C. F. Hempstead, and A. R. Strnad, “Flux-Flow Resistance in Type-II Superconductors,” *Physical Review*, vol. 139, no. 4A, pp. 1163–1172, 1965.

[7] C. P. Bean, “Magnetization of High-Field Superconductors,” *Rev. Mod. Phys.*, vol. 36, pp. 31–39, 1964.

[8] C. P. Bean, “Magnetization of hard superconductors,” *Phys Rev Lett*, vol. 8, no. 6, pp. 250–253, 1962, doi: 10.1103/PhysRevLett.8.250.

[9] Y. B. Kim, C. F. Hempstead, and A. R. Strnad, “Critical persistent currents in hard superconductors,” *Phys Rev Lett*, vol. 9, no. 7, 1962, doi: 10.1103/PhysRevLett.9.306.

[10] Adrianov V. V., Zenkevich V. B., Kurguzov V. V, Sychev V. V., and Ternvskii F. F.., “EFFECTIVE RESISTANCE OF AN IMPERFECT TYPE II SUPERCONDUCTOR IN AN OSCILLATING MAGNETIC FIELD,” *Soviet Physics JETP*, vol. 31, pp. 815–819, 1970.

[11] T. Ogasawara, Y. Takahashi, K. Kanbara, Y. Kubota, K. Yasohama, and K. Yasukochi, “Alternating field losses in superconducting wires carrying dc transport currents: Part 1 single core conductors,” *Cryogenics (Guildf)*, vol. 19, no. 12, pp. 736–740, 1979, doi: 10.1016/0011-2275(79)90192-9.

[12] T. Ogasawara, Y. Takahashi, K. Kanbara, Y. Kubota, K. Yasohama, and K. Yasukochi, “Alternating field losses in superconducting wires carrying dc transport currents. Part 2: multifilamentary composite conductors,” *Cryogenics (Guildf)*, vol. 21, no. 2, 1981, doi: 10.1016/0011-2275(81)90056-4.

[13] T. Ogasawara, K. Yasuköchi, S. Nose, and H. Sekizawa, “Effective resistance of current-carrying superconducting wire in oscillating magnetic fields 1: Single core composite conductor,” *Cryogenics (Guildf)*, vol. 16, no. 1, pp. 33–38, 1976, doi: 10.1016/0011-2275(76)90284-8.

[14] G. P. Mikitik and E. H. Brandt, “Generation of a dc voltage by an ac magnetic field in type-II superconductors,” *Phys Rev B Condens Matter Mater Phys*, vol. 64, no. 9, pp. 925021–925024, 2001, doi: 10.1103/physrevb.64.092502.

[15] M. P. Oomen, J. Rieger, M. Leghissa, B. Ten Haken, and H. H. J. Ten Kate, “Dynamic resistance in a slab-like superconductor with Jc(B) dependence,” *Supercond Sci Technol*, vol. 12, no. 6, 1999, doi: 10.1088/0953-2048/12/6/309.

[16] G. Ries and K. P. Jüngst, “Filament coupling in multifilamentary superconductors in pulsed longitudinal fields,” *Cryogenics (Guildf)*, vol. 16, no. 3, 1976, doi: 10.1016/0011-2275(76)90226-5.

[17] A. M. Campbell, “Coupling losses in filamentary superconductors with a resistive barrier,” *Supercond Sci Technol*, vol. 10, no. 12, 1997, doi: 10.1088/0953-2048/10/12/016.

[18] J. Kováč, J. Šouc, P. Kováč, and I. Hušek, “AC losses of single-core MgB2 wires with different metallic sheaths,” *Physica C: Superconductivity and its Applications*, vol. 519, 2015, doi: 10.1016/j.physc.2015.09.001.

[19] Y. Nikulshin *et. al..*, “Monel Contribution to AC Losses in MgB2 Wires in Frequencies Up to 18 kHz,” *IEEE Transactions on Applied Superconductivity*, vol. 28, no. 8, 2018, doi: 10.1109/TASC.2018.2841926.

[20] Y. Nikulshin, Y. Yeshurun, and S. Wolfus, “Effect of magnetic sheath on filament AC losses and current distribution in MgB2 superconducting wires: Numerical analysis,” *Supercond Sci Technol*, vol. 32, no. 7, 2019, doi: 10.1088/1361-6668/ab13d9.

[21] G. Blatter, M. V. Feigel’Man, V. B. Geshkenbein, A. I. Larkin, and V. M. Vinokur, “Vortices in high-temperature superconductors,” *Rev Mod Phys*, vol. 66, no. 4, 1994, doi: 10.1103/RevModPhys.66.1125.

[22] H. Zhang, Z. Wen, F. Grilli, K. Gyftakis, and M. Mueller, “Alternating current loss of superconductors applied to superconducting electrical machines,” *Energies (Basel)*, vol. 14, no. 8, 2021, doi: 10.3390/en14082234.

[23] C. A. Luongo, “Superconducting storage systems: An overview,” *IEEE Trans Magn*, vol. 32, no. 4 PART 2, 1996, doi: 10.1109/20.508607.

[24] Y. Nikulshin, Y. Wolfus, A. Friedman, and Y. Yeshurun, “Dynamic core length in saturated core fault current limiters,” *Supercond Sci Technol*, vol. 26, no. 9, 2013, doi: 10.1088/0953-2048/26/9/095013.

[25] Y. Nikulshin *et. al..*, “Saturated Core Fault Current Limiters in a Live Grid,” *IEEE Transactions on Applied Superconductivity*, vol. 26, no. 3, 2016, doi: 10.1109/TASC.2016.2524444.

[26] M. R. Beasley, W. A. Fietz, R. W. Rollins, J. Silcox, and W. W. Webb, “Annihilation instability in hard superconductors,” *Physical Review*, vol. 137, no. 4A, 1965, doi: 10.1103/PhysRev.137.A1205.

[27] A. V. Kapra, D. Y. Vodolazov, and V. R. Misko, “Vortex transport in a channel with periodic constrictions,” *Supercond Sci Technol*, vol. 26, no. 9, 2013, doi: 10.1088/0953-2048/26/9/095010.

[28] R. Zadorosny, E. C. S. Duarte, E. Sardella, and W. A. Ortiz, “Vortex-antivortex annihilation in mesoscopic superconductors with a central pinning center,” *Physica C: Superconductivity and its Applications*, vol. 503, 2014, doi: 10.1016/j.physc.2014.04.007.

[29] L. Burlachkov and S. Burov, “Effect of vortex annihilation lines on magnetic relaxation in high-temperature superconductors,” *Phys Rev B*, vol. 103, no. 2, pp. 1–7, 2021, doi: 10.1103/PhysRevB.103.024511.

[30] Lukovsky Gregory, “Mechanisms for electric field evolution in Bi2Sr2Ca2Cu3O10-δ and YBa2Cu3O7-δ tapes in a response to AC magnetic field,” *M.Sc. Thesis Bar Ilan University*, 2006.

[31] L. Burlachkov and N. Fuzailov, “Anomalous ‘ out-of-phase ’ magnetic ac response in superconducting wires,” *Phys. Rev. B*, vol. 104, pp. 1–5, 2021.

[32] P. W. Anderson and Y. B. Kim, “Hard superconductivity: Theory of the motion of abrikosov flux lines,” *Rev Mod Phys*, vol. 36, no. 1, 1964, doi: 10.1103/RevModPhys.36.39.

[33] A. M. Campbell and J. E. Evetts, “Flux vortices and transport currents in type II superconductors,” *Adv Phys*, vol. 21, no. 90, 1972, doi: 10.1080/00018737200101288.

[34] M. R. Beasley, R. Labusch, and W. W. Webb, “Flux Creep in Type-II Superconductors,” *Physical Review*, vol. 181, no. 2, pp. 682–700, 1969.

[35] Y. Yeshurun and A. P. Malozemoff, “Giant flux creep and irreversibility in an Y-Ba-Cu-O crystal: An alternative to the superconducting-glass model,” *Phys Rev Lett*, vol. 60, no. 21, 1988, doi: 10.1103/PhysRevLett.60.2202.

[36] L. Burlachkov, D. Giller, and R. Prozorov, “Collective flux creep: Beyond the logarithmic solution,” *Phys Rev B Condens Matter Mater Phys*, vol. 58, no. 22, 1998, doi: 10.1103/PhysRevB.58.15067.

[37] Y. Abulafia *et. al.*., “Local magnetic relaxation in high-temperature superconductors,” *Phys Rev Lett*, vol. 75, no. 12, 1995, doi: 10.1103/PhysRevLett.75.2404.

[38] V. M. Vinokur, M. V. Feigelman, and V. B. Geshkenbein, “Exact solution for flux creep with logarithmic U(j) dependence: Self-organized critical state in high-Tc superconductors,” *Phys Rev Lett*, vol. 67, no. 7, 1991, doi: 10.1103/PhysRevLett.67.915.

[39] J. Bardeen and M. J. Stephen, “Theory of the motion of vortices in superconductors,” *Physical Review*, vol. 140, no. 4A, 1965, doi: 10.1103/PhysRev.140.A1197.

[40] L. Burlachkov and N. Fuzailov, “Negative resistance and heat dissipation in superconducting wires in an ac magnetic field,” *Physica C: Superconductivity and its Applications*, vol. 603, 2022.

[41] N. Fuzailov, “Anomalous ‘Out-of-phase’ Magnetic AC Response in Superconducting Wires.”

[42] J. J. Rabbers, B. Ten Haken, and H. H. J. T. Kate, “Advanced ac loss measurement methods for high-temperature superconducting tapes,” *Review of Scientific Instruments*, vol. 72, no. 5, 2001, doi: 10.1063/1.1367361.

[43] E. Zeldov, J. R. Clem, M. McElfresh, and M. Darwin, “Magnetization and transport currents in thin superconducting films,” *Phys Rev B*, vol. 49, no. 14, 1994, doi: 10.1103/PhysRevB.49.9802.

[44] A. Rimikis, R. Kimmich, and T. Schneider, “Investigation of n-values of composite superconductors,” *IEEE Transactions on Applied Superconductivity*, vol. 10, no. 1, 2000, doi: 10.1109/77.828459.

[45] J. H. Kim, S. X. Dou, A. Matsumoto, S. Choi, T. Kiyoshi, and H. Kumakura, “Correlation between critical current density and n-value in MgB 2/Nb/Monel superconductor wires,” in *Physica C: Superconductivity and its Applications*, 2010. doi: 10.1016/j.physc.2010.05.075.

[46] A. Motaman *et. al.*., “Power-law relationship between critical current density, microstructure, and the n-value in MgB 2 superconductor wires,” *J Supercond Nov Magn*, vol. 27, no. 7, 2014, doi: 10.1007/s10948-014-2504-5.

[47] E. C. L. Chesneau and B. A. Glowacki, “Comparison of magnetic field profiles of Ag/BSCCO-2223 tapes carrying AC and DC currents,” *IEEE Transactions on Applied Superconductivity*, vol. 9, no. 2 PART 2, 1999, doi: 10.1109/77.785008.

[48] G. Lukovsky, A. Friedman, Y. Wolfus, L. Burlachkov, and Y. Yeshurun, “Energy loss and regimes of flux dynamics in BSCCO tapes above the engineering critical current,” in *IEEE Transactions on Applied Superconductivity*, Jun. 2007, pp. 3137–3139. doi: 10.1109/TASC.2007.900004.

תקציר

מודל תיאורטי חדש הדגיש את התרומה החשובה של קווי אפס מגנטיים על דינמיקת השטף בתוך מוליכי-על. קווים אלו הינם נקודת המפגש של שטף חיובי ושלילי ובהם השטפים מאיינים זה את זה. ההתבדרות המקומית של צפיפות הזרם על ידי קווי אפס אלו, מפלגת מחדש את צפיפות הזרם בכל שטח החתך של מוליך-העל ומובילה להאטה בדינמיקת השטף כאשר קווי האפס המגנטיים נוכחים במוליך-העל. בעבודה זו, אנו חוקרים באופן ניסיוני איך תרומה זו של קווי האפס המגנטיים משפיעה על המתח הנוצר על גבי חוטים מוליכי-על בטמפרטורות גבוהות. אנו מתחילים במצב של DC, על ידי חקירה של עקומות מתח -זרם בחוטי BSCCO-2223 הנושאים זרמי DC וחשופים לשדות מגנטיים DC חיצוניים. בעוד שהזרם יוצר באופן טבעי קו אפס במרכז החוט, השדה החיצוני מזיז את מיקום הקו ואף יכול להעלים אותו, זאת כתלות בערכי הזרם והשדה יחדיו. על ידי שינוי ערכי הזרם והשדה, הראינו באופן ניסיוני שעקומות המתח-זרם משתנות במעבר בין מצב שבו קו האפס נוכח למצב בו הוא נפקד. המשכנו וחקרנו את ההשפעות של קו האפס במצב ה-AC, שם נצפו שני מנגנונים מתחרים. במנגנון רגיל, המתח שנוצר עקב תנועת השטף לאורך החוט הוא "בפאזה" עם השדה המגנטי החיצוני. אבל, ככל שתדירות השדה גדלה או שהזרם בחוט קטן, מופיע באופן לא צפוי שיא במתח "שאינו בפאזה" עם השדה המגנטי החיצוני. עבור תנאים שונים של שדה חיצוני וזרם, שני המנגנונים מתקיימים זה לצד זה. לעומת זאת, בתנאים אחרים של שדה וזרם השיא שאינו בפאזה מתגבר על זה שבפאזה ונותר לבדו. המודל התיאורטי חוזה שהשיא במתח שאינו בפאזה נובע כתוצאה של ההאטה בתנועת השטף עקב קווי אפס מגנטיים. הוצגה דיאגרמת פאזות אשר חוזה את התנאים של זרם ושדה בהם כל אחד מהשיאים במתח שולט, ואת התנאים בהם השיאים מתקיימים זה לצד זה. תוצאות המדידה הראו שהתנהגות המתח תואמת באופן איכותי לתחזיות של דיאגרמת הפאזות התיאורתית. התוצאות הן במצב ה-DC והן במצב ה-AC תומכות בכך שיש האטה בדינמיקת השטף בנוכחות קווי אפס מגנטיים. בנוסף, גילינו תופעה חדשה ומפתיעה של אסימטריה בתגובת החוט לשדה מגנטי ולזרם הנובעת ככל הנראה מאסימטריה במבנה של החוט מוליך-העל שנמדד. אסימטריה זו משפיעה בצורה משמעותית על צורת הגל של המתח במוליך-העל. על יד התאמת התיאוריה לחוט בעל מבנה אסימטרי, הראינו שאסימטריה זו משפיעה בעיקר על השיא במתח שאינו בפאזה עם השדה ושההשפעה שלה גדולה יותר בתדרים גבוהים ובזרמים נמוכים, זאת בהתאמה לתיאוריה. עם העלייה בביקוש עבור חוטים מוליכי-על, וכן העלייה בשימוש בהם, תוצאות אלו יכולות לשחק תפקיד חשוב בשימוש בחוטים אלו בהתקנים יישומיים.

עבודה זו נעשתה בהדרכתו של דוקטור שוקי וולפוס.

המחלקה לפיזיקה של אוניברסיטת בר-אילן.

אוניברסיטת בר אילן

השפעת קווי אפס מגנטיים על שדות חשמליים בחוטים של מוליכי-על בטמפרטורה גבוהה במצב ה-DC וה-AC

אופק מרלי

עבודה זו מוגשת כחלק מהדרישות לשם

קבלת תואר מוסמך במחלקה לפיזיקה,

אוניברסיטת בר אילן

רמת גן התשפ"ד